THESIS

UNDRAINED SHEAR BEHAVIOR AND CRITICAL STATE ANALYSIS OF MIXED MINE WASTE ROCK AND TAILINGS

Submitted by

Raquel N. Borja Castillo

Department of Civil & Environmental Engineering

In partial fulfillment of the requirements

For the Degree of Master of Science

Colorado State University

Fort Collins, Colorado

Summer 2019

Master's Committee:

Advisor: Christopher A. Bareither

Joseph Scalia
Sean Gallen

ABSTRACT

UNDRAINED SHEAR BEHAVIOR AND CRITICAL STATE ANALYSIS OF MIXED WASTE ROCK AND TAILINGS

The objectives of this study were to (i) evaluate the undrained shear behavior of mine tailings and a tailings-dominated mixture of filtered tailings and waste rock (i.e. GeoWaste), (ii) identify the critical state of each material, and (iii) assess the impact of waste rock inclusions on the critical state of tailings. Mine tailings and waste rock were collected from an active mine where GeoWaste is being considered as a potential solution for mine waste management. GeoWaste was prepared at a mixture of 1.2 parts waste rock to 1 part tailings, by dry mass, which was a relevant mixture ratio for field implementation. Consolidated undrained (CU) triaxial compression tests were conducted on pure tailings and GeoWaste. Large-scale triaxial compression tests were conducted on 150-mm-diameter GeoWaste specimens, and 38-mm-diameter triaxial tests were conducted on tailings prepared to three initial conditions: filtered tailings that represented field conditions, dense filtered tailings, and paste tailings. Triaxial compression tests were conducted at effective confining pressures (σ_c') ranging between 20 and 500 kPa.

Filtered tailings prepared to represent field conditions yielded contractive, strain-hardening behavior. Dense filtered tailings exhibited strain-hardening behavior, net positive pore pressure, and a transition from contractive to dilative tendencies. Paste tailings exhibited modest strain-hardening behavior. GeoWaste exhibited strain-hardening, contractive behavior, and a modest transition from contractive to dilative behavior was observed at σ'_c = 500 kPa. The undrained shear behavior of GeoWaste was comparable to filtered tailings at σ'_c = 50 kPa and 100 kPa. However, undrained shear behavior of GeoWaste at σ'_c = 500 kPa changed related to tailings, which was characterized by a larger deviator stress and lower excess pore pressure. This

GeoWaste behavior indicated improved shear resistance compared to filtered tailings, which was attributed to (i) inter-particle reinforcing effects between the waste rock particles within a tailings-dominated structure and (ii) densification of the GeoWaste structure.

Shear strength parameters were calculated from the slope of a composite K_f Line for each material. Filtered tailings prepared to represent field conditions, and dense filtered tailings yielded effective tangent friction angle (φ'_t) = 33°, and paste tailings yielded φ'_t = 32°. Similarity in φ'_t between the three tailings prepared with different initial specimen characteristics was attributed to similar void ratios at the end of consolidation under a given σ'_c. GeoWaste yielded φ'_t = 32°. Although composite φ'_t were similar between tailings and GeoWaste, the secant friction angles of GeoWaste increased with increasing σ'_c, whereas the opposite trend was observed for tailings. The addition of waste rock particles to tailings in a fine-dominated structure to increase the shear resistance relative to tailings as effective consolidation stress increased.

An assessment was conducted between the critical state lines for tailings and GeoWaste to determine if the critical state line for tailings can represent critical state conditions in GeoWaste. An equivalent tailings void ratio (e^*_t) that can represent the tailings fraction within GeoWaste correlated with the critical state line for tailings. In this study, the e^*_t for GeoWaste was determined via optimizing a fitting parameter in the e^*_t equation to correlated with the critical state line for tailings. Although this evaluation suggests that the critical state line for the tailings can be used to represent critical state conditions in GeoWaste, additional work is needed to determine e^*_t a priori.

ACKNOWLEDGMENTS

I want to thank everybody who contributed both directly and indirectly in the completion of this work.

First, I would like to thank my advisor, Dr. Christopher Bareither, who provided constant support, guidance, and enthusiasm throughout my Master's program. His support was crucial to the completion of this work. I also would like to extend my thanks to Dr. Scalia and Dr. Gallen for serving on my graduate committee.

I appreciate the support of Geo-Group friends with whom I shared such great moments at CSU. Special thanks to Mohammad Gorakhki for his motivation and assistance during my laboratory work, which was crucial for my thesis, and to Neelufar Aghazamani for her company and moral support.

I am very grateful to my family, specially to my parents and sister for their continuous support, sacrifice, trust, and love throughout all my life. My parents did what I am today, and I am eternally grateful. I wish to thank my fiancé Geinfranco for showing true support and love to achieve my personal goals. Finally, I am thankful to God for his blessing during my time at CSU.

TABLE OF CONTENTS

LIST OF TABLES

LIST OF FIGURES

LIST OF SYMBOLS

A	Skempton's pore pressure parameter	w	water content
D_{10}	coarse fraction particle diameter at 10% finer	$\Delta\sigma_d$ or q	deviator stress
D_{50}	fine fraction particle diameter at 50% finer	$\Delta\sigma_{d,max}$	maximum deviator stress
d_{max}	maximum particle size	ε_a	axial strain
e	void ratio	ε_{af}	axial strain at failure
e_g	global void ratio	σ'_1	effective major principle stress
e_t	tailings void ratio	σ'_3	effective minor principal stress
e^*_t	Tailings equivalent void ratio	$(\sigma'_1/\sigma'_3)_{max}$	maximum principle stress ratio
f_c	fines content	σ'_c	effective confining stress
G_s	specific gravity	σ_v	vertical stress
K_f Line	failure line in p'-q space	ϕ'	effective friction angle
k	hydraulic conductivity	ψ	state parameter
LL	liquid limit		
PL	plastic limit		
PI	plasticity index		
p'	mean effective stress		
R	dry mixture ratio		
R_{opt}	optimum mixture ratio		
u_e	excess pore pressure		
$u_{e,max}$	maximum excess pore pressure		

CHAPTER 1: INTRODUCTION

1.1 Problem Statement

The two main mine waste materials are tailings and waste rock. Tailings are fine sand and silts, whereas waste rock is gravel- to cobble-sized material with some sand and fines. Waste rock usually is stored in gravity piles, which can be susceptible to acid rock drainage (ARD) if sulfide minerals are exposed to oxygen and water. Tailings are disposed of generally as slurry in tailings storage facilities (TSFs). Relevant challenges related to TSFs include mechanical stability, environmental contamination, water management, and closure and reclamation (Williams et al. 2003; Leduc et al. 2004; Wickland et al. 2006; Bussière 2007; Blight 2010). The potential for slurry-deposited mine tailings to exist in loose, contractive states can lead to low shear strength and liquefiable materials under vertical loading (static liquefaction) and/or seismic loading (dynamic liquefaction), which has resulted in numerous TSF failures over the last century (Azam and Li 2010; Kossof et al. 2014; Caldwell 2016; Morgenstern et al. 2016).

Co-disposal of waste rock and tailings (WR&T) has been evaluated as an alternative mine waste management technique (e.g., Williams et al. 2003; Wickland et al. 2006; Bussière 2007). The vision of mixing WR&T is to create a material that facilities placement in deposits that are geotechnically and geochemically stable and do not require dams or embankments necessary in TSFs constructed for slurry-deposited tailings. The addition of waste rock to tailings is envisioned to improve shear strength, aid in transitioning shear behavior from contractive to dilative tendencies (e.g., Jehring and Bareither 2016; Hamade and Bareither 2019), and reduce liquefaction potential of the tailings, which promotes geotechnical stability.

The proportion of tailings and waste rock within a given mixture influences engineering parameters of the mixture. Tailings-dominated mixtures correspond to waste rock particles that act as inclusions in a tailings matrix. For example, GeoWaste is a tailings-dominated mixture created via mixing fast-filtered mine tailings with waste rock (Burden et al. 2017; Bareither et al.

2017; Bareither et al. 2018; Gorakhki et al. 2019). The vision of GeoWaste is to encapsulate potentially acid-generating waste rock in tailings to inhibit the ingress of oxygen and mitigate ARD potential (i.e., geochemical stability) while relying on the waste rock inclusions to improve shear strength and mitigate liquefaction potential of the tailings.

The consistency of mine tailings can range from slurry to filtered tailings, depending on the water content, and also influences engineering parameters of a WR&T mixture. Filtered tailings present low porosity and water content resulting in higher shear strength and lower hydraulic conductivity compared with conventional slurry tailings (Bussière 2007). Therefore, the use of filtered tailings in a tailings-dominated mixture is envisioned to further improve shear strength while maintaining a low reduce hydraulic conductivity relative to previous WR&T mixtures prepared with thickened and paste tailings (e.g., Wickland et al. 2006; Kahlili et al. 2010; Jehring and Bareither 2016; Hamade and Bareither 2019). The low hydraulic conductivity and potential high moisture retention of filtered tailings in the mixture (Gorakhki et al. 2019) are anticipated to minimize ingress of oxygen to reduce ARD potential. Thus, the blending of filtered tailings and waste rock in a tailings-dominated mixture (i.e., GeoWaste) is an innovative co- disposal approach to mine waste management. However, limited research has been performed on the assessment of undrained shear behavior of GeoWaste and the impact that waste rock inclusions have on the shear behavior of filtered tailings.

1.2 Research, Objectives, and Tasks

The objectives of this study were to (i) evaluate the undrained shear behavior of tailings and GeoWaste, and (ii) identify the critical state of each material, and (iii) assess the impact waste rock inclusions in GeoWaste have on the critical state of pure tailings. Mine tailings and waste rock were collected from an active gold mine where GeoWaste is being considered as a potential solution for mine waste management.

The following research tasks were completed as part of this study:

1. Determined specimen preparation techniques for tailings and GeoWaste;
2. Evaluated the undrained shear behavior of tailings to establish a baseline for comparison;
3. Evaluated the undrained shear behavior of GeoWaste;
4. Evaluated critical-state behavior of tailings and GeoWaste; and
5. Compared the undrained shear behavior and the critical state of GeoWaste to pure tailings.

Consolidated undrained (CU) triaxial compression tests were conducted on pure tailings and GeoWaste. Large scale triaxial compression tests were conducted on 150-mm-diameter GeoWaste specimens, and 38-mm-diameter triaxial tests were conducted on tailings. Different specimen preparation methods were used to suit the materials tested appropriately. Triaxial compression tests were conducted at effective confining pressures (σ_c') ranging between 20 and 500 kPa.

CHAPTER 2: BACKGROUND

This study focused on the undrained shear behavior of tailings and mixed mine waste rock and tailings from a critical state perspective. Information about the main characteristics of mine waste materials and mine waste management is provided for a better understating of the state-of-art and state-of-practice of co-mixed WR&T. Key concepts about critical state soil mechanics are provided to establish a baseline for evaluating the undrained shear behavior of mixed mine waste rock and tailings.

2.1 Mine Waste

2.1.1 Waste Rock

Mine waste rock is the rock excavated in a mining operation that does not contain economically-viable quantities of metals or minerals, and generally is gravel- to cobble-sized particles with some sand and fines. In general, waste rock is characterized by low compressibility, high shear strength, and high hydraulic conductivity. Waste rock is managed in piles commonly constructed by end-dumping via truck or conveyor. The presence of sulfide minerals in mine waste rock can lead to acid generation (i.e., ARD) when waste rock is exposed to oxygen and water.

Waste rock with the potential for ARD is referred to as potentially acid generating rock (PAG), whereas waste rock without the potential for ARD is referred to as non-acid generating rock (NAG). Common mitigation solutions of ARD are to limit infiltration of atmospheric oxygen or precipitation, which can be accomplished using barrier systems for final closure. Two commonly used final cover systems to close waste facilities are conventional covers and water balance covers (WBCs). Conventional cover systems rely on low-permeability soil layers and impermeable geomembranes to minimize infiltration. Water balance covers, also known as store-and-release, evapotranspirative, or alternative covers, rely on a balance between precipitation, soil water

storage, evaporation, and transpiration to limit percolation (Albright et al. 2010; Benson and Bareither 2012). Another mitigation solution involves isolating oxygen from the system by mixing mine tailings and waste rock to form a material with limited oxygen diffusion potential (Williams et al. 2003; Wickland et al. 2006; Bussière 2007).

2.1.2 Mine Tailings

Tailings are a mine waste material obtained from the ore milling process and generally are composed of sand-, silt-, and clay-sized particles. Tailings can exhibit a wide range of characteristics depending on the nature of the parent material, and the milling and ore extraction process. Particle-size distributions (PSDs) compiled from the literature that represents the average, upper bound, and lower bound of mine tailings are shown in Fig. 2.1. In general, tailings are classified as non-plastic silts (ML), or silty sands (SM) using the Unified Soil Classification System (USCS), and have a liquid limit (LL) usually below 40% and a plastic limit (PL) ranging from 0 to 15% (Bussière 2007). The hydraulic conductivity (*k*) of tailings typically ranges from 10^{-7} to 10^{-9} m/s (Wickland et al. 2010). Results of consolidated drained (CD) triaxial tests performed on tailings yielded effective friction angles ranging from 30° to 42°, with cohesion close to zero. Results of consolidated undrained (CU) triaxial tests performed on tailings yielded total friction angles ranging between 14° and 25°, with cohesion ranging between 0 and 100 kPa (Bussière 2007).

The physical state of tailings can be described as slurry, thickened, paste, or filtered tailings depending on the solids content (SC), defined as the ratio of dry solid mass to the total mass. The yield stress (τ_y), defined as the limiting stress below which irreversible deformation and flow does not occur, can be used to differentiate the state of mine tailings. The relationship between SC and τ_y of tailings is shown in Fig. 2.2 (Boger 2009). This exponential relationship indicates that τ_y increased exponentially as a function of SC. Thus, water removal from tailings

(e.g., thickening or filtering) is conducted to increase the shear strength of mine tailings while also recovering water for subsequent tailings processing.

2.1.3 Mine Waste Management and Co-disposal

Previous studies suggest that WR&T mixtures have potential to improve mine waste management via (i) decreasing the footprint for waste disposal, (ii) reducing potential for acid mine drainage, (iii) increasing stability of the waste deposits, and (iv) facilitating post-closure and reclamation of mine waste facilities (e.g., Williams et al. 2003; Leduc et al. 2004; Wickland et al. 2006; Bussière 2007). Mine waste co-disposal is defined as the simultaneous or alternate deposition of tailings and waste rock in the same surface facility (Bussière 2007). Co-disposal of waste rock and tailings is a mine waste management alternative to mitigate risks associated with impoundment stability and ARD (Wilson et al. 2003; Wickland and Wilson 2005; Wickland et al. 2006; Khalili et al. 2010; Wickland et al. 2010).

Three main categories of co-disposal are (i) co-mixing, (ii) layering, and (iii) co-disposal in impoundments. Co-mixing consists of the combination of tailings and waste rock prior to disposal such that the coarse waste rock particles are arranged in loose contact and tailings fill void space between the waste rock particles. The objective of co-mixing is to improve the physical stability of tailings impoundments by integrating waste rock, which is a high shear strength material (Bussière 2007). Layering co-disposal consists of the addition of layers of tailings in the waste rock pile to control AMD production. The addition of fine-grained tailings layers into the waste rock pile may help to reduce oxygen flux and water infiltration (Bussière 2007). Co-disposal in impoundments consists of the placement of waste rock structures in the tailings impoundment. For example, placing waste rock along the upstream face of a tailings dam or inside the impoundment can create coarse-grained structures that act as drainage layers (Bussière 2007).

Experimental studies have been performed on co-mixed WR&T to assess the geotechnical behavior for the mixture (Leduc et al. 2004; Khalili et al. 2005; Wickland et al. 2006;

Jehring and Bareither 2016; Hamade and Bareither 2017). These studies indicate that the proportion of tailings and waste rock within a given mixture influences engineering parameters of the mixture. In general, mixtures have shear strength and compressibility governed by the waste rock and hydraulic conductivity controlled by the tailings-matrix.

2.2 Mixture Theory

The mixture ratio (R) of WR&T is defined as the ratio of the dry mass of waste rock over the dry mass of tailings. Schematics of particle arrangements in pure waste rock, pure tailings, and potential WR&T mixtures are shown in Fig. 2.3. A waste rock-dominated mixture corresponds to waste rock particles that are in contact and not all void space between waste rock particles are filled with tailings. On the other hand, a tailings-dominated mixture (e.g., GeoWaste) corresponds to waste rock particles that act as inclusions (i.e., are floating) in a tailings matrix. The mixture ratio corresponding to a state in which waste rock particles retain particle-to-particle contacts and all void space between waste rock particles are filled with tailings is called the optimum mixture ratio (R_{opt}). In general, strength and compressibility of mixtures at $R \geq R_{opt}$ are controlled by the waste rock, whereas hydraulic behavior of mixtures at $R \leq R_{opt}$ are controlled by the tailings (e.g., Wickland et al. 2006). Furthermore, the presence of waste rock particles in tailings-dominated mixtures ($R \leq R_{opt}$) has been shown to enhance shear strength and aid in transitioning shear behavior from contractive to dilative tendencies (e.g., Jehring and Bareither 2016; Hamade and Bareither 2019).

Fines content (f_c) is defined as the ratio of the dry mass of the fine fraction to the total dry mass of the bulk mixture, and has been used to describe shear behavior of silt and sand mixtures (Thevanayagam 1998). The correlation between f_c and R is shown in Eq. 2.1.

$$R = \frac{1 - f_c}{f_c} \tag{2.1}$$

2.2.1 Mixture Void Ratios

Thevanayagam (1998) investigated the effect of silt content on the undrained shear strength of silty sands and implied that the silty sand mixture can be described with three relevant void ratios: (i) global or bulk void ratio of the composite mixture, e_g, (ii) void ratio of the fine fraction, e_t, and (iii) void ratio of the coarser fraction, e_r. Equations for e_r and e_t adapted from Thevanayagam (1998) as a function of f_c are in Eqs. 2.2 and 2.3, are respectively

$$e_r = \frac{e_g + f_c}{1 - f_c} \tag{2.2}$$

$$e_t = \frac{e_g}{f_c} \tag{2.3}$$

At a fines content of 0.0, $e_r = e_g$ as the mixture contains no fines. An increase in the fines content increases the magnitude of e_r, and an increase in e_r above the maximum void ratio of the pure waste rock will correspond to a decrease in coarse particle contacts. At a fines content of 1.0, $e_t = e_g$ as the mixture contains no coarse particles. A decrease in the fines content will cause e_g to decrease as coarse particles with no internal voids begin replacing the tailings fraction. Thevanayagam (1998) reported that the three relevant void ratios (e_g, e_r, and e_t) could be used to describe a given mixture containing a distinct coarser and a finer fraction to more effectively evaluate shear behavior.

Thevanayagam (2007) considered the coarse-fraction dominated mixtures and fine-fraction dominated mixtures separately to analyze the influence of mixture ratio. For each mixture category, an equivalent void ratio was introduced to more effectively describe a fraction void ratio (i.e., e_r or e_t). Subsequent studies suggested that these equivalent void ratios are an effective tool to relate the undrained shear behavior of sand-silt mixtures to the predominant fraction of the mixture (Thevanayagam et al. 2002; Ni et al. 2004; Rahman et al. 2008; Bobei et al. 2009). The coarse-fraction equivalent void ratio (e_r^*) is

$$e_r^* = \frac{e_g + (1-b)\cdot f_c}{1-(1-b)\cdot f_c} \tag{2.4}$$

where b is a parameter that ranges from 0 to 1 and represents the influence of the finer-fraction on the transfer of stress during shear (Rahman et al. 2008). The fine-fraction equivalent void ratio (e_t^*) for fine-fraction controlled mixtures is

$$e_t^* = \frac{e_g}{f_c + \frac{1-f_c}{d_R{}^m}} \tag{2.5}$$

where d_R is the particle size disparity (i.e., D_{10} coarser fraction / D_{50} finer fraction) and m is a coefficient ranging between 0 and 1 that depends on particle characteristics and packing of the finer fraction. The b parameter in Eq. 2.4 and m parameter in Eq. 2.5 are empirical fitting parameters. In general b and m decrease with an increase in d_R (Thevanayagam et al. 2007; Rahman et al. 2008).

2.3 Undrained Shear Behavior

During undrained loading, excess in pore pressure is generated within the soil leading to a change in the effective stress. Three types of undrained behavior for soils under monotonic compression are (i) flow, (ii) non-flow, and (iii) limited-flow, as illustrated in Fig. 2.4. The effective stress paths are shown in a p'-q space, where $p' = (\sigma_1' + \sigma_3')/2$, $q = (\sigma_1' - \sigma_3')/2$, and σ_1' and σ_3' are the major and minor principal effective stresses, respectively. For flow behavior, the soil exhibits contractive tendencies to generate positive excess pore pressure that leads to a loss of shear strength such that the soil behaves as a liquid. For non-flow behavior, the soil exhibits dilative tendencies, where negative excess pore pressure produces an increase in shear strength. For limited-flow behavior, the soil presents an intermediate response between flow and non-flow conditions resulting in a slight increase or decrease in shear strength depending on the magnitude of excess pore pressure.

In general, sand and clay present a contractive behavior when prepared loose or normally consolidated, respectively, and dilative behavior when prepared dense or over-consolidated, respectively. The undrained behavior is mainly affected by the initial conditions of the soil before shearing, such as the effective confining stress and density (Lambe and Whitman 1969).

2.4 Critical State

Critical state soil mechanics (CSSM) has been adopted to provide a framework to conceptualize and develop constitutive models of soil behavior (Schofield and Wroth 1968). CSSM forms the basis of several methods of evaluation of liquefaction potential (Been et al. 1991; Plewes et al. 1992; Boulanger 2003; Jefferies & Been 2006). The critical state was defined by Roscoe et al. (1958) as the state at which soil undergoing shear continues to deform at constant stress and constant void ratio. The ultimate void ratio at which continuous deformation occurs with no change in principal stress difference is termed as the critical void ratio (e_c) (Casagrande 1936). The relationship between e_c and mean effective stress (p') is called the critical state line (CSL).

An application of the CSSM theory to assess undrained shear behavior is illustrated in Fig. 2.5. During undrained loading, any soil with an initial state defined by p' and void ratio (e) that plots above the CSL will generate positive excess pore pressure (i.e., tendency to contract during shear). This positive excess pore pressure will act to reduce p', and since the void ratio cannot change during undrained conditions, the stress path will move horizontally towards a final state of p' and e defined by the CSL. Conversely, a soil with an initial state of p' and e that plots below the CSL will generate negative excess pore pressure (i.e., tendency to dilate during shear). This negative excess pore pressure will act to increase p' and the stress path will more horizontally towards a final p' and e defined by the CSL. Once a given soil state reaches the CSL, the soil theoretically continues shearing with no change in e or p'. The tendency to contract during undrained shear corresponds to strain-softening behavior due to the reduction in effective stress.

The tendency to dilate during undrained shear corresponds to strain-hardening behavior due to an increase in effective stress. A substantial loss of strength that results from the reduction in effective stress during undrained shearing (i.e., flow behavior in Fig. 2.4) can lead to liquefaction (Jefferies and Been 2006)

The undrained shear response of soils from a CSSM perspective can be evaluated based on the state parameter (ψ), defined as the vertical difference between the initial void ratio of a given soil and the critical state void ratio (e_c) at the same p' (Been and Jefferies 1985) (see Fig. 2.5). Loose and normally consolidated soils typically have void ratios above the CSL that correspond to positive ψ, whereas dense and over-consolidated soils typically have void ratios below the CSL that correspond to negative ψ. The state parameter can be used as a predictive measure for the potential to yield flow behavior. Flow behavior is associated with positive ψ, limited-flow is associated with an initial point located near the CSL, and non-flow behavior is associated with negative ψ, or an initial state point below the CSL (Bobei et al. 2009).

The CSL is independent of the stress path, drainage conditions, and sample preparation method (Poulos et al. 1981; Been et al. 1991). However, the CSL is dependent on the fines content of a given soil. Been and Jefferies (1985) stated that the slope of a CSL increases with increasing fines content, which also indicates that greater compressibility occurs when increasing the fines content. The shape of the CSL depends on the stresses range. On a semi-logarithmic plot, the CSL is linear at low stress, highly non-linear and steeper for medium stress, and nearly linear and much steeper at high stress level (Been et al. 1991). The stresses level at which the slope of the CSL changes is dependent on the soil. Been et al. 1991 also states that particle breakage could change the slope of CSL. If this particle breakage is significant, the grain size distribution of the material would be modified, and because the critical state is sensitive to grain size (Poulos et al. 1981), the CSL would be affected.

The CSL can be obtained from drained and undrained triaxial compression tests regardless. Critical state points are selected from the shear behavior of a given triaxial test at the

state at which a soil continues to deform at constant stress and void ratio. For CU triaxial tests, void ratio is constant since volume change is not allowed during shear; consequently, critical state points are defined at the state at which deformation occurs at constant deviator stress and excess pore pressure. A typical stress-strain and pore pressure response from a CU triaxial test that reaches a well-defined critical state are shown in Fig. 2.6a. In some cases, the soil appears to reach the critical state, but then the undrained shear response changes with subsequent axial deformation. A typical case that does not reach a well-defined critical state is shown in Fig. 2.6b. The temporary condition identified in Fig. 2.6b is called the quasi-steady state (Alarcon et al. 1988) and should not be interpreted as a critical state. The quasi-steady state is influenced by the test conditions and fabric of the soil specimen. For undrained shear that exhibits a quasi-steady state, the recommended interpretation is to plot conditions at the end of the test on a state diagram to determine the CSL and indicate that the specimen was still evolving towards the critical state (Jefferies and Been 2006; Been et al. 1991).

2.5 Liquefaction potential

2.5.1 Mine Tailings

The effect of fine particles on the liquefaction potential of sandy soils has been assumed to be insignificant (Kuerbis et al. 1988, Pitman et al. 1994). These past studies indicated that fines tend to make the soil more resistant to liquefaction by occupying void space between the large particles, and in effect reducing the bulk void ratio and making the soil appear denser. However, more recent studies concluded that fines content influences the liquefaction potential of soils (e.g., Bray and Sancio 2006; Wijewickreme et al. 2005). These studies indicate that soils with high fines content may liquefy under loading when void ratios are high and representative of soil fabrics with a tendency to collapse with the application of dynamic loading or a rapid increase in excess pore pressure.

Mine tailings deposited in a TSF with high water contents (e.g., slurry to paste tailings) often exist in an unconsolidated state as continuous deposition of tailings generates positive excess pore pressure that must dissipate. The physical structure of mine tailings, characterized by high fines content, angular particles, and high void ratios, can create deposits with potential for structural collapse upon dynamic or static loading. Mine tailings have been shown to liquefy, a compilation of case histories of tailings liquefaction is presented by Puri et al. (2013).

The liquefaction potential of tailings can be determined based on previous work (Bray and Sancio 2006; Boulanger and Idriss 2007) that focused on soil index properties of plasticity index (PI), liquid limit (LL), and natural water content (w_c) to determine liquefaction potential. A chart of plasticity index versus the ratio of w_c/LL is shown in Fig. 2.7 with zones of "non-susceptible", "moderately susceptible", and "susceptible" liquefaction were identified based on the observations of samples that did or did not experience liquefaction (Bray and Sancio 2006). A w_c/LL ratio of 0.80 is identified as the threshold below which the soil will not liquefy (Bray and Sancio 2006).

Liquefaction potential of mine tailings also can be assessed from the critical state approach. Bedin and Schaid (2012) performed undrained triaxial tests on gold tailings. Results indicated that tailings present positive excess pore pressure during shear (i.e., contractive behavior), which can lead to liquefaction. This behavior was confirmed with results from drained triaxial compression and extension tests. Anderson and Eldridge (2011) used piezocone penetration test (CPTu) profiles within the critical state framework to indicate that silt tailings were expected to behave in a highly strain softening manner, which could potentially result in liquefaction.

2.5.2 WR&T mixture

Wijewickreme et al. (2010) conducted a liquefaction assessment on WR&T mixtures in which tailings just filled void spaces between waste rock particles. Monotonic and cyclic undrained triaxial shear tests were conducted. This study indicated that WR&T mixture was unlikely to liquefy

under cyclic loading since strain-softening behavior accompanied by loss of shear strength did not develop. In general, results indicated that WR&T mixtures behaved similarly to a coarse rock material as opposed to fine-grained tailings alone. However, WR&T mixtures had a higher potential for strain development under cyclic loading in comparison with coarse material alone. The presence of tailings in the pore space of rock particles appeared to decrease the ability of rock particles to engage and develop inter-particle stresses in comparison with the coarse material alone.

Jehring and Bareither (2016) stated that for WR&T mixtures with $R < R_{opt}$, tailings composition of the finer fraction and R were important factors that can lead to differences in undrained shear behavior. Hamade and Bareither (2019) suggested that as R increases from $R < R_{opt}$ to $R \approx R_{opt}$ via the addition of waste rock to the mixtures, shear behavior transitions from a contractive, strain-softening response to a more dilative, strain-hardening response. This transition was attributed to more pronounced interaction between waste rock inclusions in a fine-dominated structure that mitigated the development of flow behavior.

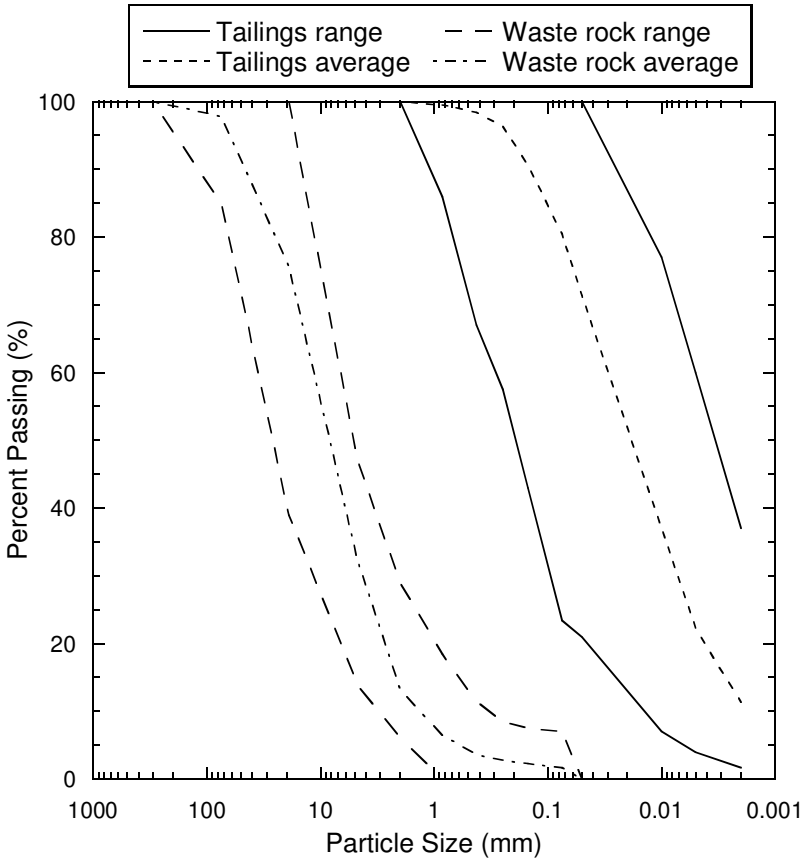

Fig. 2.1. Range and average particle-size distributions for mine tailings and waste rock compiled from Qiu and Sego (2001), Morris and Williams (1997), Khalili et al. (2005), Wickland and Wilson (2005), Wickland et al. (2006) Bussière (2007), Khalili et al. (2010), and Wickland et al. (2010).

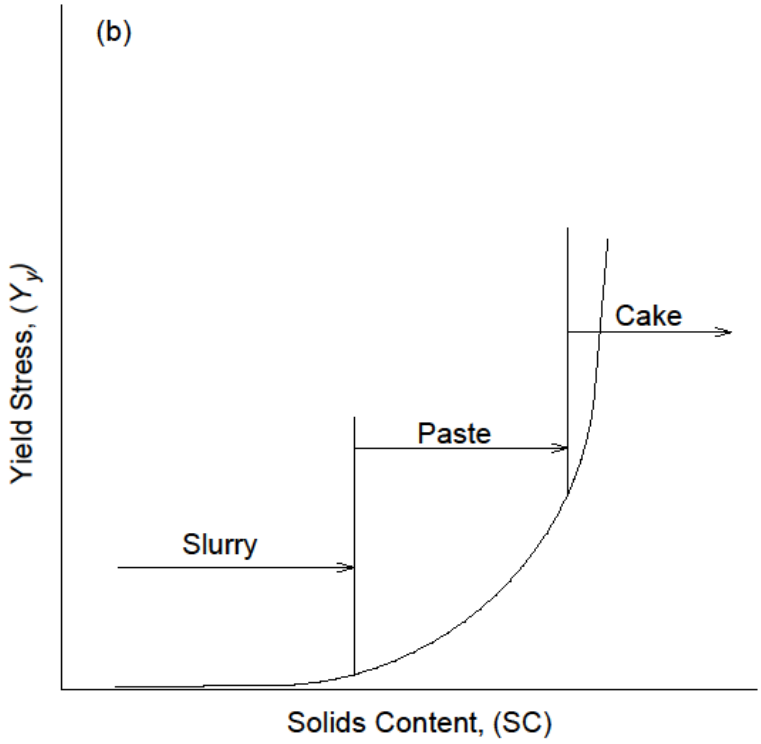

Fig. 2.2. Typical curve for yield stress for different types of tailings based on solids content. Adapted from Boger 2009.

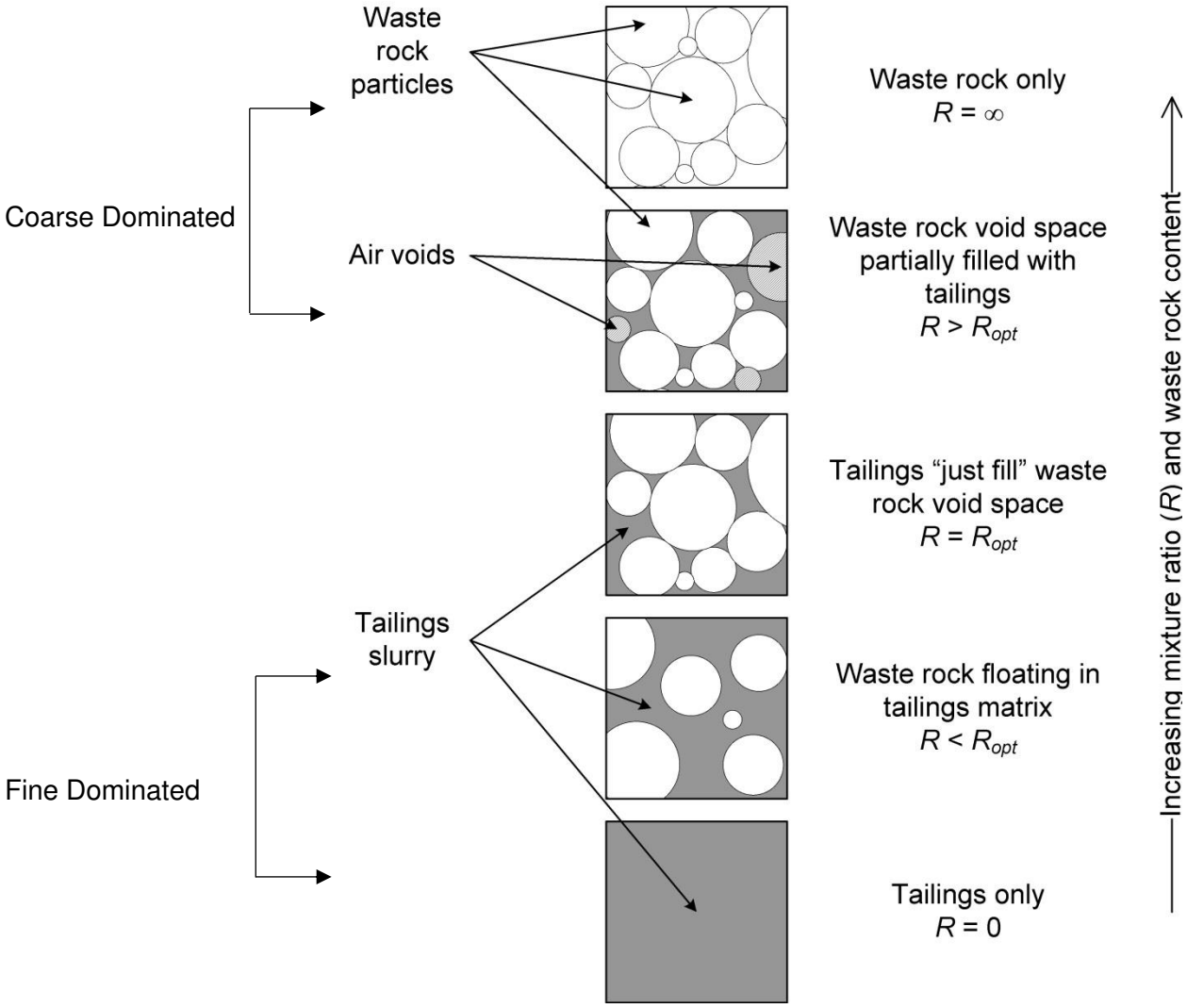

Fig. 2.3. Particle structure of co-mixed waste rock and tailings for different mixture ratios, R. Adapted from Wickland et al. (2006).

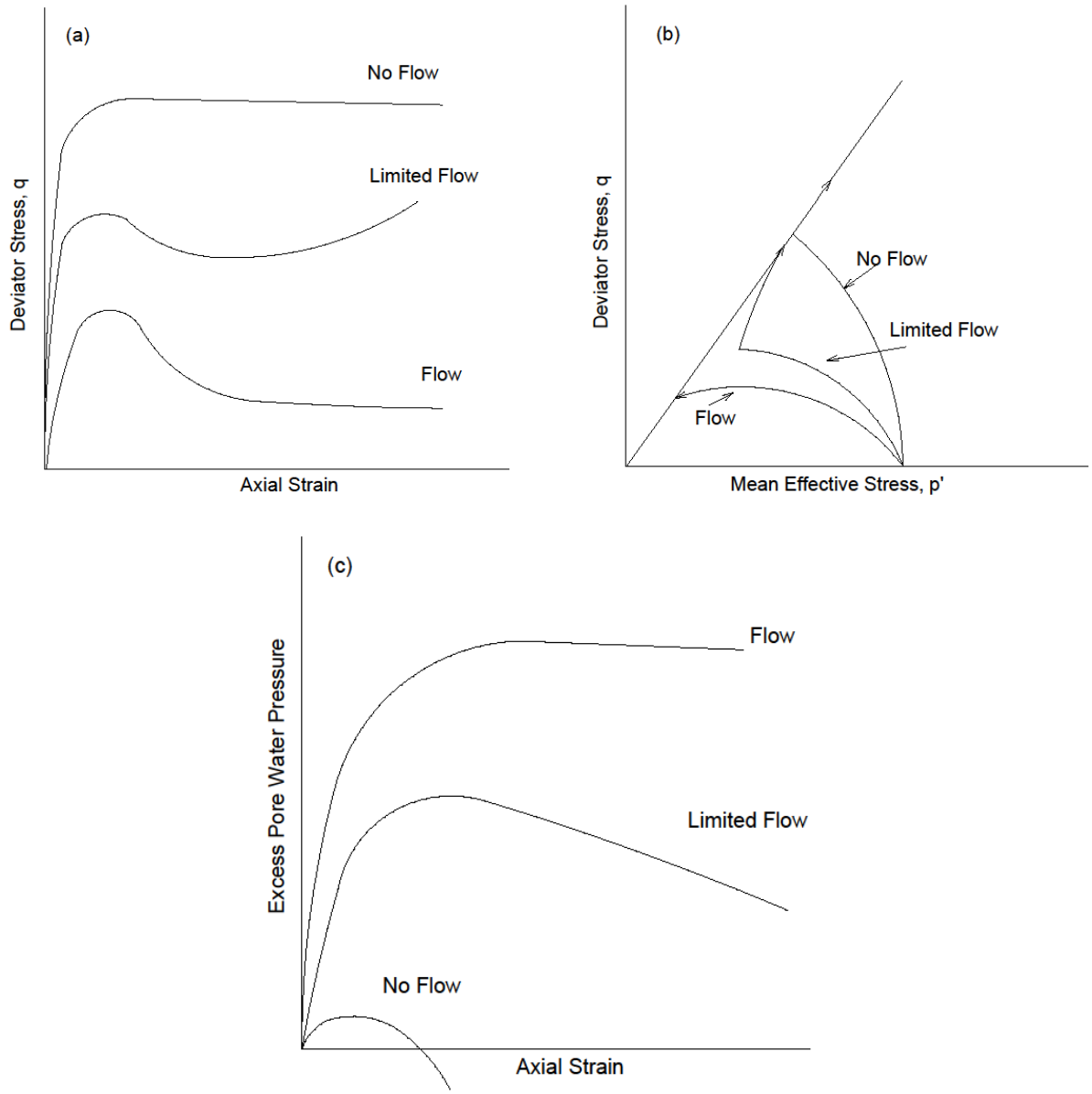

Fig. 2.4. Schematics of three possible undrained shear flow behaviors for (a) deviator stress ($\Delta\sigma$) versus axial strain (ε_a), (b) effective stress paths, and (c) excess pore water pressure (u_e) versus axial strain (ε_a). Modified from Bobei et al. (2009).

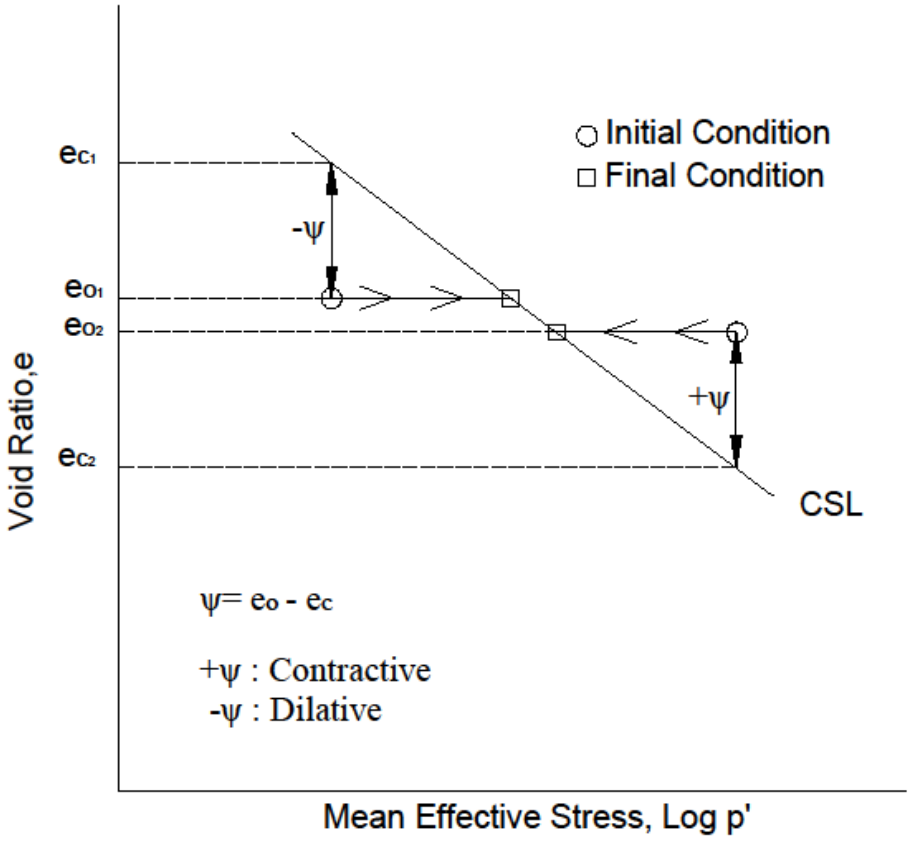

Fig. 2.5. Schematic showing the relationship between void ratio and mean effective stress with definition of state parameter (ψ); adapted from Been & Jefferies (1985).

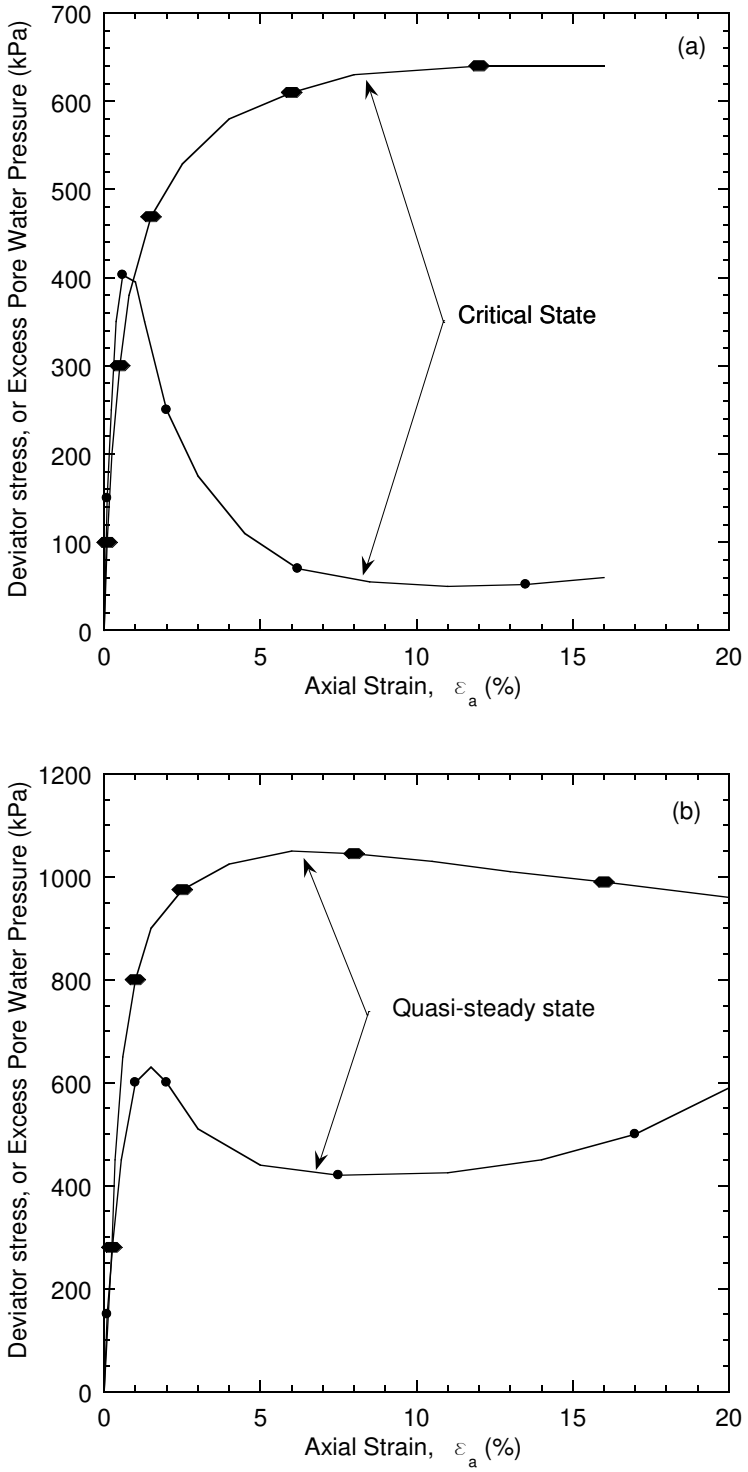

Fig. 2.6. Typical stress-strain and pore water pressure behavior from consolidated undrained (CU) triaxial tests. Modified from Jefferies and Been 2006.

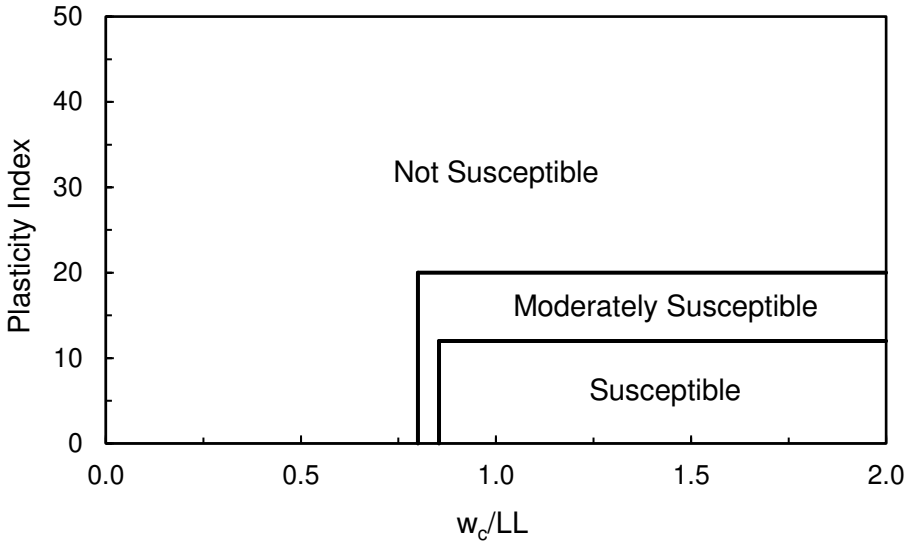

Fig. 2.7. Criteria for evaluating liquefaction potential based on soil index properties. Modified from Bray and Sancio (2006)

CHAPTER 3: MATERIALS AND METHODS

3.1 Materials

Mine tailings and mine waste rock from an active gold mine in North America were used in this study. Waste rock was non-potentially acid generating (Non-PAG) material. GeoWaste was created in the laboratory via mixing mine tailings and waste rock to form tailings-dominated mixtures with waste rock particles acting as inclusions within the tailings matrix.

3.1.1 Waste Rock

Geotechnical characteristics of waste rock are summarized in Table 3.1. Particle-size distribution (PSD) of virgin waste rock is shown in Fig. 3.1 along with an average PSD of waste rock compiled from the literature. The maximum particle size of the waste rock was 76.2 mm, which corresponded to the sieve size used when sampling waste rock at the mine. The waste rock consisted of greater than 95% gravel-sized particles and classified as well-graded gravel (GP) in accordance with the USCS (ASTM D2487). The waste rock sample collected contained minor sand (2.8%) and fines (2.1%) contents. The as-received water content was 2.2%. The specific gravity (G_s) of the waste rock was 2.73, which was measured using the water pycnometer method described in ASTM D854.

3.1.2 Tailings

The PSD for tailings is shown in Fig. 3.2 along with an average, upper-bound, and lower-bound PSD based on a compilation from literature. Geotechnical characterization of tailings included mechanical sieve and hydrometer (ASTM D422), Atterberg limits (ASTM D4318), specific gravity (ASTM D854), and standard-effort compaction (ASTM D698). Geotechnical characteristics of tailings are summarized in Table 3.1. Tailings classified as a low plasticity silt (ML) in accordance with the USCS (ASTM D2487) with liquid limit (*LL*) of 20.9% and plasticity

index (*PI*) of 1.3%. The *LL*, plastic limit (*PL*), and *PI* of tailings are shown in Fig. 3.3 along with a range of values for tailings compiled from the literature. The *PL* of tailings was similar to averages of the compiled ranges, whereas the *LL* and *PI* of tailings plotted near the lower bounds of the compiled ranges. In general, tailings used in this study were comparable with average tailings properties.

Compaction tests were conducted on tailings with standard-effort compaction to obtain the optimum water content (w_{opt}) and maximum dry density ($\rho_{d\text{-}max}$). The w_{opt} was 14.2% that corresponded to a $\rho_{d\text{-}max}$ of 1.82 Mg/m^3. The as-received water content of the mine tailings was 20.3%, which was representative of the fast-filtering process at the mine to prepare mine tailings to be mixed with waste rock to form GeoWaste. The G_s of the mine tailings was 2.76, which was measured using the water pycnometer method described in ASTM D854.

3.1.3 GeoWaste

GeoWaste specimens were prepared by mixing tailings and waste rock at water contents representative of their as-received water contents. All mine tailings and waste rock were oven dried for subsequent characterization testing and storage. Thus, water was added to dry tailings or waste rock, mixed, and allowed to equilibrate for 24 hr prior to mixing the two materials together to create GeoWaste. All GeoWaste mixtures were prepared with R = 1.2, which was the target mixture ratio for field implementation.

Standard-effort compaction tests were conducted on GeoWaste at R of 1.2 following Method C described in (ASTM D698). The w_{opt} for GeoWaste was 6.0%, which corresponded to a $\rho_{d\text{-}max}$ of 2.09 Mg/m^3. The addition of waste rock to mine tailings increased $\rho_{d\text{-}max}$ and reduced w_{opt} compared to pure tailings (Table 3.1). The increase in $\rho_{d\text{-}max}$ of GeoWaste was due to solid waste rock particles displacing void space of the tailings fraction.

The water content of the tailings fraction in the GeoWaste was calculated based on R and G_s of waste rock. The w_{opt} for the tailings fraction in GeoWaste was estimated to be 13.2% and corresponded to a calculated $\rho_{d\text{-}max}$ = 1.69 Mg/m^3 for the tailings fraction. The water content of the tailings fraction in GeoWaste at w_{opt} was comparable to w_{opt} of pure tailings; however, ρ_d of the tailings fraction in GeoWaste at $\rho_{d\text{-}max}$ was lower than $\rho_{d\text{-}max}$ of pure tailings (Table 3.1).

3.2 Triaxial Compression Testing

3.2.1 Consolidated Undrained Compression

Consolidated undrained (CU) triaxial tests were conducted on pure tailings and GeoWaste in accordance with ASTM D4767. Specimens were back-pressure saturated to achieve a B-value ≥ 0.95. This method consists of the linear increase of cell and back pressures keeping a constant effective stress. Specimens were sheared at an axial strain rate of 1 %/h to a maximum axial strain of 20%. The strain rate was determined via ASTM D4767 to promote pore pressure equilibration throughout the specimen during shear. Pore water pressure was measured during shear.

3.2.1.1 Small-Scale Triaxial Testing

Conventional 38-mm-diameter triaxial tests were performed on paste and filtered tailings because the maximum particle diameter (d_{max}) for tailings was ≤ 2 mm. Filtered tailings were prepared at as-received water content of 20.3% at two different densities. Filtered tailings prepared at ρ_d = 1.45 Mg/m^3, which corresponds to the 80% of $\rho_{d\text{-}max}$, were called filtered tailings at field condition. Filtered tailings prepared at ρ_d = 1.70 Mg/m^3, which corresponds to the 93% of $\rho_{d\text{-}max}$, were called dense filtered tailings.

Paste tailings specimens were prepared to a target solids content of 70 % (described subsequently) and then anisotropically consolidated via vertical stress application. A schematic

of the vertical consolidation setup is shown in Fig 3.4. The vertical load was applied incrementally via dead weights, with a load increment ratio of unity (i.e., the load was doubled for each increment). Vertical deformation was monitored using a dial gage during the increase in effective vertical stress (σ_v') to determine when consolidation was completed for each load increment. Complete consolidation was assumed when no further deformation was observed. After achieving a σ_v' equivalent to the target effective confining stress (σ_c'), specimens were then transferred to a triaxial cell and subjected to an isotropic σ_c'. The target σ_c' for paste tailings were 100 and 250 kPa. Specimen volume change during vertical loading was attributed to vertical deformation and measured via a dial gauge. Specimen volume change during application of a confining stress in a triaxial cell was monitored via an outflow burette connected to drainage lines for the specimen and vertical deformation of the specimen.

Filtered tailings specimens were prepared to a target water content, moist tamped in a split mold (described subsequently), and then isotropically consolidated within the triaxial cell prior to shear. Vertical stress application similar to the paste tailings was not conducted on filtered tailings specimens. Specimen volume change during consolidation was measured using an outflow burette connected to the drainage lines of the specimen and vertical deformation of the specimen. The target σ_c' for filtered tailings at field condition were 20, 50, 100, 250, and 500 kPa, and for dense filtered tailings were 100 and 250 kPa.

The void ratio (e) of all tailings specimens was determined after shearing via Eq. 3.1:

$$S \cdot e = w \cdot G_s \tag{3.1}$$

where S is the degree of saturation and w is water content. The final water content of the tailings specimens after shear was determined using the total sample freezing method described in Sladen and Handford (1987). The final void ratio was computed, assuming specimens were 100% saturated.

Measurements of axial load, axial displacement, cell pressure, and pore pressure within the tailings specimen were measured during triaxial testing. Axial load was measured using a load cell (Artech Industries, Inc., 8900 ± 0.4 N) and axial displacement was measured with a LVDT (Novotechnik, 50 ± 0.003 mm). Cell and pore pressure were monitored with pressure transducers (GeoTac, 1378 ± 0.07 kPa; ELE International, Ltd., 700 ± 0.07 kPa). All data were collected by a data acquisition system (CU Triaxial Mode, GeoTac).

3.2.1.2 Large-Scale Triaxial Testing

Large-scale triaxial tests were conducted on 150-mm-diameter specimens for GeoWaste and mine tailings. The d_{max} of GeoWaste was constrained to be 25 mm to adhere with stipulations in ASTM D 4767. Thus, waste rock used in the GeoWaste specimens was scalped on a 25.4-mm sieve. GeoWaste specimens were prepared to target conditions, moist tamped in a split-mold (described subsequently), and isotropically consolidated within the triaxial cell prior to shear. The change in specimen volume during consolidation was measured using an outflow burette connected to the drainage lines of the specimen. The target σ_c' for GeoWaste were 50, 100, 250, and 500 kPa. A single large-scale triaxial test on mine tailings was conducted on filtered tailings consolidated under 100 kPa. The large-scale triaxial tests on tailings were conducted to compare and verify that similar shear behavior was obtained in small- and large-scale CU triaxial compression. Void ratio for all large-scale triaxial specimens after shear was determined via Eq. 3.1 using the final water which was determined from a representative sample exhumed from a given specimen.

Measurements of axial load, axial displacement, cell pressure, and pore pressure within the tailings specimen were measured during triaxial testing. A LVDT was used to measure vertical displacement (Macro Sensors Model PR 750 2000, 100 ± 0.07 mm) and a load cell was used to measure axial load (Tovey Engineering, Inc. Model SW20-25K-B00, 110 ± 0.29 kN). Pressure transducers were used to measure cell and pore pressures (Omega Engineering, Inc. Model SR-

PR-OM-1000, 1000 ± 0.1 kPa). All measurements were collected by a data acquisition system (CATS Triaxial Mode 1.85, GCTS).

3.2.2 Specimen Preparation

3.2.2.1 Tailings Specimens

Tailings were prepared by mixing de-aired tap water with dried tailings using a stirring rod. Paste tailings were prepared to a target solids content of 70 %. Slurry tailings were used to get paste tailings. Slurry tailings specimens were prepared via slurry deposition method described by Wang et al. (2011). A schematic of the specimen preparation apparatus is shown in Fig. 3.4. Tailings slurries were poured into a 38-mm-diameter by 101-mm-tall split mold lined with a 0.25-mm-thick latex membrane. A 70-mm-tall extension collar was added to the top of the split mold to increase the height such that a sufficient height to diameter ratio of the specimen was maintained after consolidation. A 0.05-mm-thick paper mold was placed around the outside of the latex membrane prior to assembling the split mold and depositing the tailings slurry. The paper mold was held together with tape and provided stability to the test specimen following removal of the split mold. Once water was added to the triaxial cell to apply the confining pressure, the paper mold lost strength and tape lost adhesion such that the paper mold fell apart prior to shear.

Slurry deposited specimens were initially allowed to consolidate under self-weight for 24 hr after pouring the slurry into the split mold. After this time, tailings particles and water were separated due to sedimentation. Separated water was extracted, which increased the solids content to 70%, corresponding to paste tailings. Subsequently, the specimens were subjected to consolidation under an applied vertical stress in the consolidation frame (Fig. 3.4) and later under an all-around confining stress in the triaxial cell.

Filtered tailings were prepared to their as-received water content. Triaxial specimens consisting of filtered tailings were prepared via a moist-tamping method in five layers to target

final dimensions of 38-mm diameter and 95-mm tall. Filtered tailings specimens only were consolidated isotropically in the triaxial cell prior to shearing.

3.2.2.2 GeoWaste Specimens

GeoWaste was created by mixing waste rock and tailings at their as-received water contents to a mixture ratio of $R = 1.2$, which corresponded to tailings-dominated mixtures. GeoWaste triaxial specimens were prepared in a 150-mm-diameter and 300-mm-tall split mold via moist-tamping method in five layers to achieve uniform specimen densities. A 2.5-mm-thick rubber membrane was used for GeoWaste specimens to avoid membrane puncture from to the angular rock particles. Membrane correction calculations presented in La Rochelle et al. (1998) were applied to large-scale triaxial test data to account for additional strength contributed by the membrane.

Table 3.1. Summary of physical characteristics and classification for mine tailings and waste rock.

Material	*LL* (%)	*PI* (%)	USCS	Gravel Content (%)	Sand Content (%)	Fines Content (%)	Clay-Size Content (%)	As-Received Water Content (%)	G_s	w_{opt} *(%)*	ρ_{max} (Mg/m^3)
Tailings	20.9	1.3	ML	0	35.8	64.2	17.4	20.3	2.76	14.2	1.82
Waste Rock	NA	NA	GP	95.1	2.8	2.1	NA	2.2	2.73	NM	NM

Notes: *LL* = liquid limit; *PI* = plasticity index; USCS = Unified Soil Classification System; clay-size content taken as percent particles by mass < 0.002 mm; G_s = specific gravity; w_{opt} = optimum water content and ρ_{max} = maximum dry unit density determined from Standard-effort compaction tests; NA = not applicable; NM = not measured.

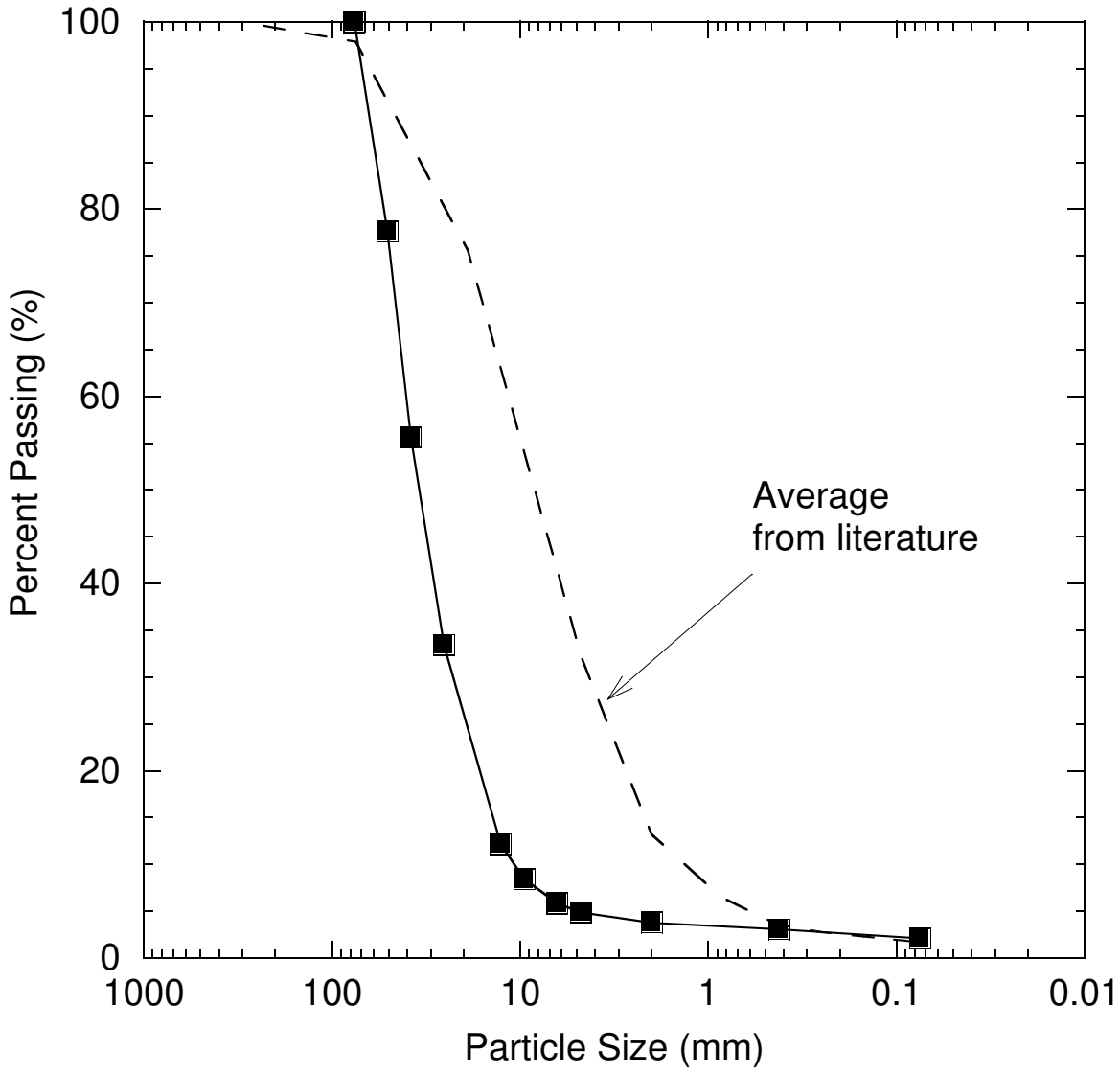

Fig. 3.1. Particle-size distributions for waste rock. Average PSD based on literature compilation. Adapted from Hamade and Bareither (2017).

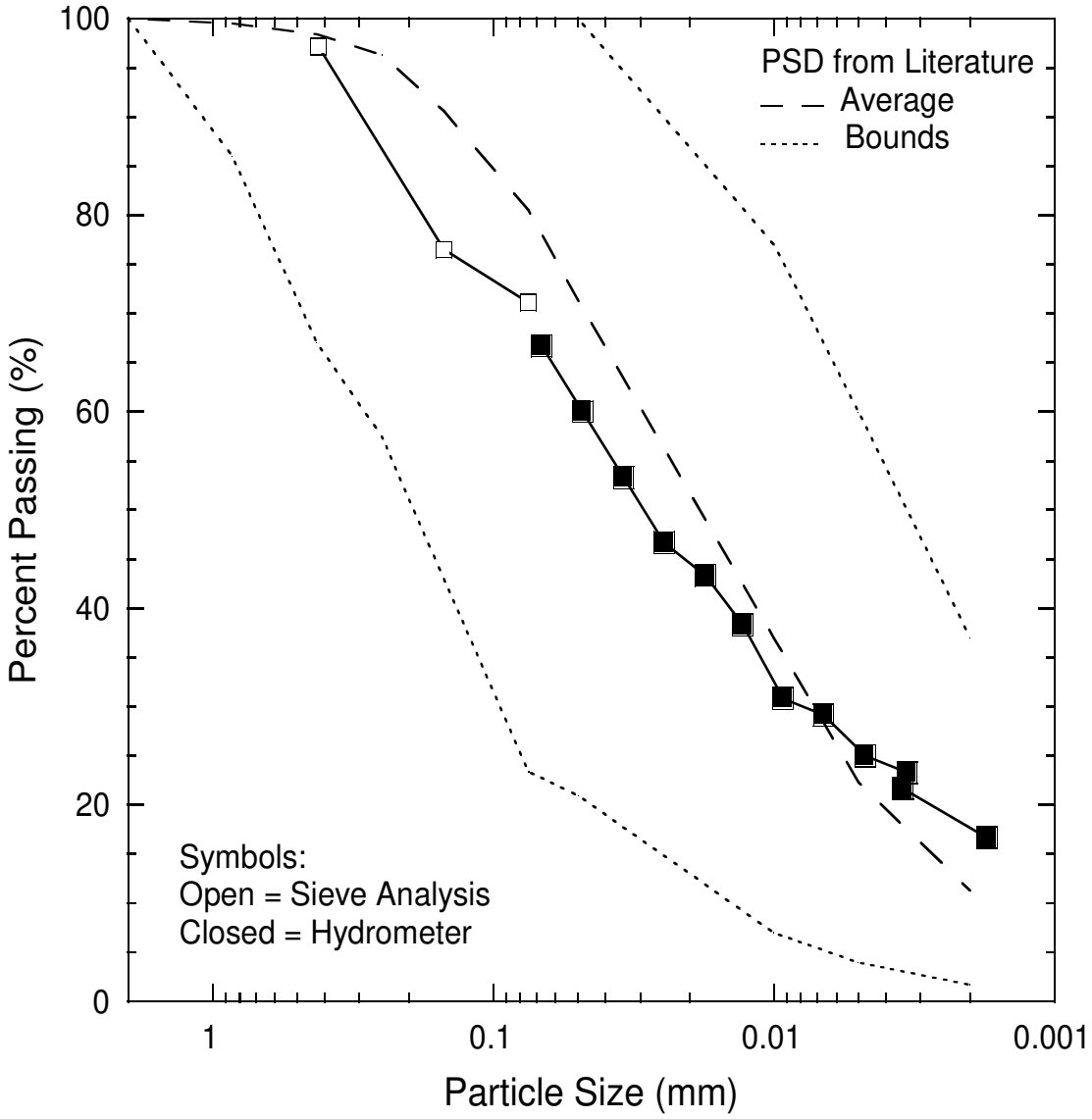

Fig. 3.2. Particle-size distributions (PSDs) for tailings based on mechanical sieve analysis and hydrometer. Dashed lines are the average PSD and upper and lower bounds of PSDs of mine tailings compiled from the literature. Adapted from Hamade and Bareither (2017).

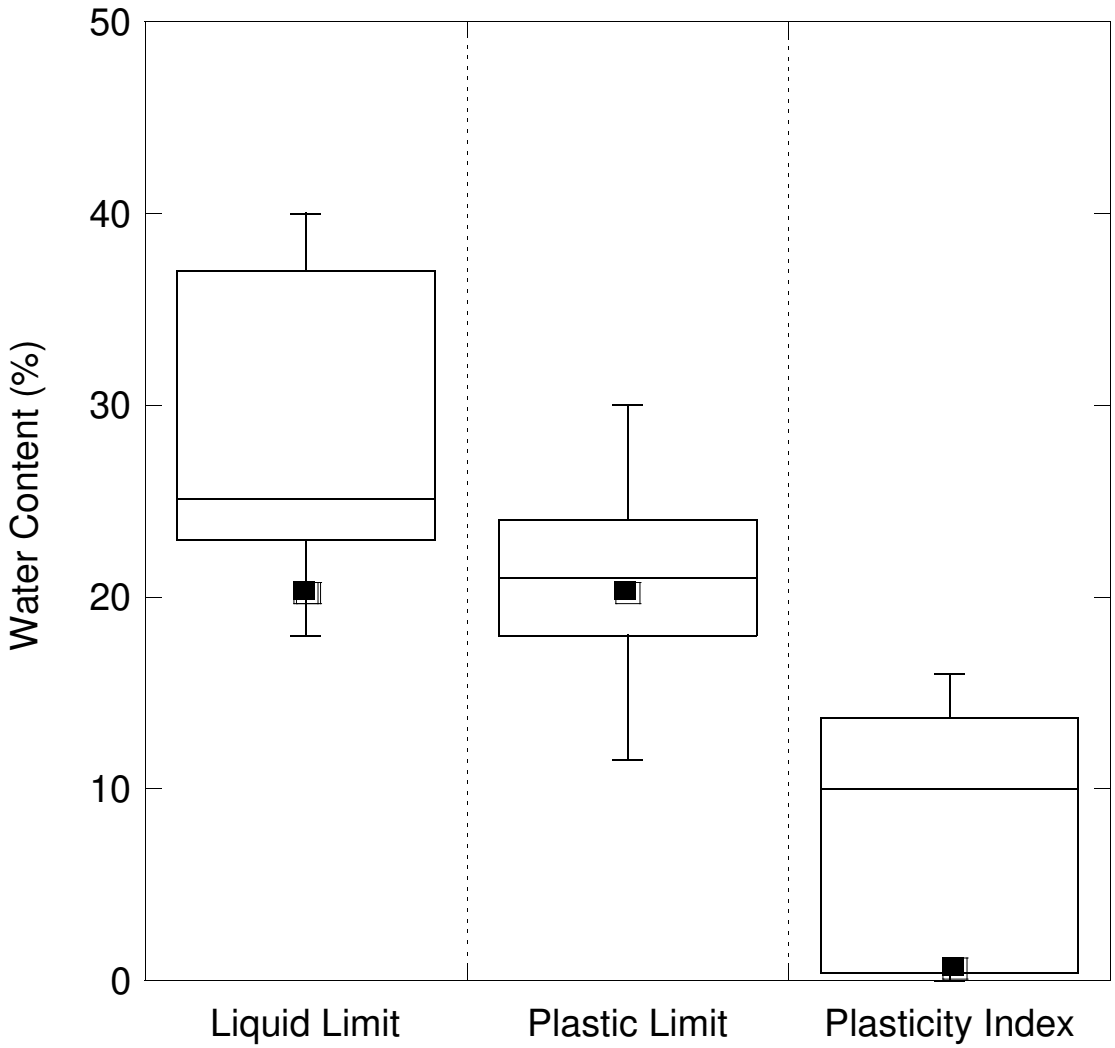

Fig. 3.3. Atterberg limits of tailings, and box and whisker plots for the ranges of Atterberg limits compiled from Matyas et al. (1984), Aubertin et al. (1996), Qiu and Sego (2001), Wickland and Wilson (2005), Wickland et al. (2010), Khalili et al. (2010), Dailiri et al. (2014), Gorakhki and Bareither (2017). The middle line in each box is the median literature value, the upper and lower bounds of each box mark the upper and lower quartiles. The upper and lower whiskers denote the maximum and minimum literature values.

.

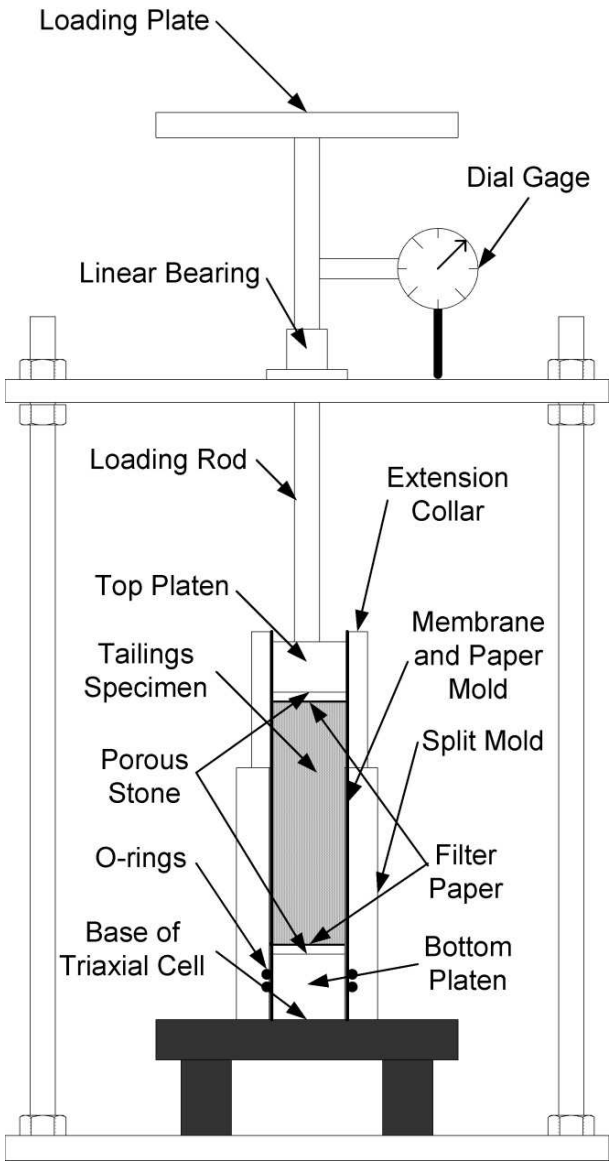

Fig. 3.4. A schematic of the consolidation frame used for the preparation of specimens for triaxial tests. Adapted from Jehring and Bareither (2016).

CHAPTER 4: RESULTS AND DISCUSSION

A summary of the consolidated undrained (CU) triaxial tests conducted on tailings is in Table 4.1 and on GeoWaste is in Table 4.2. The data compilation includes the following: target and actual σ'_c, axial strain at failure ($\varepsilon_{a,f}$), deviator stress at failure ($\Delta\sigma_d$), effective major (σ'_{1f}) effective minor (σ'_{3f}) principal stresses at failure, secant friction angle (φ'_{sc}), *B*-value (*B)*, and other parameters described subsequently. Test results were analyzed to determine the stress state related to failure and the stress state related to the critical state. Select triaxial tests were repeated to check results and assess repeatability. A compilation of the results of the CU triaxial compression tests performed in this study is shown in the Appendix.

4.1 Shear Behavior

4.1.1 Mine Tailings

Relationships of deviator stress ($\Delta\sigma$), excess pore water pressure (u_e), and effective principal stress ratio (σ'_1/σ'_3) versus axial strain (ε_a) for the CU triaxial tests conducted on filtered tailings prepared to represent field conditions (subsequently referred to as filtered tailings) are shown in Fig. 4.1. In general, undrained shear behavior was similar for all filtered tailings specimens, whereby deviator stress and excess pore pressure increased until an axial strain of approximately 3% and then remained constant through the end of shearing at $\varepsilon_a \approx 20\%$ (Fig. 4.1a). The filtered tailings specimen tested at σ'_c = 500 kPa exhibited modest dilative tendencies as observed in the reduction in excess pore pressure after $\varepsilon_a \approx 5\%$ (Fig. 4.1b), which led to strain-hardening behavior and an increase in deviator stress until the end of the experiment.

The relationships of σ'_1/σ'_3 versus ε_a (Fig. 4.1c) indicate that a maximum ratio was achieved in nearly all tests at $\varepsilon_a \approx$ 8% to 10%. Furthermore, the σ'_1/σ'_3 for all filtered tailings specimens decreased with an increase in effective confining stress, whereby the largest σ'_1/σ'_3 was measured for tests conducted at σ'_c = 20 kPa and lowest σ'_1/σ'_3 were measured for tests

conducted at σ'_c = 250 kPa and 500 kPa. A decreasing trend of σ'_1/σ'_3 with increasing σ'_c has been reported by (Kolymbas 1999) and corresponds to a decreasing secant friction angle with increasing σ'_c (Table 4.1). Repeat tests performed σ'_c = 20, 100, and 250 kPa exhibited similar shear behavior to one another, which supports the CU triaxial test method and measured data.

Relationships of $\Delta\sigma$, u_e, and σ'_1/σ'_3 versus ε_a for the CU triaxial tests conducted on dense filtered tailings are shown in Fig. 4.2 and for paste tailings are shown in 4.3. Undrained shear behavior for the dense filtered tailings exhibited strain-hardening behavior, characterized by a continuous increase in deviator stress and transition from contractive to dilative tendencies (Fig. 4.2a). Dense filtered tailings all exhibited net positive pore pressure; however, the u_e versus ε_a relationships all changed the slope at approximately 1-2% strain, which identifies a phase change and shifts from a contractive to dilative tendency (Fig. 4.2b). Undrained shear behavior of the paste tailings exhibited modest strain-hardening behavior (Fig. 4.3). The relationships of σ'_1/σ'_3 versus ε_a for both the dense filtered tailings and paste tailings increase to a maximum and then remained approximately constant until the end of the experiments (Fig. 4.2c, 4.3c). The dense filtered tailings exhibited a stiffer response as observed in the more rapid increase to a maximum σ'_1/σ'_3 at $\varepsilon_a \approx$ 2-3%, whereas maximum σ'_1/σ'_3 of the paste tailings was achieved at a larger axial strain.

Comparisons among the relationships of σ'_1/σ'_3 versus ε_a for all three tailings (field conditions, dense, and paste) tested at σ'_c = 100 kPa and 250 kPa are shown in Fig. 4.4. The dense filtered tailings exhibited the stiffest response to shearing and yielded the largest σ'_1/σ'_3 at nearly the entire range of axial strain. In contrast, the paste and filtered tailings exhibited a less stiff response to shearing, and the lowest σ'_1/σ'_3 was measured for paste tailings at a given σ'_c. This stiffer response and overall larger σ'_1/σ'_3 of the dense filtered tailings was attributed to the resultant tailings fabric of the denser prepared specimens.

4.1.2 GeoWaste

Relationships of $\Delta\sigma$, u_e, and σ'_1/σ'_3 versus ε_a for GeoWaste are shown in Fig. 4.5. Undrained shear behavior for GeoWaste developed positive u_e with axial deformation that ultimately reached a maximum value and remained constant for the remainder of shearing. The deviator stress relationships were similar and exhibited an increase to a maximum deviator stress that then remained nearly constant for the duration of shearing. The relationships of σ'_1/σ'_3 versus ε_a also exhibited similar behavior to deviator stress and excess pore pressure, and a maximum σ'_1/σ'_3 was achieved at approximately 10% axial strain. However, the σ'_1/σ'_3 for GeoWaste increased with increasing σ'_c, which was opposite to the trend observed for tailings. Thus, the GeoWaste appeared to develop increased shear resistance with an increase in effective confining stress. This behavior was hypothesized to develop from the densification of the GeoWaste. An increase in GeoWaste density is characterized by a denser tailings matrix and waste rock particles that are in closer proximity to one another. The increase in shear resistance of GeoWaste specimens at higher σ'_c was attributed to both enhanced interference between the waste rock particles during shear and denser tailings matrix.

4.1.3 Filtered Tailings and GeoWaste Comparison

Comparisons of undrained shear behavior were made between the filtered tailings prepared to represent field conditions and GeoWaste, because the GeoWaste specimens were prepared with tailings at the same water content. Relationships of $\Delta\sigma$ and u_e versus ε_a for filtered tailings and GeoWaste at σ'_c = 50, 100 and 500 kPa is shown in Fig. 4.6. The relationships for σ'_c = 50 kPa and 100 kPa were similar between the filtered tailings and GeoWaste, which suggests that the tailings matrix in the GeoWaste at low σ'_c was controlling the undrained shear behavior (Fig. 4.6a,b). In contrast, $\Delta\sigma$ increased and u_e decreased for the GeoWaste specimen tested at σ'_c = 500 kPa relative to filtered tailings (Fig. 4.6c). These changes in undrained shear behavior of GeoWaste relative to filtered tailings documents the influence of the waste rock inclusions. As

the GeoWaste densified and hypothetically, there was more interaction between adjacent waste rock particles during shear, shear resistance was enhanced.

Relationships of the σ'_1/σ'_3 and Skempton's A parameter ($u_e/\Delta\sigma$) versus ε_a for tests conducted on filtered tailings and GeoWaste are shown in Fig. 4.7. The σ'_1/σ'_3 of GeoWaste was higher than filtered tailings at σ'_c = 500 kPa. These trends indicate improved shear resistance of GeoWaste when compared to filtered tailings. The *A* parameters for filtered tailings at all σ'_c were positive and exhibited similar behavior. Similarity in the A parameter for GeoWaste to the filtered tailings at σ'_c = 50 kPa and 100 kPa is an additional assessment the documents the filtered tailings controlled shear behavior of GeoWaste at low σ'_c. However, the increase in σ'_c to 500 kPa for GeoWaste decreased the A parameter, which corresponds to mitigation of the contractive tendencies of the filtered tailings during undrained shear. The comparisons of undrained shear behavior between filtered tailings and GeoWaste indicate a change in GeoWaste behavior occurred with an increase in effective confining stress, and this change in behavior was characterized by enhanced shear behavior.

4.2 Shear Strength

4.2.1 Evaluation and Definition of Failure

A definition of failure is needed to determine shear strength parameters from a given laboratory experiment. Brandon et al. (2006) evaluated the undrained shear behavior and shear strength of silty soils and identified six failure criteria: (1) maximum deviator stress, $\Delta\sigma_{d,max}$; (2) maximum principal stress ratio, $(\sigma'_1/\sigma'_3)_{max}$; (3) maximum excess pore pressure, $u_{e,max}$; (4) limiting value of Skempton's pore pressure parameter *A* (e.g., *A* = 0); (5) stress path reaches the failure line (K_f Line) in *p'-q* space; and (6) limiting axial strain (e.g., ε_a = 5 or 10 %). These failure criteria were evaluated in Brandon et al. (2006) as well as in Wang and Luna (2012) and Jehring and Bareither (2016). The latter study considered all possible failure interpretations for mine tailings and identified three methods (i.e., $\Delta\sigma_{d,max}$, K_f Line, and ε_a = 15%) that were applicable to different

mine tailing tested in CU triaxial compression and yielded the smallest bias in determining shear strength parameters. In regards to recommendations in Brandon et al. (2006) and Jehring and Bareither (2016), failure defined by reaching the K_f Line was considered in this study.

Effective stress paths in p'-q space reach failure and theoretically maintain a constant q/p' ratio for the remainder of axial deformation in a CU triaxial test. In this study, all tailings and GeoWaste specimens were normally consolidated materials such that K_f Lines were assumed to pass through the origin (i.e., $p' = 0$ and $q = 0$). The p'-q data from an individual CU test specimen were evaluated, and all data points that yielded approximately the same q/p' ratio were taken as representative of failure conditions. The first p'-q data point in the data set representing failure conditions (i.e., smallest ε_a) was taken as the point at which the stress path reached the K_f Line, which represented the stress state at failure (Table 1). Secant friction angles (φ'_{sc}) for each triaxial test were determined via linear regression of q/p' data sets representing failure conditions for the individual tests. A composite K_f Line was determined via linear regression of the composite single data points representing stress states at failure for multiple σ'_c for a given material (e.g., filtered tailings). The slope of the composite K_f Lines was then used to compute effective friction angles (φ'_t) which are compiled for each material in Tables 4.1 and 4.2.

4.2.2 Shear Strength of Tailings

Effective stress paths and the composite K_f Line in p'-q space for filtered tailings are shown in Fig. 4.8. All effective stress paths are non-linear and exhibit typical undrained behavior associated with positive generation of excess pore pressure. The stress states at failure for each triaxial test are shown in Fig. 4.8b along with the K_f Line determined via linear regression with the constraint to pass through the origin. The φ'_t determined from the slope of the K_f line was 33º and yielded a coefficient of determination (R^2) or 0.995. Secant friction angles for the filtered tailings displayed a general decreasing trend with increasing σ'_c (Table 4.1). Thus, stress paths and stress states at failure for triaxial tests conducted at $\sigma'_c \leq 100$ kPa plot above the composite K_f Line.

Effective stress paths, stress states at failure, and the composite K_f Line in *p'-q* space for dense filtered tailings are shown in Fig. 4.9. The dense filtered tailings exhibit similar non-linear effective stress paths as observed for the filtered tailings. However, the magnitude of positive pore pressure was lower in the dense filtered tailings such that the effective stress paths reach the K_f line at larger *q* and *p'* and then trend along the K_f Line. The φ'_t for dense filtered tailings was 33º, which was identical to the filtered tailings prepared to represent field conditions. A similar friction angle for the dense filtered tailings was attributed to similar void ratios achieved in all filtered tailings specimens for consolidation under a given σ'_c. Although the initial high degree of compaction for the dense filtered tailings samples yielded stiffer specimens with more pronounced dilative behavior and higher σ'_1/σ'_3 (Fig. 4.6), aggregating the CU triaxial tests yielded a similar shear strength parameter to the filtered tailings prepared to represent field conditions.

Effective stress paths, stress states at failure, and the composite K_f Line in *p'-q* space for paste tailings are shown in Fig. 4.10. The paste tailings yielded non-linear effective stress paths with positive pore pressure generation that appeared similar to the dense filtered tailings. The composite K_f Line for the paste tailings yielded $\varphi'_t = 32º$. The slightly lower friction angle for the paste tailings was also observed in lower secant friction angles for the two paste tailings triaxial tests relative to triaxial tests on filtered tailings (field conditions and dense) at σ'_c = 100 kPa and 250 kPa. Similarity in undrained shear behavior and shear strength between the paste tailings and dense filtered tailings, was attributed to similar void ratios achieved at the end of consolidation under a given σ'_c (Table 4.1).

4.2.3 Shear Strength of GeoWaste

Effective stress paths, stress states at failure, and the composite K_f Line in *p'-q* space for GeoWaste are shown in Fig. 4.11. The effective stress paths for GeoWaste exhibit similar non-linear behavior as observed in the tailings. All effective stress paths for the GeoWaste reached failure identified by reaching the K_f Line and then trended upward along the failure line. The

composite K_f Line for GeoWaste yielded φ'_t = 32º, which was identical to the φ'_t = 32º to 33º determined for tailings. However, secant friction angles for the GeoWaste triaxial tests increased from 30º at σ'_c = 50 kPa to 40º at σ'_c = 500 kPa, which was opposite the behavior observed for tailings. Although the composite φ'_t were similar between tailings and GeoWaste, the increase in secant friction angle suggests that the addition of waste rock particles to tailings in a fine-dominated structure can increase shear strength relative to tailings. This phenomenon was attributed to overall densification of the GeoWaste that led to closer packing of the waste rock particles within the tailings matrix. The enhanced shear resistance of mine tailings via the addition of waste rock that develops interparticle reinforcing effects agrees with previous research on co-mixed waste rock and tailings (Wickland et al. 2010, Jehring and Bareither 2016 and Hamade and Bareither 2019).

4.3 Critical State Analysis

A summary of key parameters in the critical state analysis for tailings and GeoWaste is in Table 4.3. The compilation includes initial effective principal stress (p'_i), critical state effective principal stress (p'_{cs}), tailings void ratio (e_t), global void ratio (e_g) for the GeoWaste, and tailings equivalent void ratio (e^*_t) for the GeoWaste. The e_g and e_t in Table 4.3 are void ratios of specimens after consolidation and before shear. These void ratios are also representative of final specimen conditions since no volume change was allowed during undrained shear. The e_t listed for the GeoWaste specimens is a direct calculation of the tailings fraction void ratio assuming the waste rock particles were crystalline, and all void volume in GeoWaste was retained within the tailings fraction. The direct computations of e_t in GeoWaste led to void ratios higher than any tailings specimens prepared in this study. The equivalent tailings void ratio was computed for the GeoWaste based on Eq. 2.5 with an optimized m parameter (discussed subsequently).

The true critical state of a soil is defined at a given effective stress state and void ratio during shear for which the material continues to shear with no change in stress or void ratio. This

definition applied to undrained shear corresponds to a soil shearing at constant deviator stress and excess pore pressure. A true critical state may not have been reached in all CU triaxial tests conducted on tailings and GeoWaste because some specimens did not reach a constant deviator stress and/or excess pore pressure. Thus, conditions at the end of each CU triaxial test were taken to represent a quasi-steady state of the material to determine the CSL (Jefferies and Been 2006; Been et al. 1991). End state conditions were used for all tests for consistency in the critical state analysis.

4.3.1 Mine Tailings

The initial conditions and critical state conditions in *e-p′* space for filtered tailings at field conditions are shown in Fig 4.12, for dense filtered tailings are shown in Fig. 4.13a, and for paste tailings are shown in Fig 4.13b. Arrows included in the plots show the direction of stress change during undrained shear, whereby a dilative material shifts to the right in response an increase in *p′*, and a contractive material shifts to the left in response to a decrease in *p′*. The composite CSL based on all tailings specimens is shown in Fig. 4.14. The CSL was defined by logarithmic regression of the *e-p′* points at critical state. The CSL for tailings is statistically significant with an R^2 = 0.90 for the regression line.

The two CU triaxial tests conducted at σ'_c = 25 kPa for filtered tailings exhibited a tendency to dilative behavior, whereas the rest of the tests performed at higher σ'_c exhibited a tendency to contract (Fig. 4.12). Although all filtered tailings prepared had different initial *e* and *p′*, the data points exhibit migration towards a single CSL (Fig. 4.14). Tests conducted at σ'_c = 100 kPa and 250 kPa on dense filtered tailings exhibited an increase in *p′* and shift to the right at critical state, whereas the test performed σ'_c = 500 kPa yielded a small decrease in *p′* to shift modestly to the left at critical state. Dense filtered tailings specimens had different initial *e-p′* points, but also moved towards a single CSL (Fig. 4.14). The change from initial to critical state conditions for the paste tailings was similar to dense filtered tailings in that the test conducted at σ'_c = 100 kPa

shifted to the right at critical state and the test performed σ'_c = 250 kPa shifted slightly to the left at critical state (Fig. 4.13b). The critical state conditions of the paste tailings also agree with the aggregate CSL for the tailings (Fig. 4.14). In general, initial conditions of the tailings defined by *e-p'* points below the CSL exhibited a tendency to dilative and increased *p'* at failure, whereas initial conditions defined by *e-p'* points above the CSL exhibited a tendency contract and decreased *p'* at failure.

4.3.2 GeoWaste

The initial conditions and critical state conditions in *e-p'* space for GeoWaste are shown in Fig 4.15. Logarithmic regression of the critical state points yielded a unique CSL that was statistically significant with an R^2 = 0.959. The initial and critical state points in *e-p'* space did not exhibit pronounced change in *p'*. The tests at σ'_c = 50 kPa and σ'_c = 100 kPa exhibited modest contractive tendencies and a slight decrease in *p'* at critical state, whereas, the test at σ'_c = 500 kPa exhibited modest dilative tendencies and a slight increase in *p'* at critical state.

An assessment was conducted between the CSLs for tailings and GeoWaste to determine if the CSL for the tailings can be used to represent critical state conditions in GeoWaste. The composite CSL for tailings is reproduced in Fig. 4.16 along with three potential critical state conditions for GeoWaste based on (i) global void ratio, (ii) tailings fraction void ratio, or (iii) equivalent tailings void ratio. The *p'* at critical state for GeoWaste was the same for the three potential representations of void ratio. The critical state of GeoWaste defined with global void ratio plot considerably below the CSL for tailings, whereas the critical state of GeoWaste defined with the tailings fraction void ratio, plots considerably above the CSL for tailings. These potential representations of critical state conditions for GeoWaste do not coincide with the CSL for tailings.

The e^*_t and *p'* at critical state for GeoWaste are shown in Fig. 4.16 to be in agreement with the CSL for tailings. Equivalent void ratios were computed with Eq. 2.5 such that the *m* parameter was optimized via the Solver function in Excel to minimize the sum of squared residuals

between e^*_t computed based on Eq. 2.5 and e^*_t predicted via the tailings CSL. The optimization procedure yielded m = 0.156 that corresponded to an R^2 = 0.937. The comparison in Fig. 4.16 suggests that the critical state of GeoWaste can be directly related to the critical state of the tailings fraction alone via an equivalent void ratio. However, computing e^*_t for any potential mine waste rock and tailings mixture requires that m is known. The assessment conducted herein provides a methodology for determining m for a given mixture. Additional evaluations are required to demonstrate that the CSL for GeoWaste defined with e^*_t can be used as a predictive tool for GeoWaste specimens prepared with the same mixture ratio, but to different initial densities.

4.4 Practical Implications

This study was performed to evaluate the influence waste rock inclusions in GeoWaste have on undrained shear behavior and critical state of filtered tailings. In general, the evaluation suggests improved shear resistance of GeoWaste when compared to filtered tailings due to the addition of waste rock.

The main practical implications of this study are (i) definition of undrained shear behavior and shear strength of GeoWaste, and (ii) prediction of the CSL of GeoWaste from the critical state of the tailings fraction alone via an equivalent void ratio. The target applications for GeoWaste are placement in piles for mine waste disposal and long-term management, and use in a final cover for the closure of mine waste facilities. The shear strength behavior and relevant parameters need to be defined for stability analyses. The results on GeoWaste obtained from this study can be used for slope stability analyses and as a preliminary evaluation for liquefaction potential. Contractive behavior is an indicator for liquefaction potential; however, more sophisticated laboratory experiments, such as cyclic triaxial, are required for a formal evaluation of liquefaction potential.

The other practical implication is that the CSL for GeoWaste can be related to the CSL of tailings alone via a tailings equivalent void ratio of GeoWaste. This relationship suggests that

knowing the CSL of tailings, which is easier to obtain via laboratory testing, the CSL of GeoWaste can be obtained. However, additional testing is required to (i) evaluate how the CSL of GeoWaste varies as a function of mixture ratio and (ii) determine how to obtain estimates of the equivalent void ratio a priori. The latter is particularly important for relating the CSL of tailings alone to predict potential shear behavior of GeoWaste via the equivalent tailings void ratio in field applications without conducting individual shear experiments on GeoWaste.

Table 4.1. Summary of tests, parameters, and results for tailings. Failure criterion of reaching K_f line was used to determine the effective friction angle and test parameters at failure.

Material	Target σ'_c [a]	σ'_c (kPa)	$\varepsilon_{a,f}$ (%)	$\Delta\sigma_f$ (kPa)	σ'_{3f} (kPa)	σ'_{1f} (kPa)	p' (kPa)	q (kPa)	A_f	$u_{e,f}$ (kPa)	Φ'_{sc} (º)	B	e	φ'_t (º)
Filtered Tailings (Field condition)	20 kPa (T1)	15.89	12	30.6	8.2	38.8	23.5	15.3	0.3	252.7	40.7	0.97	0.64	33
	20 kPa (T2)	14.27	13	37.9	7.3	45.1	26.2	18.9	0.2	222.0	46.2	0.99	0.65	
	50 kPa	46.53	6	39.2	7.9	47.1	27.5	19.6	1.0	282.1	45.4	1.00	0.62	
	100 kPa (T1)	95.03	16	57.6	20.9	78.5	49.7	28.8	1.3	434.7	35.5	0.97	0.60	
	100 kPa (T2)	96.08	9	71.0	21.9	92.9	57.4	35.5	1.0	433.6	38.2	0.97	0.59	
	100 kPa (T3)	97.57	9	79.8	24.7	104.5	64.6	39.9	0.9	457.3	38.1	1.00	0.58	
	250 kPa (T1)	249.60	9	191.0	77.9	268.9	173.4	95.5	0.9	420.6	33.4	1.00	0.55	
	250 kPa (T2)	251.94	14	159.1	78.1	237.2	157.7	79.5	1.1	389.0	30.3	0.98	0.54	
	500 kPa	490.65	8	393.2	168.7	561.8	365.2	196.6	0.8	432.4	32.6	1.00	0.47	
Dense Filtered Tailings	100 kPa	96.71	3	161.5	58.2	219.6	138.9	80.7	0.2	293.9	35.5	1.00	0.58	33
	250 kPa	248.23	5	266.6	95.2	361.8	228.5	133.3	0.6	375.2	35.7	1.00	0.54	
	500 kPa	506.00	4	403.7	178.9	582.5	380.7	201.8	0.8	440.7	32.0	0.97	0.50	
Paste Tailings	100 kPa	97.18	9	122.1	52.3	174.4	113.3	61.1	0.4	58.2	32.6	0.98	0.56	32
	250 kPa	248.88	4	207.5	92.9	300.5	196.7	103.8	0.8	442.1	31.8	1.00	0.54	

Notes: σ_c' = effective confining stress; $\varepsilon_{a,f}$ = axial strain at failure; $\Delta\sigma_f$ = deviator stress at failure; σ'_{3f} = minor effective principle stress at failure; σ'_{1f} = major effective principle stress at failure; p' = mean effective stress at failure; q = mean shear stress at failure; A_f = Skempton's pore pressure parameter; $u_{e,f}$ = excess pore pressure at failure; ϕ'_{sc} = secant friction angle; B = B-check for saturation; e = void ratio before shear; φ'_t = tangent friction angle.

[a] T1 = Test 1, T2 = Test 2, and T3 = Test 3 for repeated tests (if applicable)

Table 4.2. Summary of tests, parameters, and results for GeoWaste. Failure criterion of reaching K_f line was used to determine the effective friction angle and test parameters at failure.

Material	Target σ'_c	σ'_c (kPa)	$\varepsilon_{a,f}$ (%)	$\Delta\sigma_f$ (kPa)	σ'_{3f} (kPa)	σ'_{1f} (kPa)	p' (kPa)	q (kPa)	A_f	$u_{e,f}$ (kPa)	Φ_{sc}' (º)	B	e_g	φ'_t (º)
GeoWaste	50 kPa	49.68	12	42.4	21.5	63.9	42.7	21.2	0.8	298.3	29.8	0.95	0.39	40
	100 kPa	96.72	9	75.6	29.7	105.3	67.5	37.8	1.0	429.6	34.0	0.97	0.39	
	500 kPa	476.15	9	655.3	188.0	843.3	515.7	327.7	0.4	469.3	39.5	0.96	0.34	

Note: σ_c' = effective confining stress; $\varepsilon_{a,f}$ = axial strain at failure; $\Delta\sigma_f$ = deviator stress at failure; σ'_{3f} = minor effective principle stress at failure; σ'_{1f} = major effective principle stress at failure; p' = mean effective stress at failure; q = mean shear stress at failure; A_f = Skempton's pore pressure parameter; $u_{e,f}$ = excess pore pressure at failure; ϕ'_{sc} = secant friction angle; B = B-check for saturation; e_g = global void ratio before shear; φ'_t = tangent friction angle.

Table 4.3. Void ratio at initial conditions and steady-state with equivalent void ratios and parameters used in calculation

Material	m	R_d	d_R	Target σ'_c	p'_i (kPa)	p'_{cs} (kPa)	e_g	e_t	e^*_t
Filtered Tailings (Field conditions)	-	-	-	20 kPa (T1)	15.89	24.8	-	0.64	-
				20 kPa (T2)	14.27	32.6	-	0.65	-
				50 kPa	46.53	35.0	-	0.62	-
				100 kPa (T1)	95.03	53.3	-	0.60	-
				100 kPa (T2)	96.08	68.6	-	0.59	-
				100 kPa (T3)	97.57	73.4	-	0.58	-
				250 kPa (T1)	249.60	189.8	-	0.55	-
				250 kPa (T2)	251.94	165.5	-	0.54	-
				500 kPa	490.65	429.5	-	0.47	-
Dense Filtered Tailings	-	-	-	100 kPa	96.71	199.1	0.58	0.64	-
				250 kPa	248.23	350.2	0.54	0.65	-
				500 kPa	506.00	499.1	0.50	0.62	-
Paste Tailings	-	-	-	100 kPa	97.18	129.4	0.56	0.60	-
				250 kPa	248.88	244.2	0.54	0.59	-
GeoWaste	0.16	1.2	391	50 kPa	49.68	48.7	0.39	0.87	0.59
				100 kPa	96.72	78.0	0.39	0.86	0.58
				500 kPa	476.15	538.8	0.34	0.74	0.50

Note: m = calculation parameter for tailings equivalent void ratio; p'_i = initial mean effective stress; p'_{cs} = critical state mean effective stress; e_g = global void ratio; e_t = tailings void ratio; e_t^* = tailings equivalent void ratio.

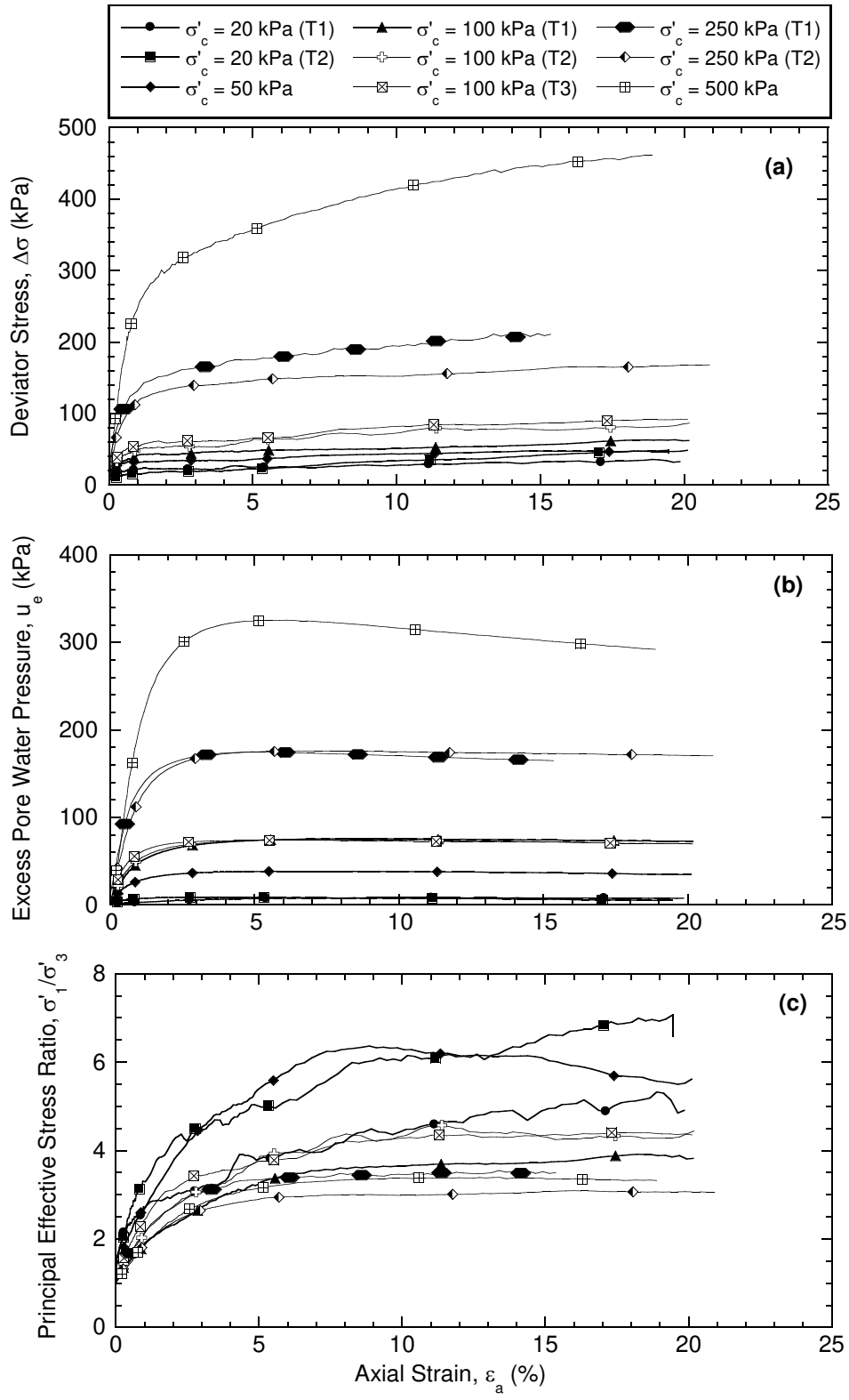

Fig. 4.1. Deviator stress (a), excess pore water pressure (b), and principal effective stress ratio (c) versus axial strain for consolidated undrained triaxial compression tests on filtered tailings prepared to represent field conditions.

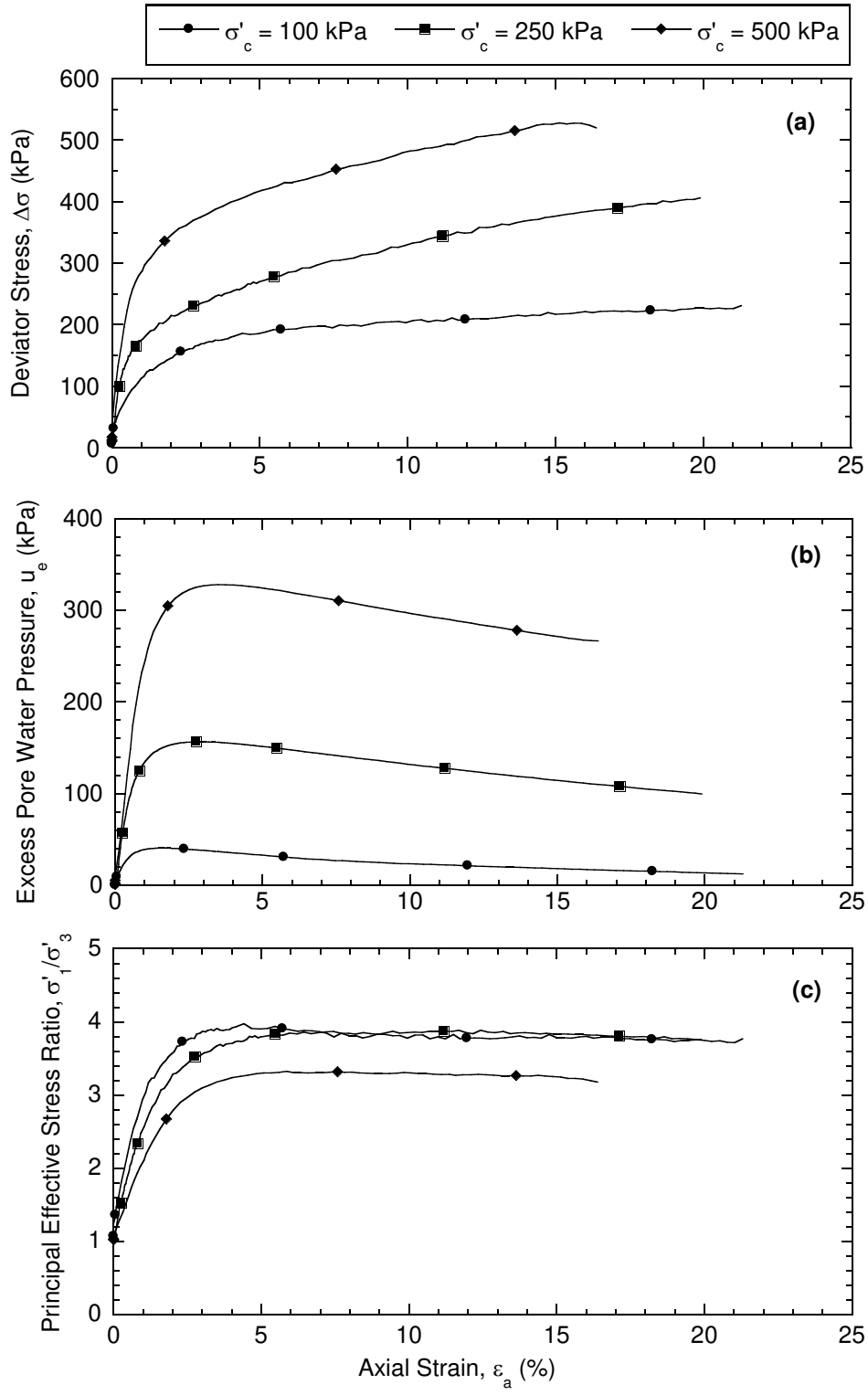

Fig. 4.2. Deviator stress (a), excess pore water pressure (b), and principal effective stress ratio (c) versus axial strain for consolidated undrained triaxial compression tests on dense filtered tailings.

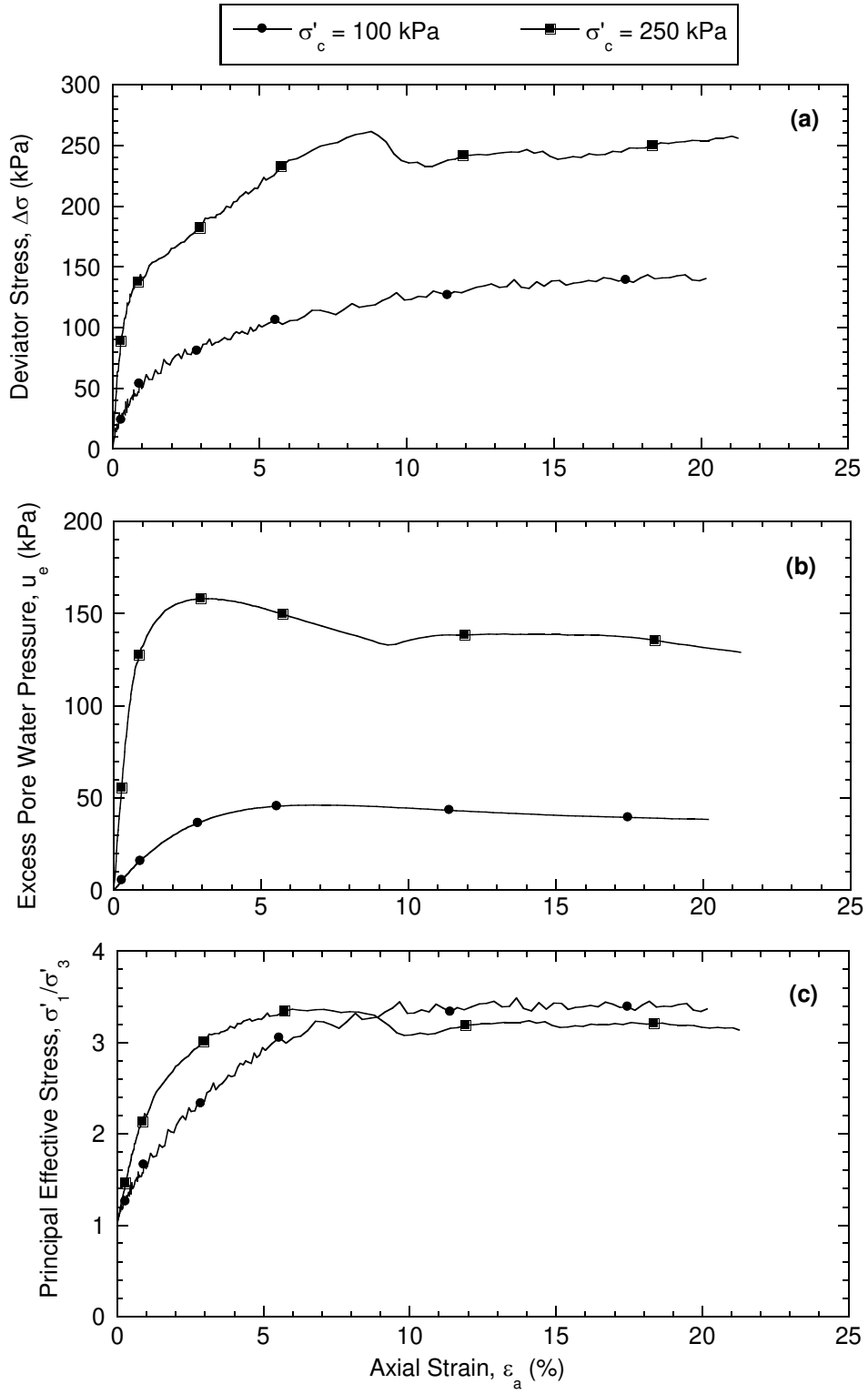

Fig. 4.3. Deviator stress (a), excess pore water pressure (b), and principal effective stress ratio (c) versus axial strain for consolidated undrained triaxial compression tests on paste tailings.

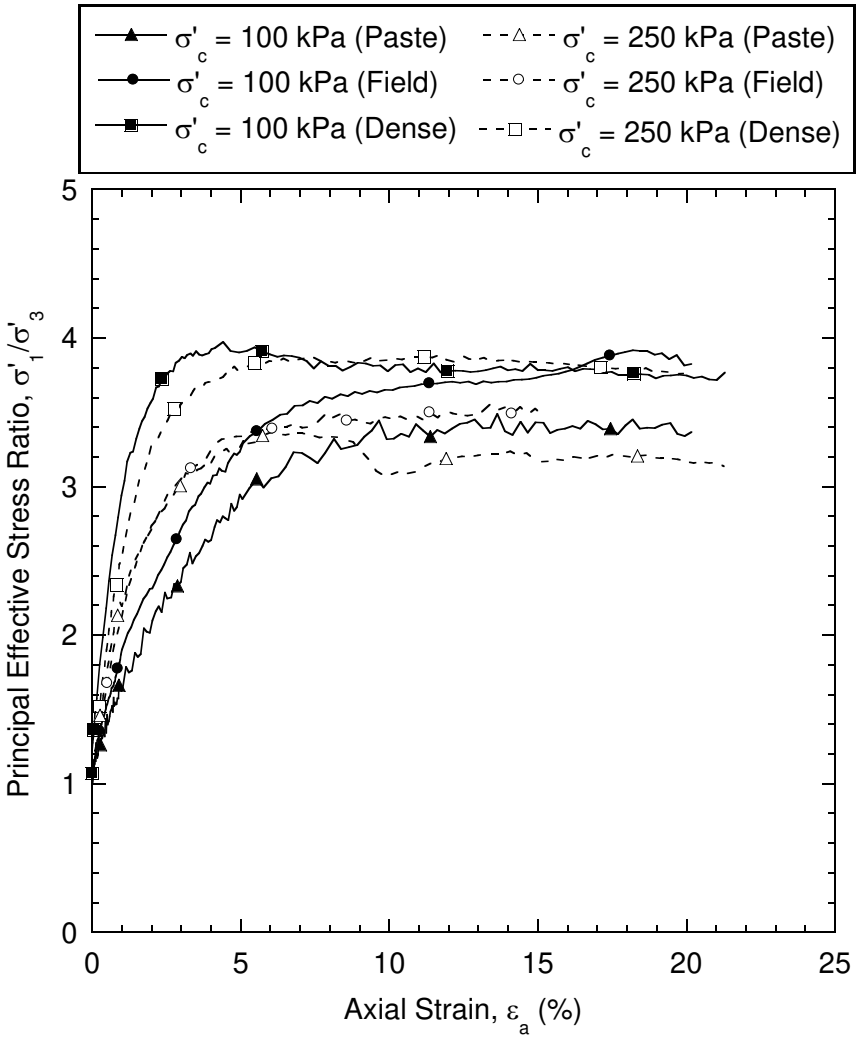

Fig. 4.4. Comparison of the principal effective stress ratio versus axial strain for consolidated undrained triaxial compression tests conducted at target effective confining stress (σ'_c) or 100 kPa and 250 kPa on filtered tailings prepared to represent field conditions (Field), dense filtered tailings (Dense), and paste tailings (Paste).

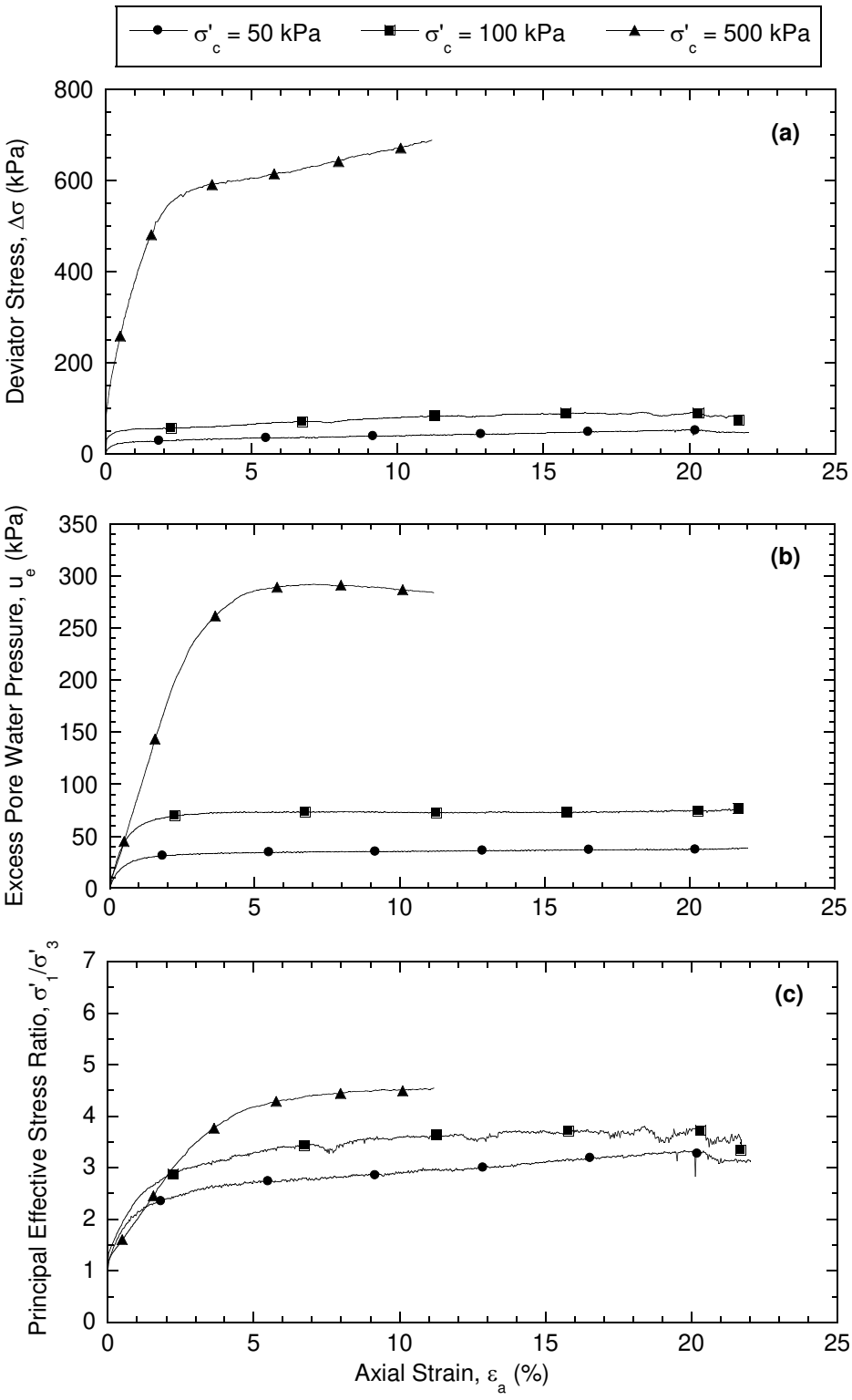

Fig. 4.5. Deviator stress (a), excess pore water pressure (b), and principal effective stress ratio (c) versus axial strain for consolidated undrained triaxial compression tests on GeoWaste.

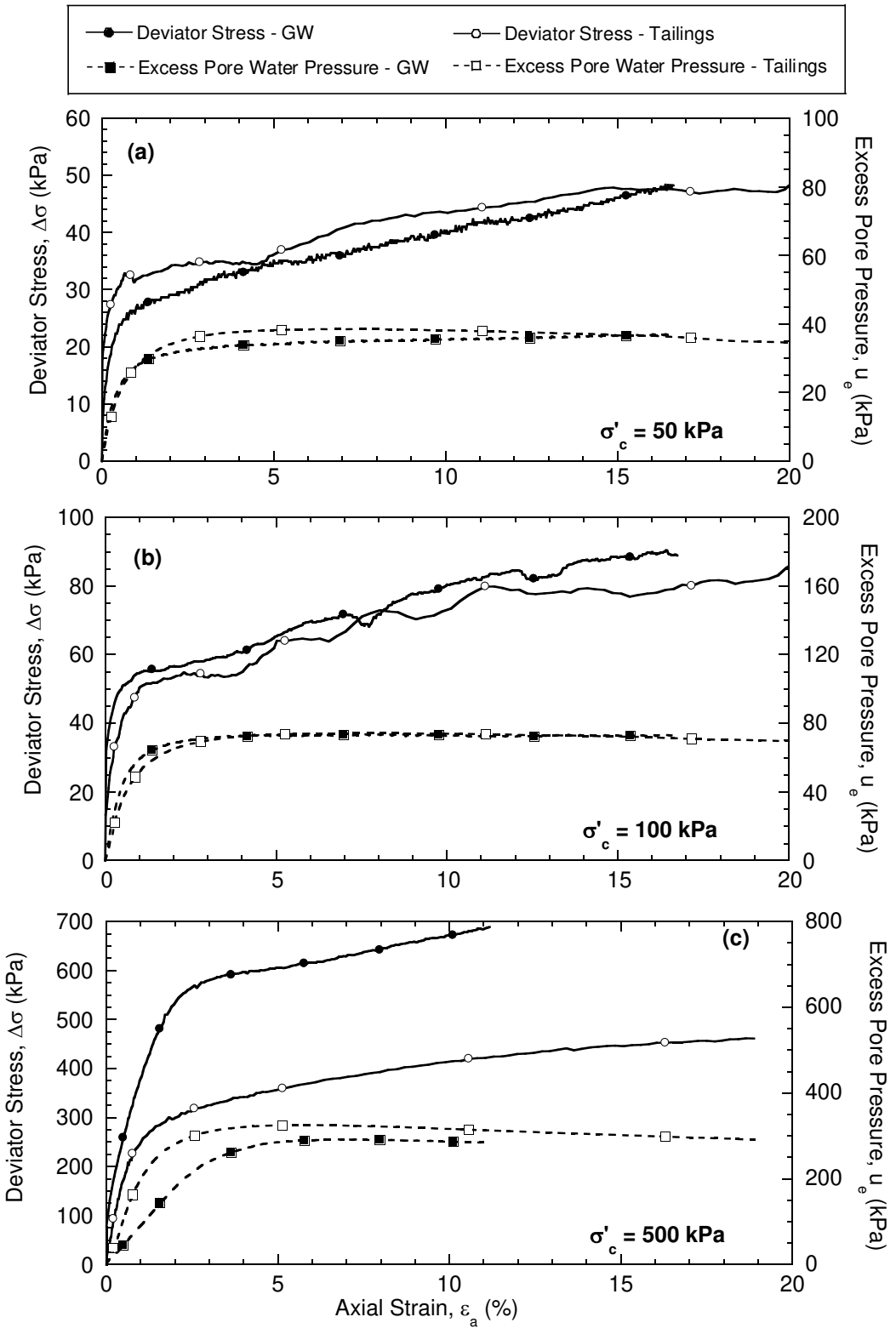

Fig. 4.6. Deviator stress and excess pore pressure versus axial strain for consolidated undrained triaxial compression tests on filtered tailings and GeoWaste at effective confining stresses (σ'_c) of 50 kPa (a), 100kPa (b), and 500 kPa (c).

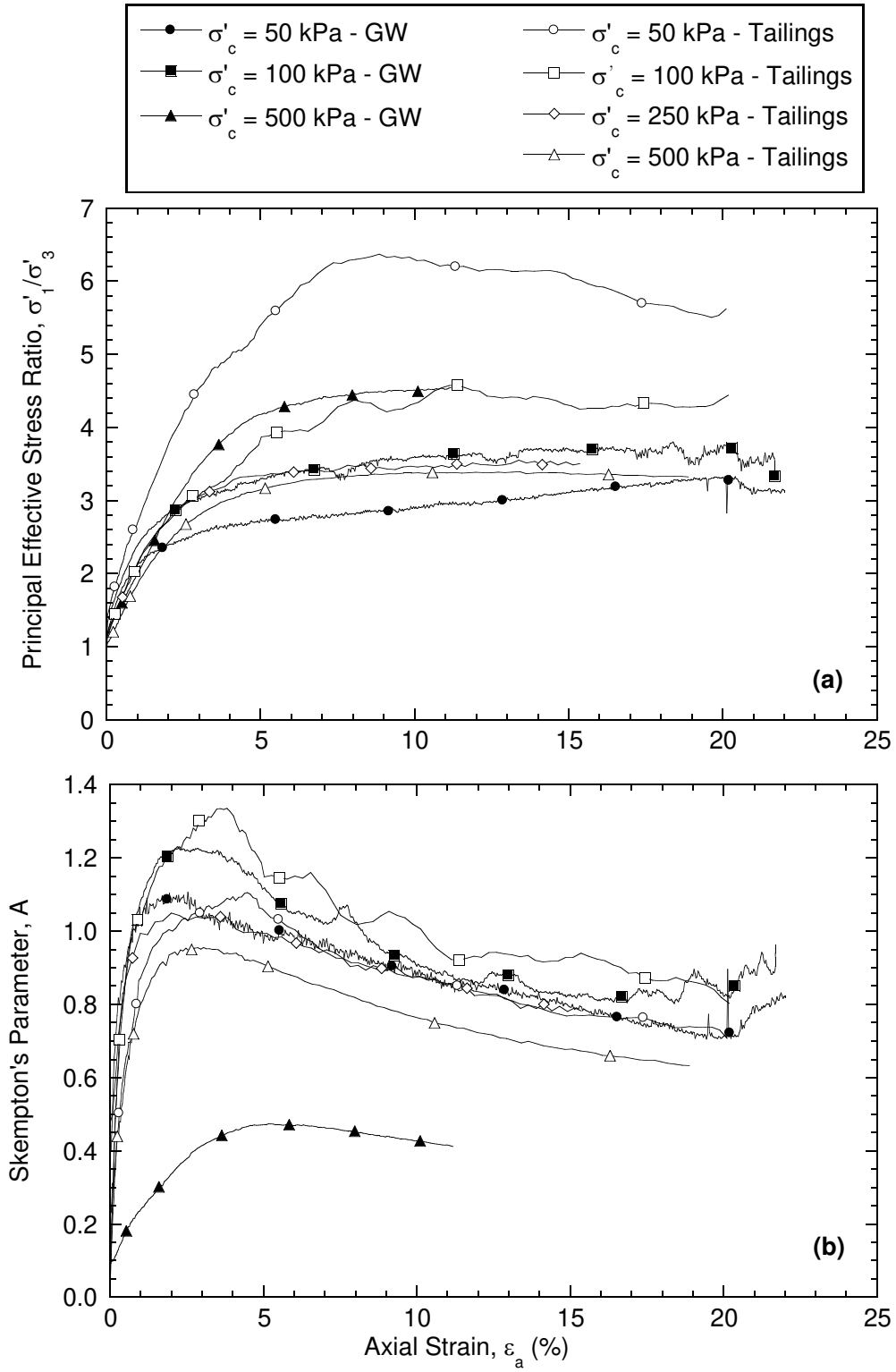

Fig. 4.7. Effective principal effective stress ratio (a) and Skempton's *A* pore pressure parameter (b) versus axial strain for consolidated undrained triaxial compression tests on filtered tailings and GeoWaste.

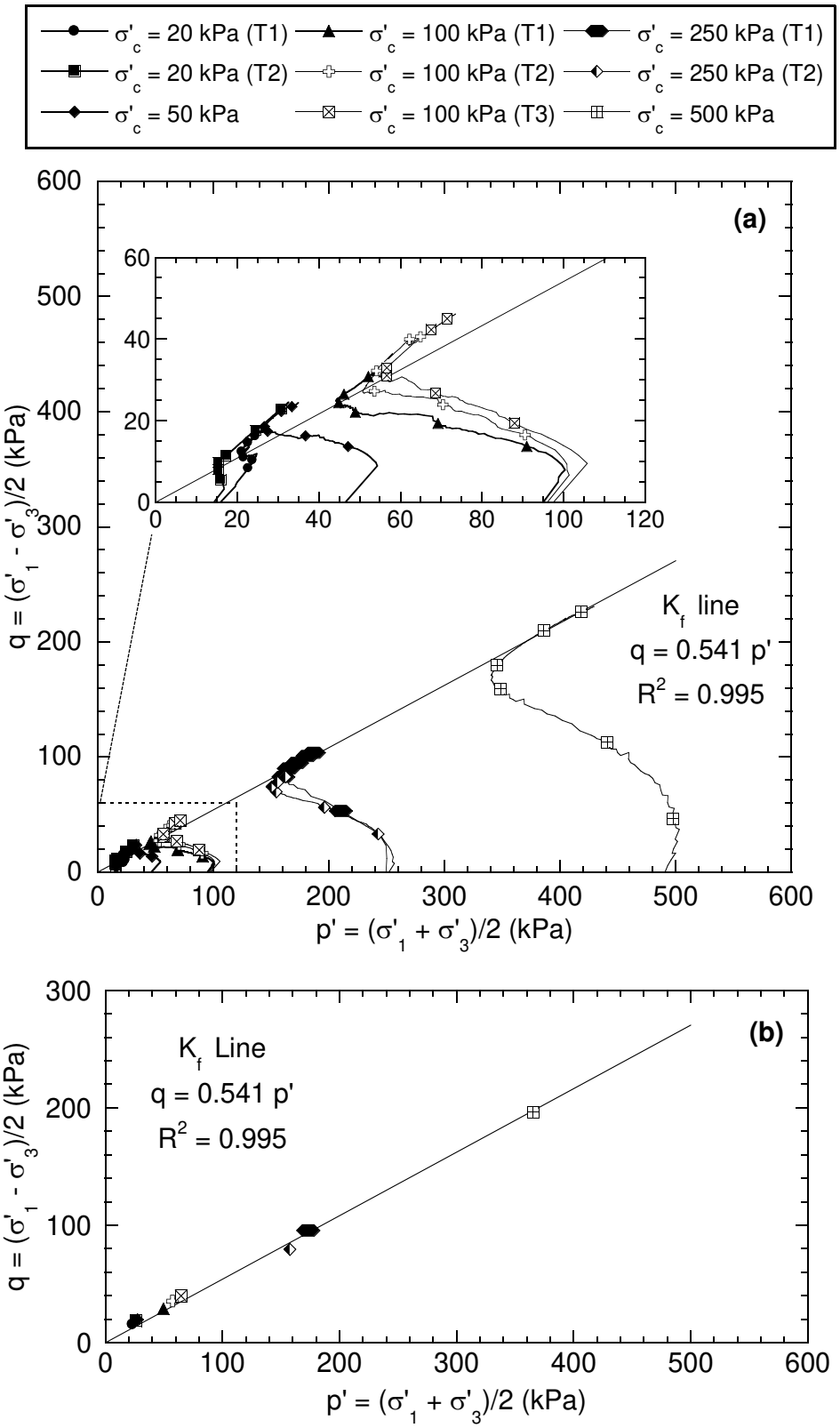

Fig. 4.8. Effective stress paths (a) and *p'-q* stress states at failure (b) for consolidated undrained triaxial compression tests conducted on filtered tailings prepared to represent field conditions. The K_f Line was regressed through all failure points and the origin.

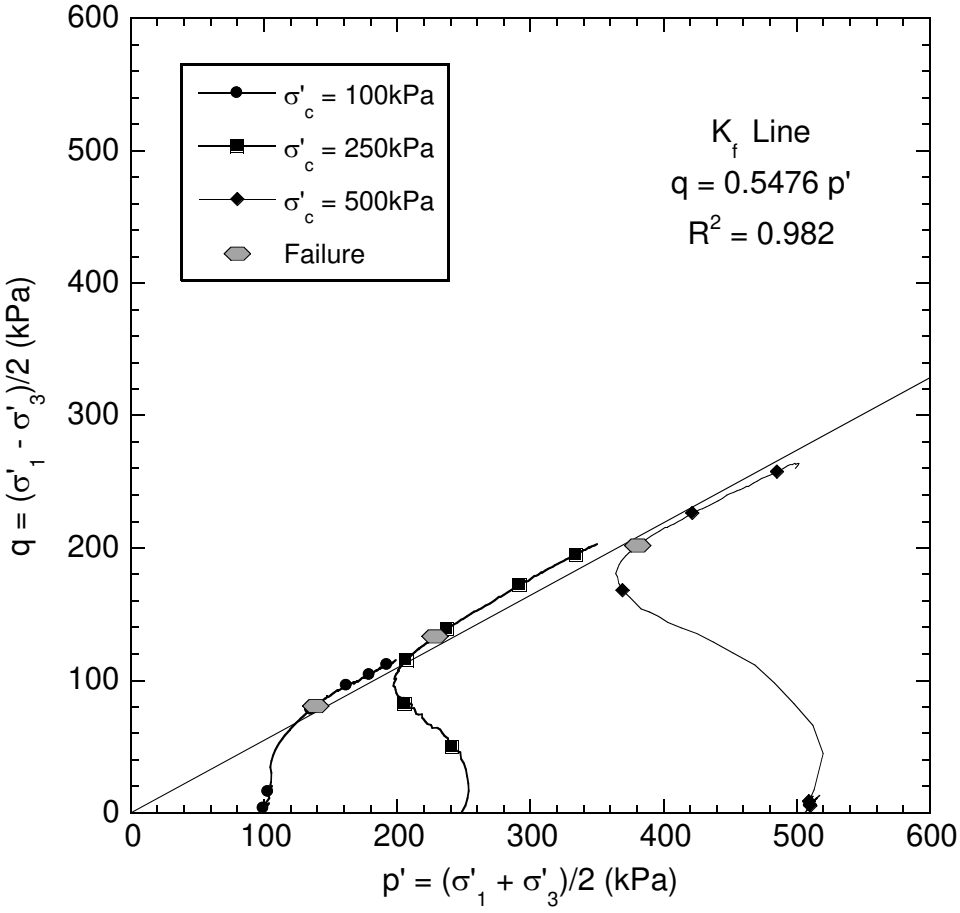

Fig. 4.9. Effective stress paths (a) and *p'-q* stress states at failure (b) for consolidated undrained triaxial compression tests conducted on dense filtered tailings. The K_f Line was regressed through all failure points and the origin.

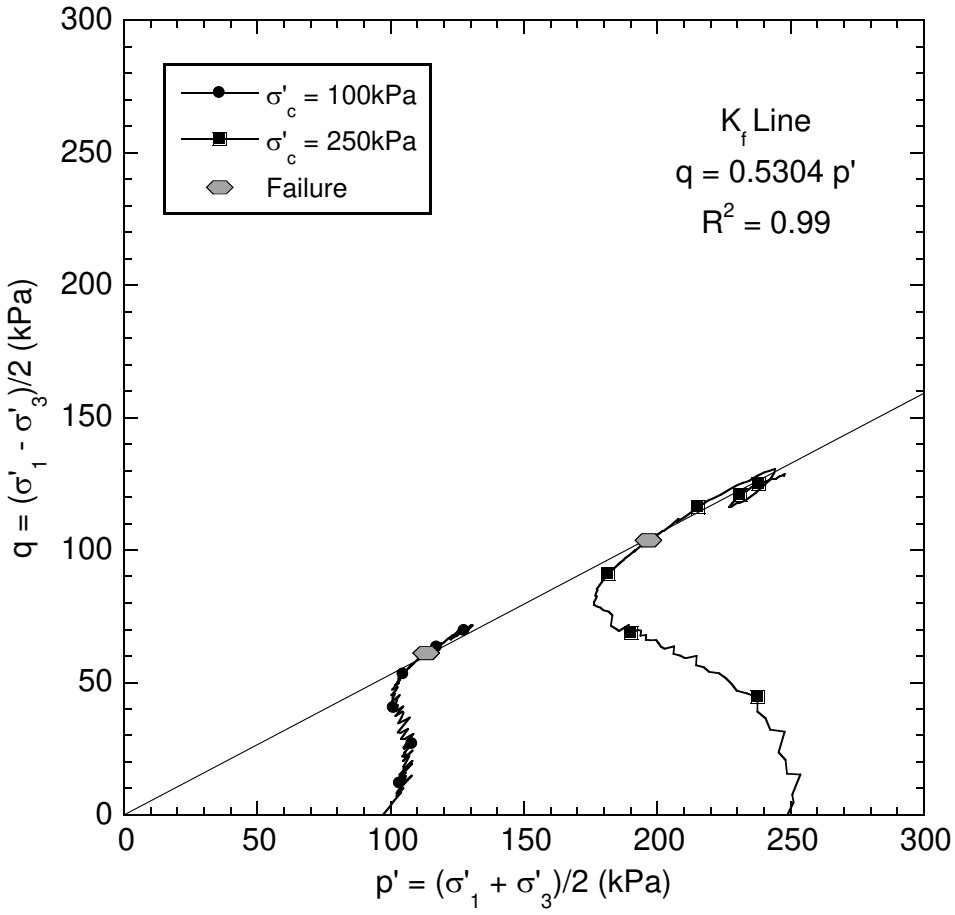

Fig. 4.10. Effective stress paths (a) and *p'-q* stress states at failure (b) for consolidated undrained triaxial compression tests conducted on paste tailings. The K_f Line was regressed through all failure points and the origin.

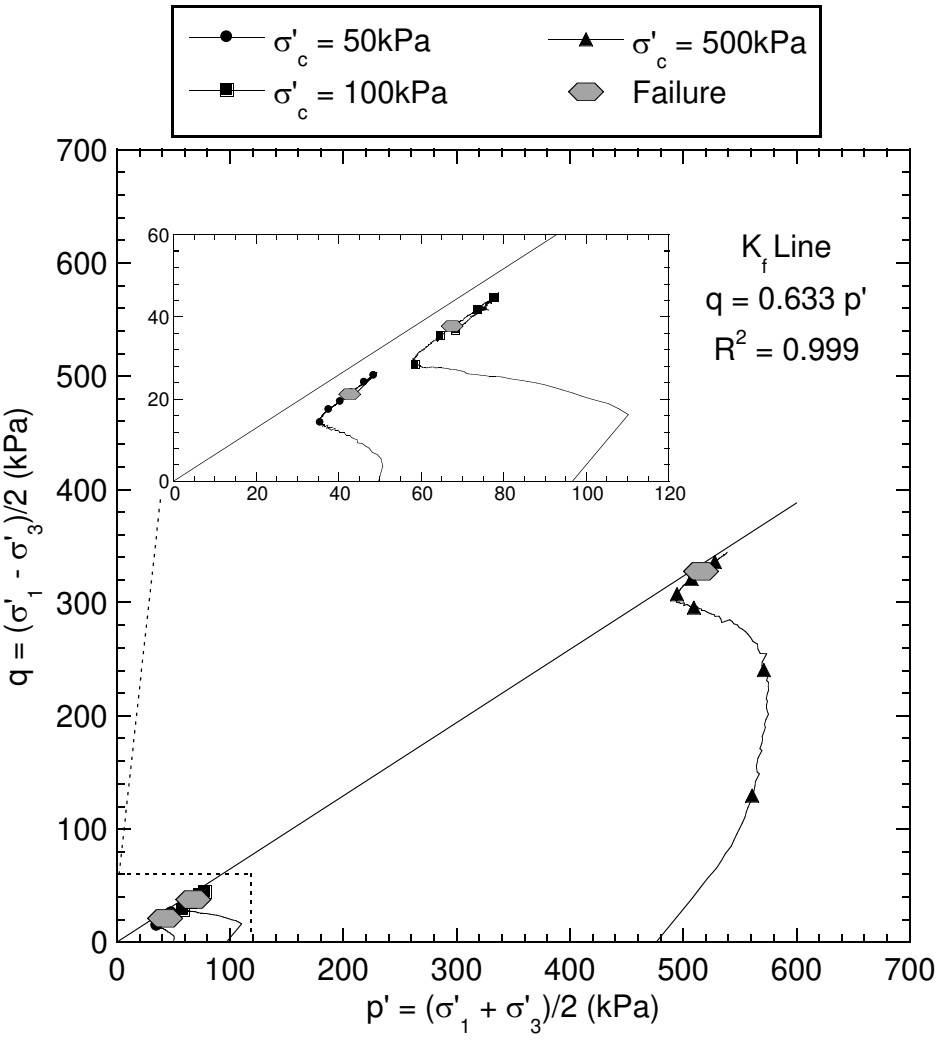

Fig. 4.11. Effective stress paths (a) and *p'-q* stress states at failure (b) for consolidated undrained triaxial compression tests conducted on GeoWaste. The K_f Line was regressed through all failure points and the origin.

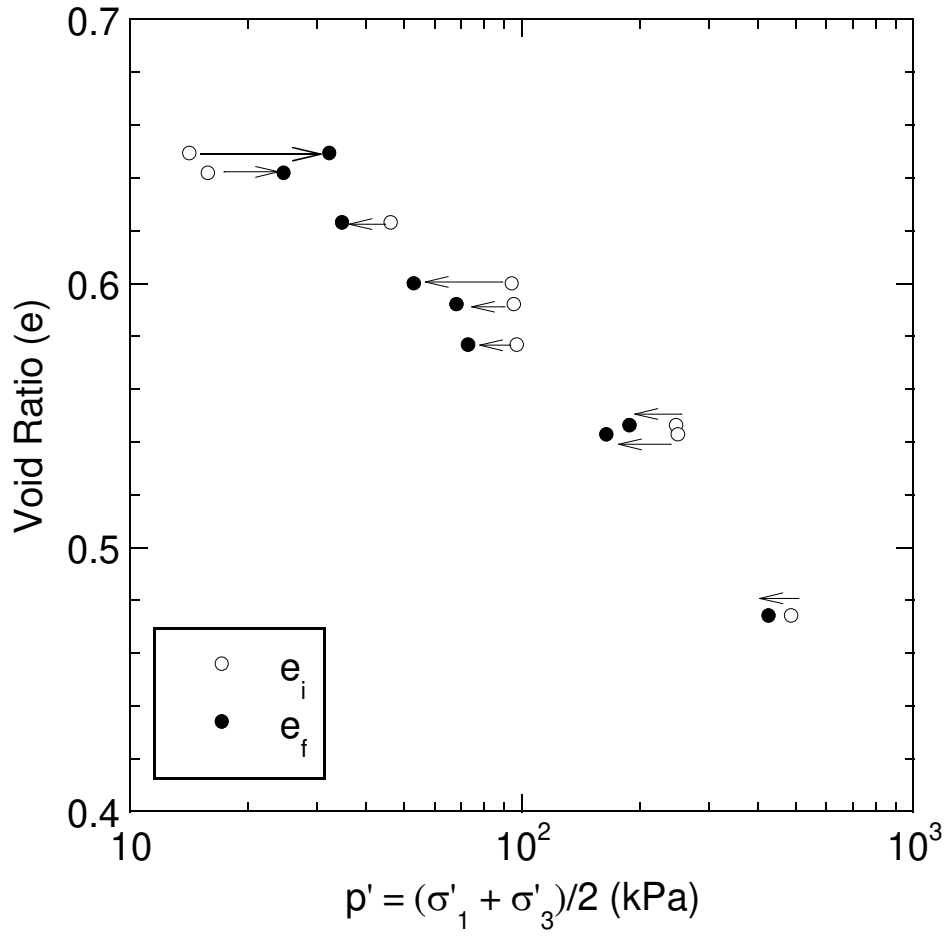

Fig. 4.12. Relationships of void ratio with mean effective stress for consolidated undrained triaxial compression tests on pure filtered tailings at field conditions.

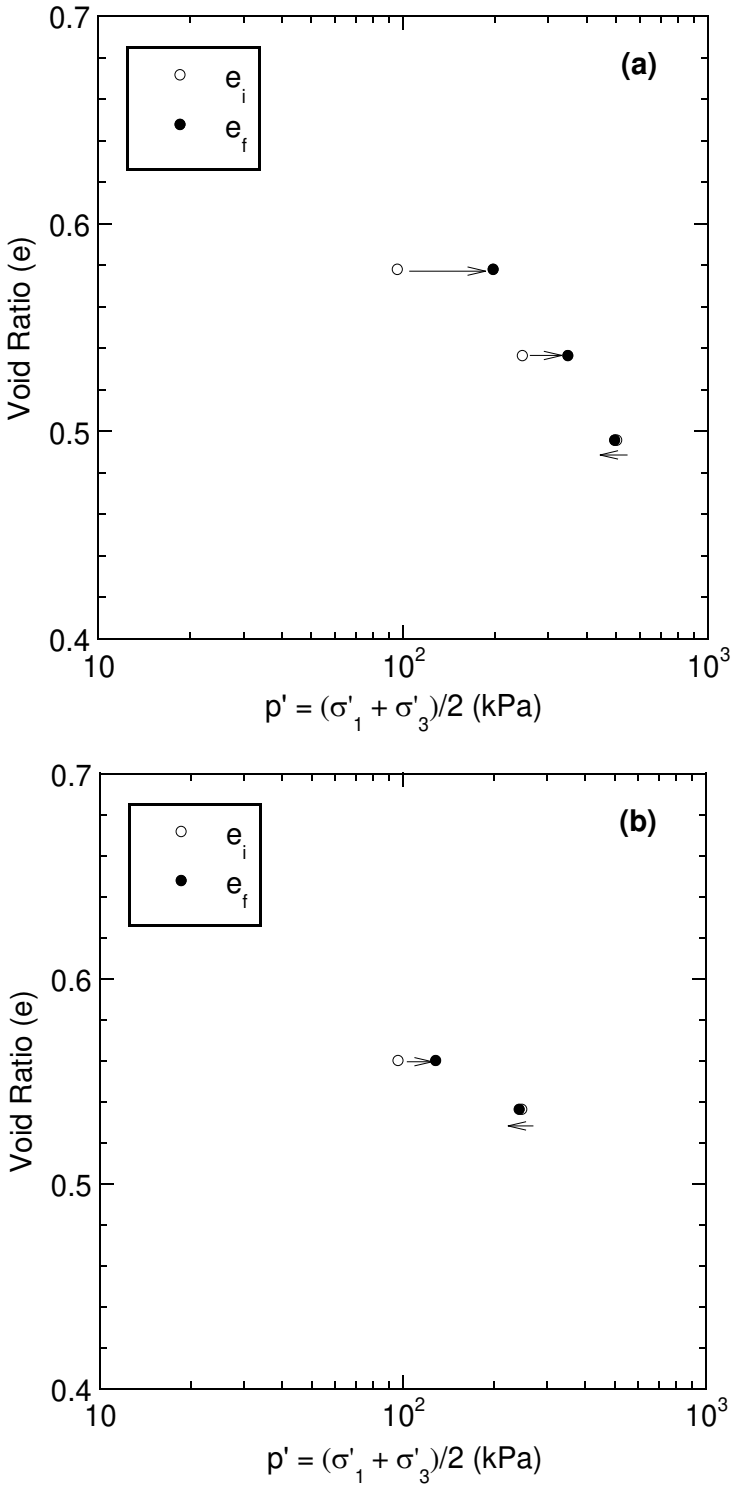

Fig. 4.13. Relationships of void ratio with mean effective stress for consolidated undrained triaxial compression tests on pure dense filtered tailings (a) and paste tailings (b).

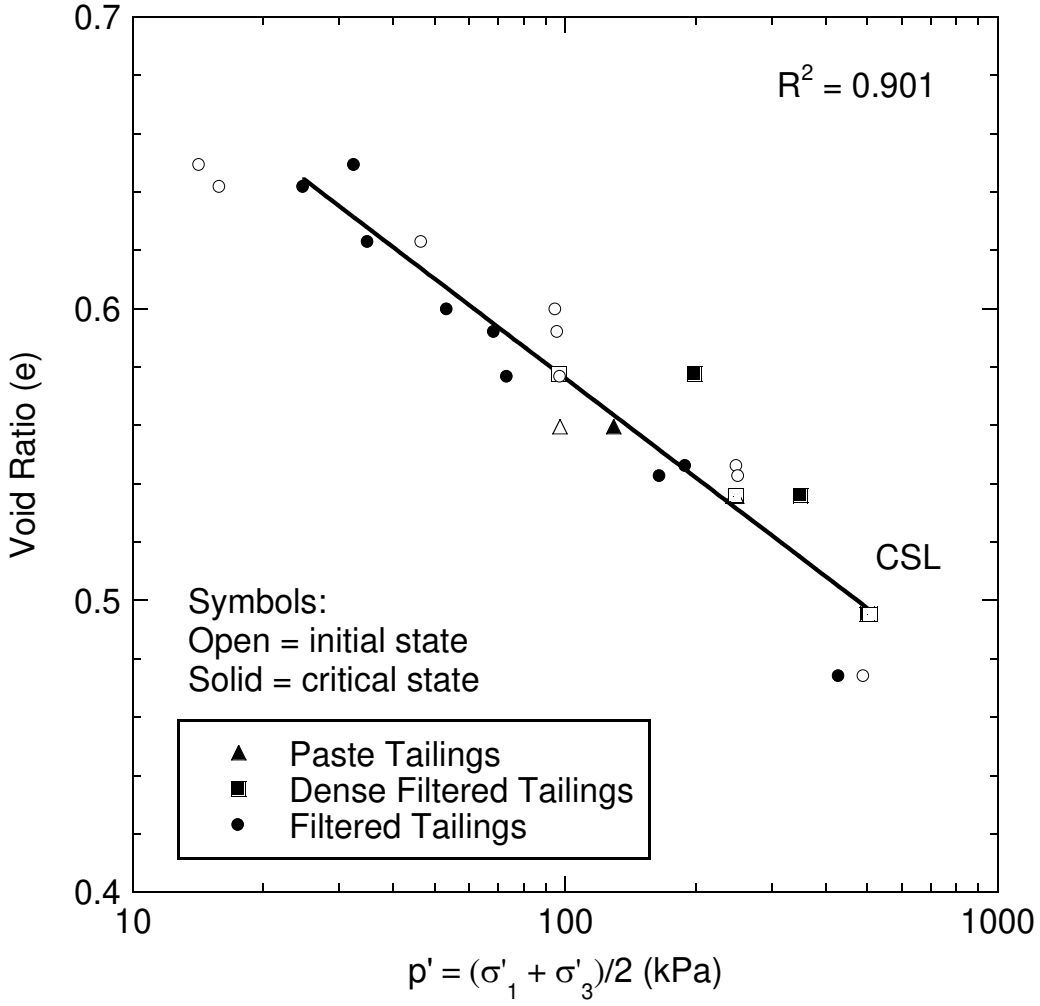

Fig. 4.14. Relationships of global void ratio with mean effective stress for consolidated undrained triaxial compression tests on all pure tailings. Critical state line (CSL) is shown as a logarithmic regression line.

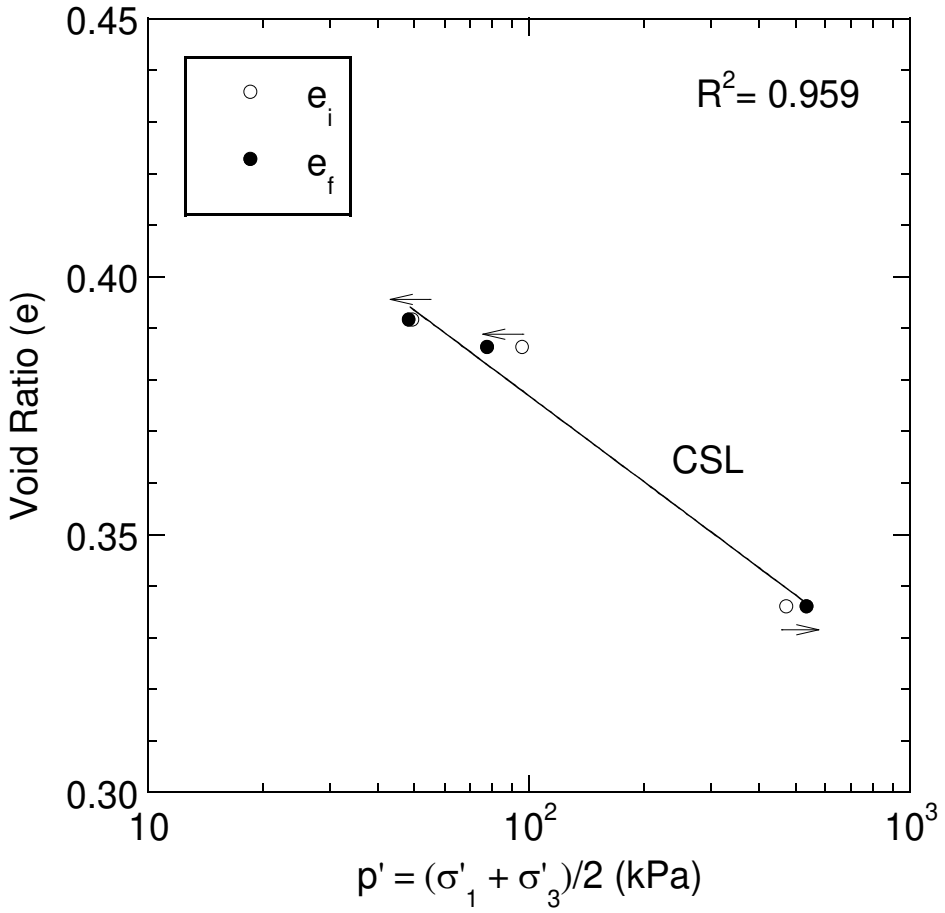

Fig. 4.15. Relationships of global void ratio with mean effective stress for consolidated undrained compression triaxial tests on GeoWaste.

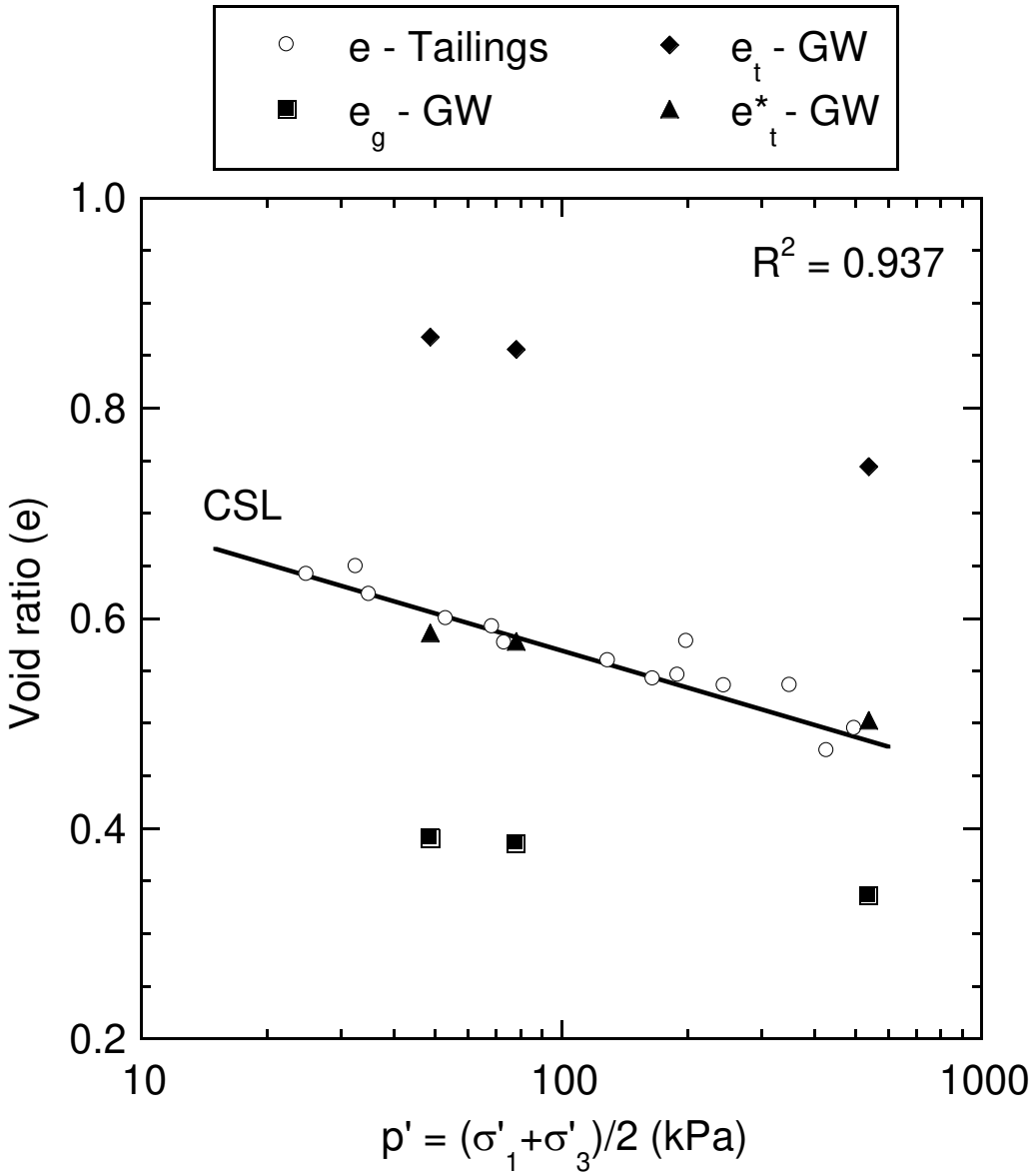

Fig. 4.16. Relationships of tailings void ratio (e), global void ratio of GeoWaste (e_g), tailings fraction void ratio in GeoWaste (e_t), and tailings equivalent void ratio in GeoWaste (e^*_t) versus effective stress for consolidated undrained triaxial compression tests.

CHAPTER 5: SUMMARY, CONCLUSIONS, AND FUTURE WORK

5.1 Summary and Conclusions

The effect of waste rock inclusions in a tailings-dominated mixture created via mixing filtered tailings with waste rock (i.e., GeoWaste) was evaluated. Consolidated undrained (CU) triaxial compression tests were performed on filtered tailings prepared to represent field conditions, dense filtered tailings, paste tailings, and GeoWaste. The undrained shear behavior and critical state of tailings were evaluated to establish a baseline for comparison with GeoWaste. The following conclusions were drawn from this study.

- Filtered tailings prepared to represent field conditions yielded contractive and strain-hardening behavior with a tangent friction angle (φ'_t) = 33º. The filtered tailings specimen tested at an effective confining stress (σ'_c) = 500 kPa exhibited a transition from contractive to dilative response during undrained shear.
- Dense filtered tailings exhibited strain-hardening behavior, net positive pore pressure, transition from contractive to dilative behavior, and φ'_t = 33º. Undrained shear behavior of the paste tailings exhibited modest strain-hardening behavior and φ'_t = 32º. The overall similarity of the undrained shear behavior and shear strength between paste tailings and dense filtered tailings was attributed to similar void ratios achieved at the end of consolidation under a given σ'_c.
- The dense filtered tailings exhibited the stiffest response to shearing and yielded the largest effective principal stress ratio (σ'_1/σ'_3). In contrast, paste and filtered tailings exhibited a less stiff response to shearing, and the lowest σ'_1/σ'_3 was measured for paste tailings. This stiffer response and larger σ'_1/σ'_3 of the dense filtered tailings were attributed to the resultant tailings fabric of the denser prepared specimens.

- GeoWaste exhibited strain-hardening, contractive behavior with $\varphi'_t = 32º$. The GeoWaste specimen tested at σ'_c = 500 kPa exhibited a transition from contractive to dilative response during undrained shear.
- GeoWaste and tailings prepared to represent field conditions exhibited similar undrained shear behavior at σ'_c = 50 and 100 kPa. However, at σ'_c = 500 kPa, the σ'_1/σ'_3 for GeoWaste increased relative to filtered tailings, which indicated that GeoWaste developed increased shear resistance. This behavior was attributed to enhanced interference between waste rock particles during shear and a denser tailings matrix of the GeoWaste at σ'_c = 500 kPa.
- The compilation of CU triaxial compression tests on tailings produced a single critical state line (CSL), which was unique and independent of initial void ratio, water content, or specimen preparation method. In general, initial tailings conditions of effective stress and void ratio of tailings that plotted above the CSL exhibited a tendency to contract (i.e., generate positive excess pore pressure) during undrained shear.
- The CSL for GeoWaste defined with global void ratio plotted below the CSL for tailings, and direct calculation of the tailings fraction void ratio, assuming all void volume in GeoWaste resided within the tailings fraction, yielded void ratios that plotted above the CSL for tailings. An equivalent tailings void ratio in GeoWaste (e^*_t) was computed via optimization to yield a GeoWaste CSL based on e^*_t that aligned with the tailings CSL. Thus, the CSL for tailings and GeoWaste can be related to one another via computing e^*_t of the GeoWaste.

5.2 Future Work

This study was conducted to evaluate the undrained shear behavior and critical state of pure tailings and GeoWaste. Additional research is needed to evaluate the effects of waste rock

inclusions in GeoWaste at higher σ'_c to further assess the potential increase in shear resistance of GeoWaste as σ'_c increases. Further testing and data compilation also are needed for GeoWaste prepared to different mixture ratios and prepared with different mine waste rock and tailings. These experimental efforts would aid in comparing critical state lines between the tailings and GeoWaste, and most importantly, aid in establishing empirical methods to determine the equivalent tailings void ratio in GeoWaste.

REFERENCES

Albright, W.H., Benson, C.H., Waugh, W.J. (2010). *Water Balance Covers for Waste Containment, Principles and Practice. ASCE*. Reston, VA.

Alarcon, A., Leonards, G., Chameau, J.L. (1988). Undrained monotonic and cyclic strength of sands. *Journal of Geotechnical Engineering*, 114(10), 1089–1109.

Anderson, C.D., Eldridge, T.L. (2011). Critical state liquefaction assessment of an upstream constructed tailings sand dam. *Tailings and Mine Waste Conference*, 101-112.

Azam, S., and Li, Q. (2010). Tailings dam failures: a review of the last one hundred years. *Geotechnical News*, 28(4), 50-54.

ASTM D422-63e2 (2007). *Standard Test Method for Particle-Size Analysis of Soils* (Withdrawn 2016), ASTM International, West Conshohocken, PA.

ASTM ASTM D698-12e2 (2012). *Standard Test Methods for Laboratory Compaction Characteristics of Soil Using Standard Effort (12 400 ft-lbf/ft3 (600 kN-m/m3))*, ASTM International, West Conshohocken, PA.

ASTM D2487-17 (2017). *Standard Practice for Classification of Soils for Engineering Purposes*, (Unified Soil Classification System), ASTM International, West Conshohocken, PA.

ASTM D4767-11 (2011). *Standard Test Method for Consolidated Undrained Triaxial Compression Test for Cohesive Soils*, ASTM International, West Conshohocken, PA.

ASTM D854-14 (2014). *Standard Test Methods for Specific Gravity of Soil Solids by Water Pycnometer*, ASTM International, West Conshohocken, PA.

ASTM D4318-17e1 (2017). *Standard Test Methods for Liquid Limit, Plastic Limit, and Plasticity Index of Soils*, ASTM International, West Conshohocken, PA.

Aubertin, M., Bussière, B., Chapuis, R. P. (1996). Hydraulic conductivity of homogenized tailings from hard rock mines, *Canadian Geotechnical Journal*, 33(3), 470-482.

Azam, S., Li, Q. (2010). Tailings dam failures: a review of the last one hundred years. *Geotechnical News*, 28(4), 50-54.

Bareither, C.A., Scalia, J., Gorakhki, M.H., Borja, R., Kent, T. (2017). Evaluation of Hydraulic Conductivity and Moisture Retention Characteristics of GeoWaste. *Department of Civil and Environmental Engineering, Colorado State University*.

Bareither, C.A., Gorakhki, M.H., Scalia, J., Jacobs, M. (2018). Compression Behavior of Filtered Tailings and Waste Rock Mixtures: GeoWaste. *Tailings and Mine Waste Conference*.

Bedin, J., Schnaid, F. (2012). Gold tailings liquefaction under critical state soil mechanics. *Geotechnique*, 263-267.

Been, K., Jefferies, M.G. (1985). A state parameter for sands, *Géotechnique*, 35(2), 99-112.

Been, K., Jefferies, M.G., Hachey, J. (1991). The critical state of sands. *Geotechnique* 41(3), 365-381.

Benson, C. H., Bareither, C. A. (2012). Designing water balance covers for sustainable waste containment: Transitioning state of the art to state of the practice. *GeoCongress 2012: State of the Art and Practice in Geotechnical Engineering, GSP 226,* K. Rollins and D. Zekkos, eds., ASCE, Reston, VA, 1–33

Blight, G. (2010). *Geotechnical Engineering for Mine Waste Storage Facilities*, CRC Press, Taylor & Francis Group, London, UK.

Bobei, D.C., Lo, S.R., Wanatowski, D., Gnanendran, C.T., Rahman, M.M. (2009). Modified state parameter for characterizing static liquefaction of sand with fines. *Canadian Geotechnical Journal*, 46(3), 281-295.

Boger, D.V. (2009), Rheology and the resource industries. *Chemical Engineering Science*, 64 (09) 4525-4536.

Boulanger, R.W. (2003). Relating Ka to Relative State parameter index. *Journal of Geotechnical and Geoenvironmental Engineering,* 129(8): 770-773.

Boulanger, R.W., Idriss, I.M. (2007). Evaluation of cyclic softening in silts and clays. *Journal of Geotechnical and Geoenvironmental Engineering* 133(6): 641-652.

Burden, R.N., Williams, D., Ward W. (2017). Summary of results for the University of Alberta/University of Queensland, Eco-tails Testing Program, Draft. *Department of Civil & Environmental Engineering, University of Alberta*.

Brandon, T.L., Rose, A.T., Duncan, J.M. (2006). Drained and undrained strength interpretation for low-plasticity silts. *Journal of Geotechnical and Geoenvironmental Engineering*, 132(2), 250-257.

Bray, J.D., Sancio, R.B. (2006). Assessment of the liquefaction susceptibility of fine-grained soils. *Journal of Geotechnical and Geoenvironmental Engineering*, 132 (9): 1165-1177.

Bussière, B. (2007). Colloquium 2004: Hydrogeotechnical properties of hard rock tailings from metal mines and emerging geoenvironmental disposal approaches. *Canadian Geotechnical* Journal, 44(9), 1019-1052.

Caldwell, J. (2006). British Columbia Tailings Failure at The HB Mine Near Salmo, British Columbia. *TechnoMine*. July 6, 2006.

Casagrande, A. (1936). Characteristics of cohesionless soils affecting the stability or earth fills. *Journal of Boston Society of Civil Engineers*, 23, 257-276.

Daliri, F., Kim, H., Simms, P., Sivathayalan, S. (2014). Impact of desiccation on monotonic and cyclic shear strength of thickened gold tailings. *Journal of Geotechnical and Geoenvironmental Engineering*, 140(9), 1-13.

Fourie, A.B., Papgeorgiou, G.V. (2001). Defining an appropriate steady state line for Merriespruit gold tailings. *Canadian Geotechnical Journal*, 695-706.

Gorakhki, M.H., Bareither, C.A. (2017). Unconfined compressive strength of synthetic and natural mine tailings amended with fly ash and cement. *Journal of Geotechnical and Geoenvironmental Engineering*, 143(7), 1-14.

Gorakhki, M.H., Bareither, C.A., Scalia, J., Jacobs, M. (2019). Hydraulic Conductivity and Soil Water Retention of Waste Rock and Tailings Mixtures. *Geo-Congress*, 41-50.

Hamade, M.M.P. (2017). *Undrained Shear Behavior of Mixed Mine Waste Rock and Tailings*. Masters Thesis, Dept. of Civil & Environmental Engineering, Colorado State University, Fort Collins, Colorado, USA.

Jefferies, M. Been, K. (2006). *Soil Liquefaction, A Critical State Approach*. Taylor and Francis.

Jehring, M.M., Bareither, C.A. (2016). Tailings composition effects on shear strength behavior of co-mixed mine waste rock and tailings. *Acta Geotechnica*, 1-20.

Khalili, A., Wijewickreme, D., Wilson, G.W. (2005). Some observations on the mechanical response of mixtures of mine waste and tailings. *Proc. 58th Canadian Geotechnical Conference*.

Khalili, A., Wijewickreme, D., Wilson, W. (2010). Mechanical response of highly gap-graded mixtures of waste rock and tailings. Part I: Monotonic shear response, *Canadian Geotechnical Journal*, 47(5), 552-565.

Kolymbas, D. (1999). *Introduction to Hypoplasticity*, A. A. Balkema.

Kossoff, D., Dubbin, W.E., Alfredsson, M., Edwards, S.J., Macklin, M.G., Hudson-Edwards, K.A. (2014). Mine Tailings Dams: Characteristics, Failure, Environmental Impacts, and Remediation, *Applied Geochemistry*, V.51, 2014 PP 229-245.

Kuerbis, R.H., Negussey, D. Vaid, Y.P. (1988). Effect of gradation and fines content on the undrained response of sand. *ASCE Conference on Hydraulic Fill Structures, GSP 21*, 330-345.

Lambe, T.W. and Whitman, R.V. (1969). *Soil Mechanics*. John Wiley & Sons, Inc. New York.

La Rochelle, P., Leroueli, S., Trak, B., Blais-Leroux, L., Tavenas, F. (1988). Observational approach to membrane and area corrections in triaxial tests, *Advanced Triaxial Testing of Soils and Rock*, ASTM, STP 977, 715-731.

Leduc, M., Backens, M., Smith, M.E. (2004). Tailings co-disposal at the Esquel gold mine Patagonia, Argentina. *Proc. SME Annual Meeting, Denver, Colorado*, 5 pp.

Matyas, E.L., Welch, D.E., Reades, D.W. (1984). Geotechnical parameters and behaviour of uranium tailings, *Canadian Geotechnical Journal*, 21(3), 489-504.

Morgenstern, N.R., Vick, S.G., Viotti, C.B., Watts, B.D. (2016). Fundão Tailings Dam Review Panel – Report on the Immediate Causes of the Failure of the Fundão Dam, Copyright – *Cleary Gottlieb Steen & Hamilton LLP, Vale S.A., BHP Billiton Brasil Ltda. and Samarco Mineração S.A*,

Morris, P.H., Williams, D.J. (1997). Results of field trials of co-disposal of coarse and fine coal waste, *Transactions of the Institution of Mining and Metallurgy*, 106, A38-A41.

Ni, Q., Tan, T. S., Dasari, G. R., Hight, D. W. (2004). Contribution of fines to the compressive strength of mixed soils. *Géotechnique*, 54(9), 561-569.

Pitman, T.D., Robertson, P.K., Sego, D.C. (1994). Influence of fines on the collapse of loose sands. *Canadian Geotechnical Journal*, 31, 5, 728-739.

Plewes, H.D., Davies, M.P., Jefferies, M.G. (1992). CPT based screening procedure for evaluating liquefaction susceptibility. *45th Canadian Geotechnical Conference*, Proc., Toronto, Ont. 26-28.

Poulos, J. (1981). The steady state of deformation. *Journal of Geotechnical Engineering Division*, ASCE, 107(GT5), 553- 562.

Puri, V.K. Kostecki, T.R. (2013). Liquefaction of mine tailings. *International Conference on Case Histories in Geotechnical Engineering.*

Qiu, Y., Sego, D.C. (2001). Lab properties of mine tailings, *Canadian Geotechnical Journal*, 38(1), 183-190.

Rahman, M. M., Lo, S. R., Gnanendran, C. T. (2008). On equivalent granular void ratio and steady-state behavior of loose sand with fines. *Canadian Geotechnical Journal,* 45(10), 1439-1456.

Roscoe, K. Shofield, A.S., Wroth, C.P. (1958). On the yielding of soils. *Geotechnique*, 8(1), 22-53.

Schofield, A., Wroth, C.P (1968). *Critical State Soil Mechanics*. London, McGrawHill.

Sladen, J.A., Handford, G. (1987). A potential systematic error in laboratory testing of very loose sands. *Canadian Geotechnical Journal*, 24, 462–466.

Thevanayagam, S. (1998). Effect of fine and confining stress on undrained shear strength of silty sands, *Journal of Geotechnical and Geoenvironmental Engineering*, 124(6), 479-491.

Thevanayagam, S., Shenthan, T., Mohan, S., Liang, J. (2002). Undrained fragility of clean sands, silty sands, and sandy silts, *Journal of Geotechnical and Geoenvironmental Engineering*, 128(10), 849-859.

Thevanayagam, S. (2007). Intergrain contact density indices for granular mixes I - Framework, *Journal of Earthquake Engineering and Engineering Vibrations*, 6(2), 123-134.

Wang, S., Luna, R., Stephenson, R.W. (2011). A slurry consolidation approach to reconstitute low-plasticity silt specimens for laboratory triaxial testing, *Geotechnical Testing Journal*, 34(4), 1-9.

Wang, S., Luna, R. (2012). Monotonic behavior of Mississippi River Valley silt in triaxial compression. *Journal of Geotechnical and Geoenvironmental Engineering*, 138(4), 516-525.

Wickland, B.E., Wilson, G.W. (2005). Self-weight consolidation of mixtures of mine waste rock and tailings, *Canadian Geotechnical Journal*, 42(2), 327-339.

Wickland, B.E., Wilson, G.W., Wijewickreme, D., Klein B. (2006). Design and evaluation of mixtures of mine waste rock and tailings. *Canadian Geotechnical Journal*, 43, 928-945.

Wickland, B.E., Wilson, G.W. Wijewickreme, D. (2010). Hydraulic conductivity and consolidation response of mixtures of mine waste rock and tailings. *Canadian Geotechnical Journal*, 47(4), 472-485.

Wijewickreme, D., Sanin, M.V., Greenaway, G.R. (2005). Cyclic shear response of fine-grained mine tailings. *Canadian Geotechnical Journal* 42(5): 1408-1421.

Wijewickreme, D., Khalili, A., Wilson, G. W. (2010). Mechanical response of highly gap-graded mixtures of waste rock and tailings. Part II: Undrained cyclic and post-cyclic shear response. *Canadian Geotechnical Journal, 47*, 566-582.

Williams, D., J., Wilson, G.W., Panidis, C. (2003). Waste rock and tailings mixtures as a possible seal for potentially acid forming waste rock. *Proc. 6th Intl Conf. on Acid Rock Drainage*, Cairns, QLD, 427-435.

Wilson, G.W., Plewes, H.D., Williams, D., Roberston, J. (2003). Concepts for co-mixing of tailings and waste rock. *Proc. 6th Intl Conf. on Acid Rock Drainage, Cairns, QLD*, 437-443.

APPENDIX: Results from Consolidated Undrained Triaxial Compression Tests

Material: **Filtered tailings prepared at field conditions**
Test: **20kPa (T1)**

Failure criterion: K_f Line

σ'_c	15.89	kPa
ρ_d	1.48	g/cm^3
ρ_t	1.76	g/cm^3
e_0	0.86	-
B	97	%

$\Delta\sigma_{df}$	30.6	kPa
u_{ef}	252.7	kPa
σ'_{1f}	38.8	kPa
σ'_{3f}	8.2	-
ξ_{af}	12	%

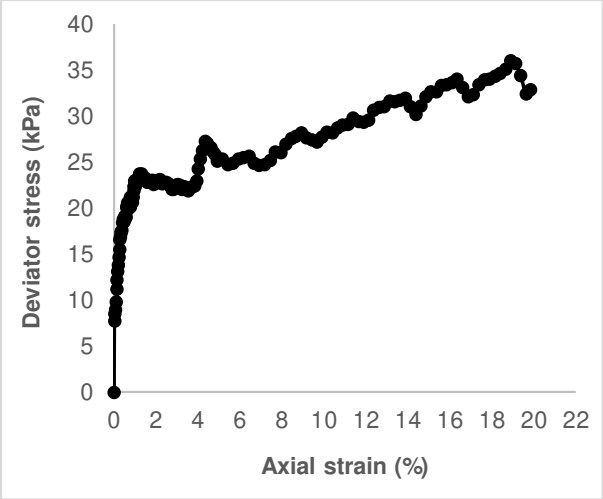

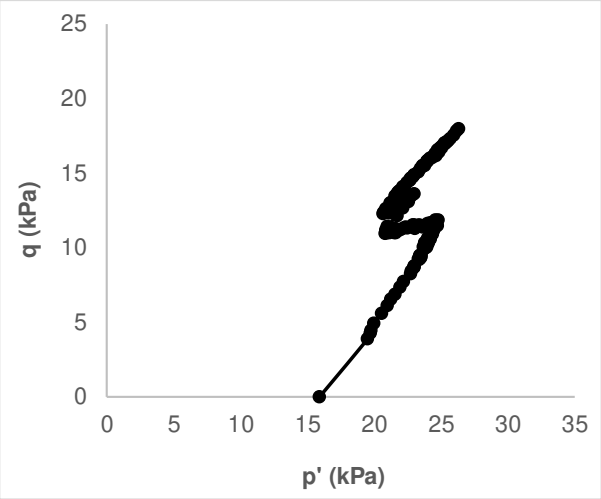

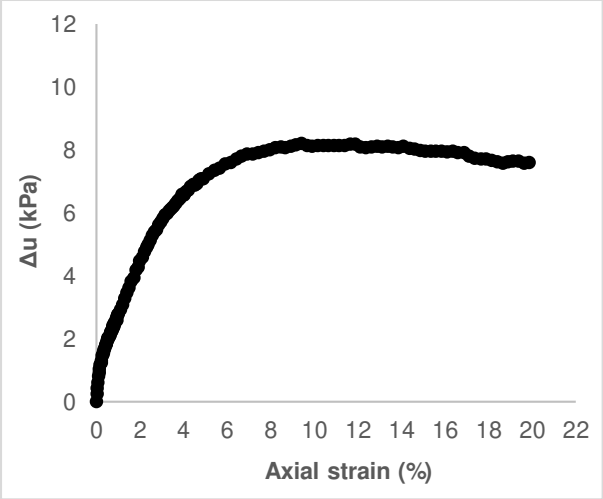

Material: **Filtered tailings prepared at field conditions**
Test: **20kPa (T2)**

Failure criterion: K_f Line

σ'_c	14.27	kPa
ρ_d	1.46	g/cm^3
ρ_t	1.76	g/cm^3
e_0	0.89	-
B	99	%

$\Delta\sigma_{df}$	37.9	kPa
u_{ef}	222.0	kPa
σ'_{1f}	45.1	kPa
σ'_{3f}	7.3	-
ξ_{af}	13	%

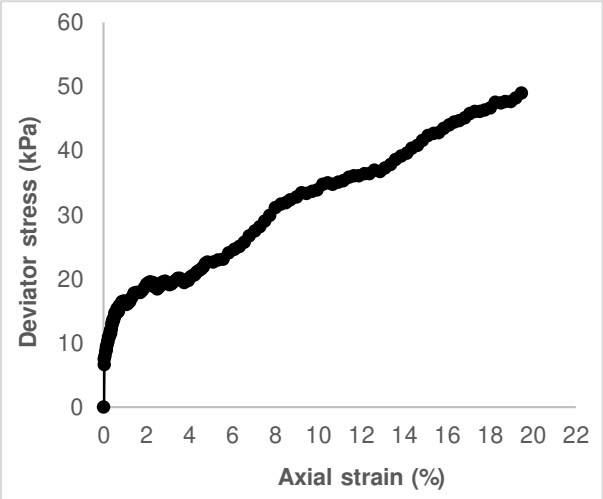

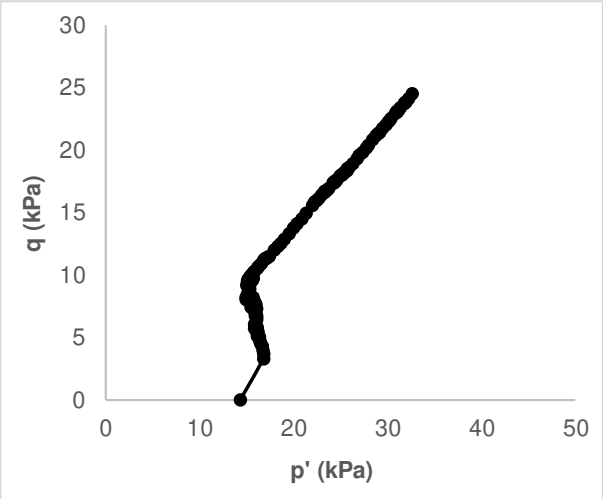

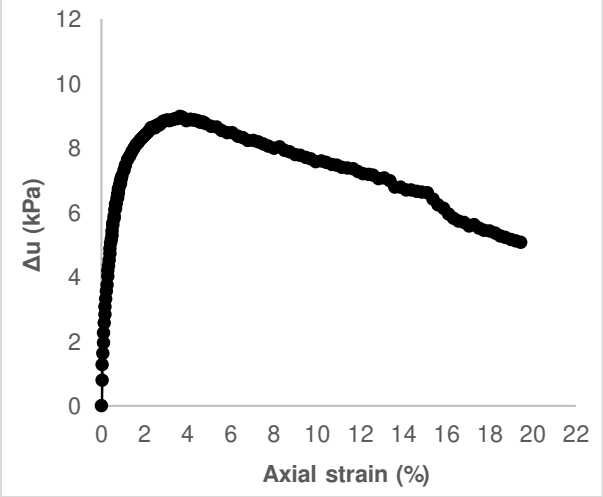

Material: **Filtered tailings prepared at field conditions**
Test: **50kPa**

Failure criterion: K_f Line

σ'_c	46.53	kPa
ρ_d	1.54	g/cm^3
ρ_t	1.85	g/cm^3
e_0	0.80	-
B	100	%

$\Delta\sigma_{df}$	39.2	kPa
u_{ef}	282.1	kPa
σ'_{1f}	47.1	kPa
σ'_{3f}	7.9	-
ξ_{af}	6	%

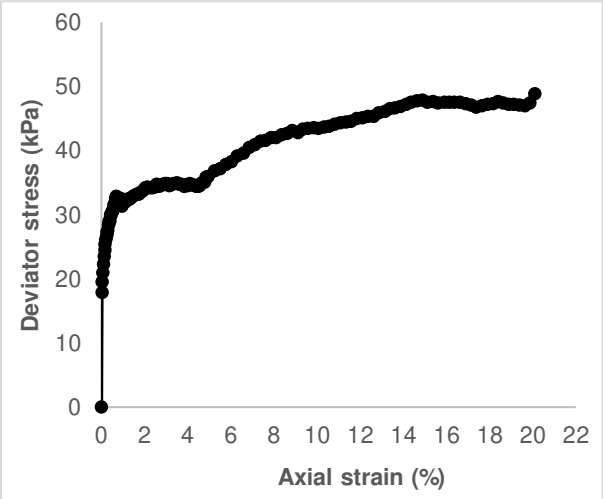

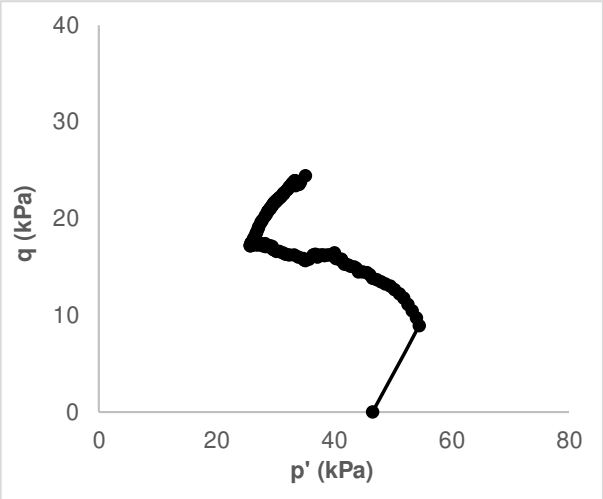

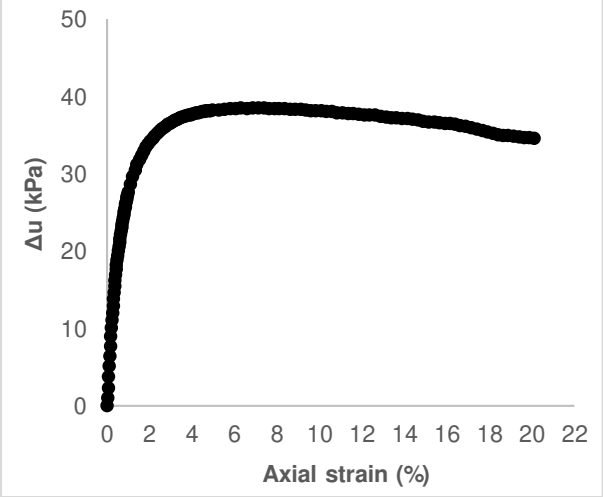

Material: **Filtered tailings prepared at field conditions**
Test: **100kPa (T1)**

Failure criterion: K_f Line

σ'_c	95.03	kPa
ρ_d	1.48	g/cm^3
ρ_t	1.78	g/cm^3
e_0	0.86	-
B	97	%

$\Delta\sigma_{df}$	57.6	kPa
u_{ef}	434.7	kPa
σ'_{1f}	78.5	kPa
σ'_{3f}	20.9	-
ξ_{af}	16	%

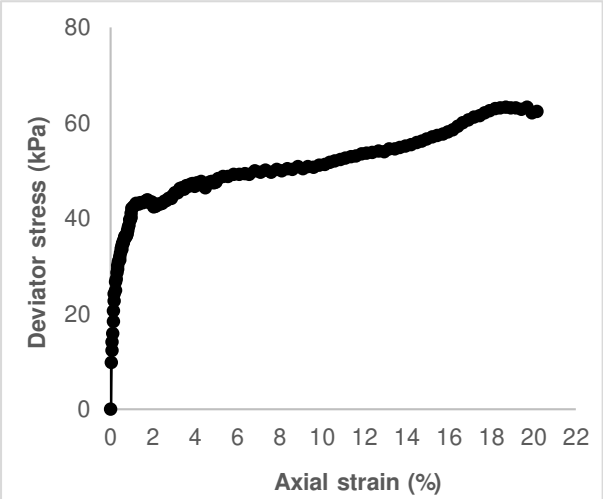

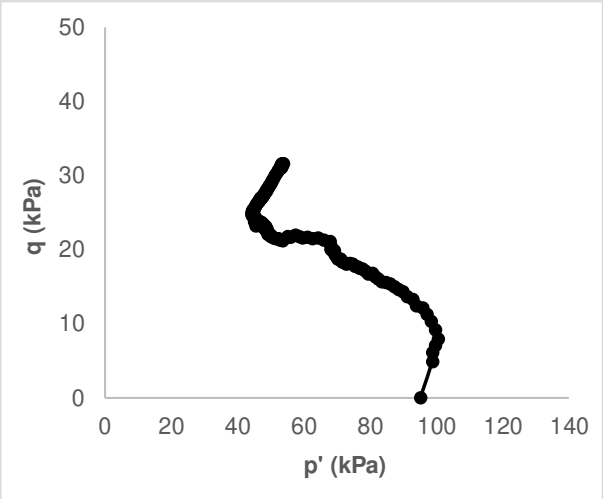

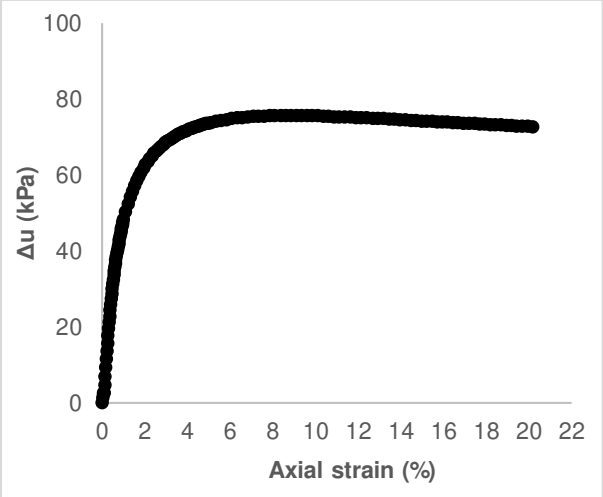

Material: **Filtered tailings prepared at field conditions**
Test: **100kPa (T2)**

Failure criterion: K_f Line

σ'_c	96.08	kPa
ρ_d	1.48	g/cm^3
ρ_t	1.79	g/cm^3
e_0	0.86	-
B	97	%

$\Delta\sigma_{df}$	71.0	kPa
u_{ef}	433.6	kPa
σ'_{1f}	92.9	kPa
σ'_{3f}	21.9	-
ξ_{af}	9	%

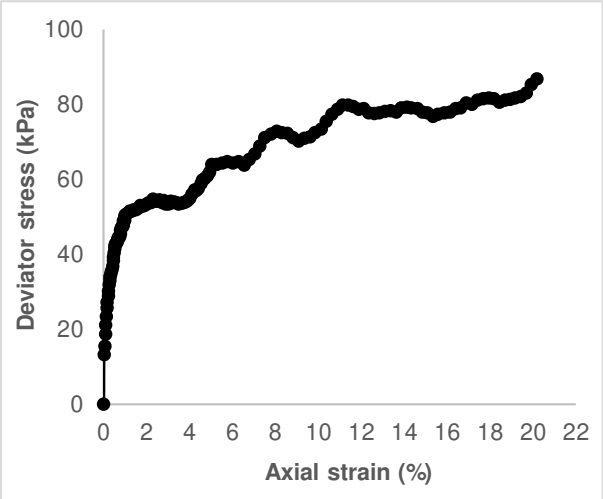

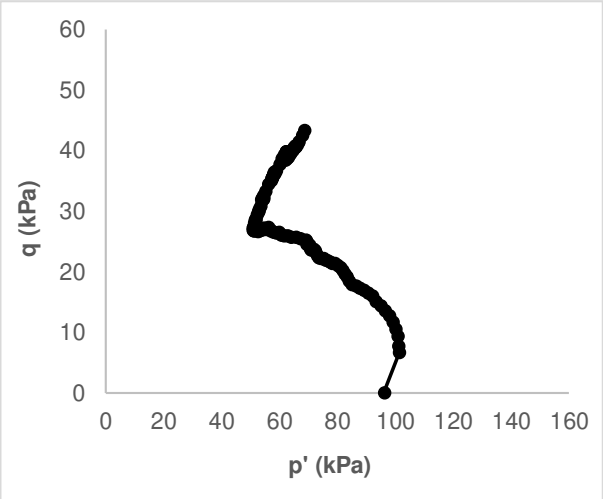

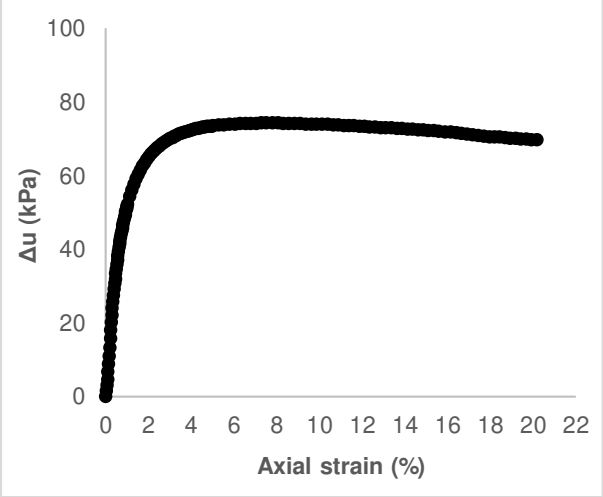

Material: **Filtered tailings prepared at field conditions**
Test: **100kPa (T3)**

Failure criterion: K_f Line

σ'_c	97.57	kPa
ρ_d	1.54	g/cm^3
ρ_t	1.81	g/cm^3
e_0	0.79	-
B	100	%

$\Delta\sigma_{df}$	79.8	kPa
u_{ef}	457.3	kPa
σ'_{1f}	104.5	kPa
σ'_{3f}	24.7	-
ξ_{af}	9	%

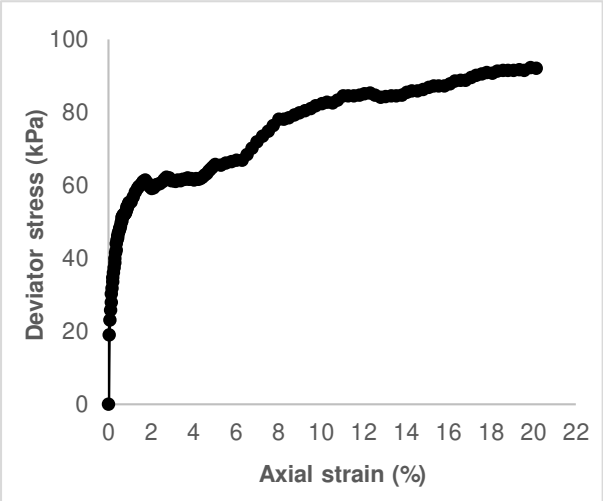

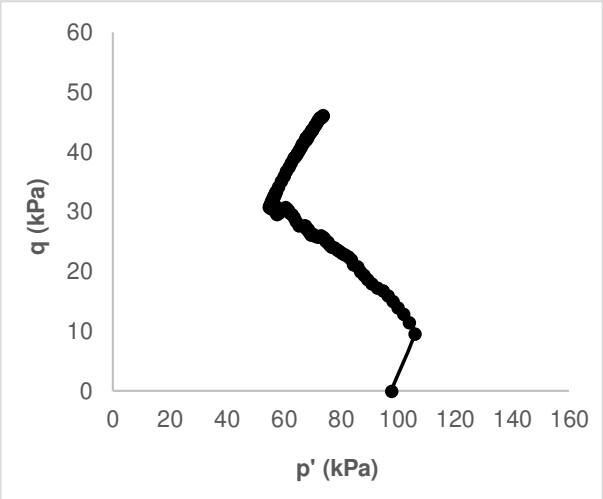

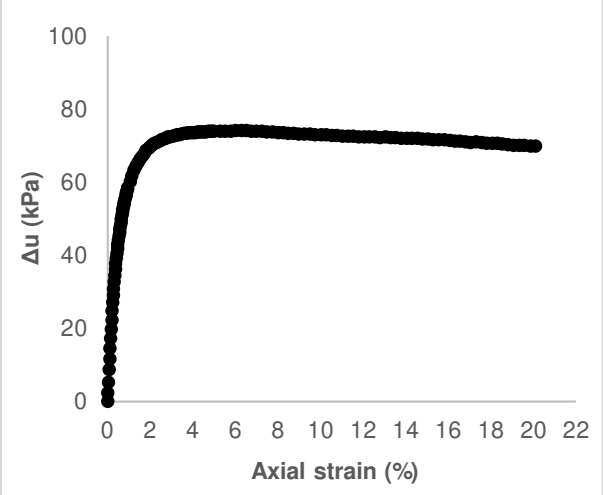

Material: **Filtered tailings prepared at field conditions**
Test: **250kPa (T1)**

Failure criterion: K_f Line

σ'_c	249.60	kPa
ρ_d	1.51	g/cm^3
ρ_t	1.81	g/cm^3
e_0	0.82	-
B	100	%

$\Delta\sigma_{df}$	191.0	kPa
u_{ef}	420.6	kPa
σ'_{1f}	268.9	kPa
σ'_{3f}	77.9	-
ξ_{af}	9	%

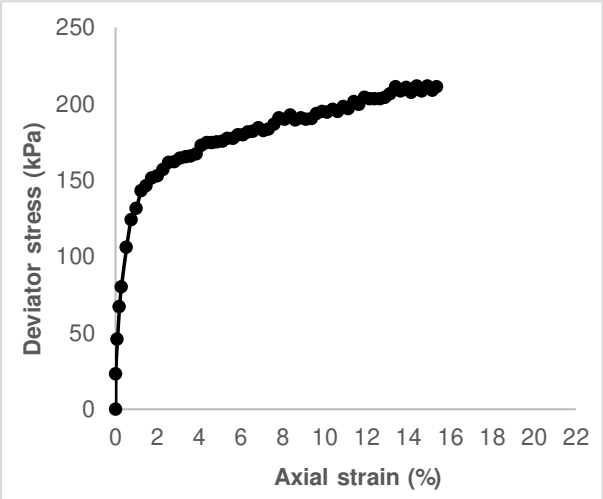

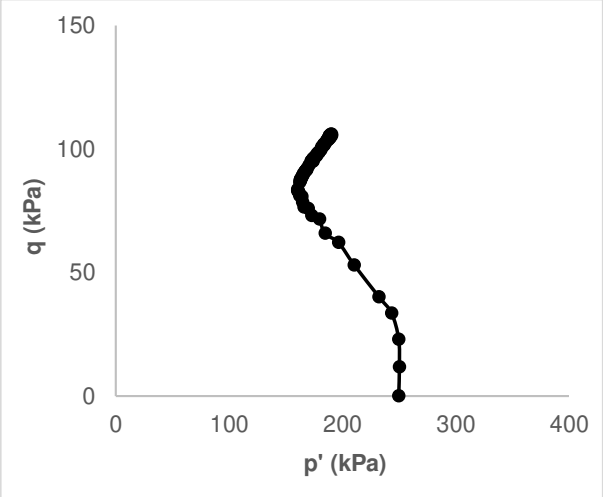

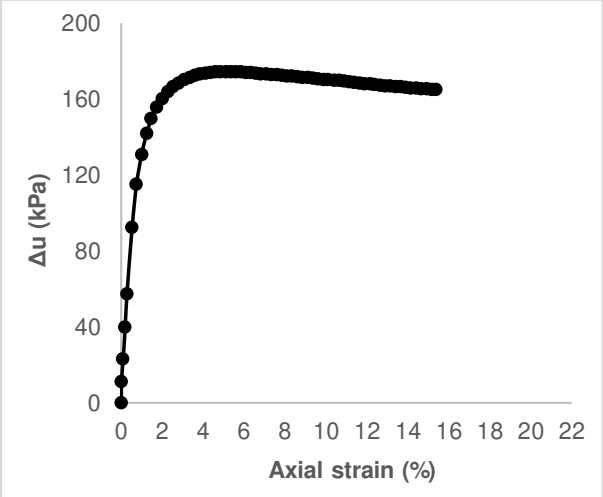

Material: **Filtered tailings prepared at field conditions**
Test: **250kPa (T2)**

Failure criterion: K_f Line

σ'_c	251.94	kPa
ρ_d	1.53	g/cm^3
ρ_t	1.81	g/cm^3
e_0	0.80	-
B	98	%

$\Delta\sigma_{df}$	159.1	kPa
u_{ef}	389.0	kPa
σ'_{1f}	237.2	kPa
σ'_{3f}	78.1	-
ξ_{af}	14	%

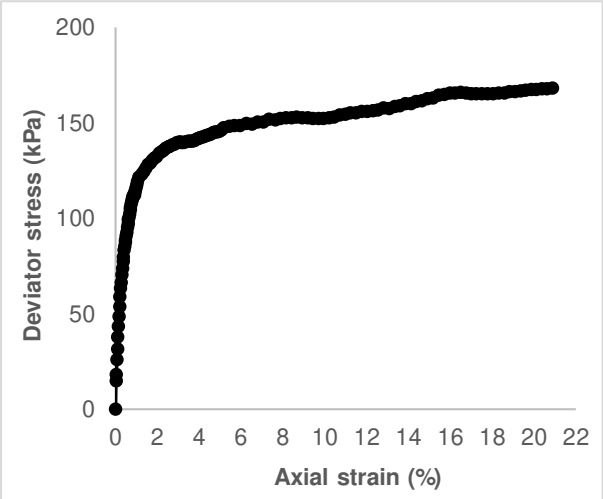

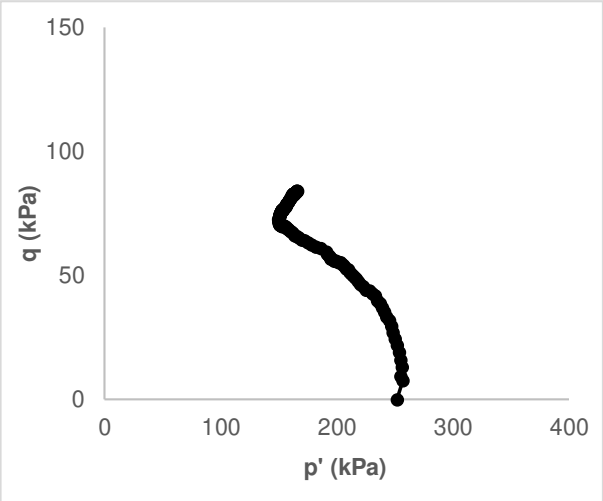

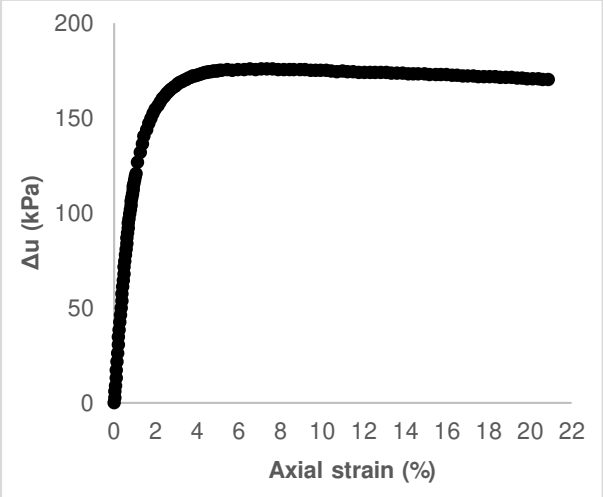

Material: **Filtered tailings prepared at field conditions**
Test: **500kPa**

Failure criterion: K_f Line

σ'_c	490.65	kPa
ρ_d	1.52	g/cm^3
ρ_t	1.82	g/cm^3
e_0	0.82	-
B	100	%

$\Delta\sigma_{df}$	393.2	kPa
u_{ef}	432.4	kPa
σ'_{1f}	561.8	kPa
σ'_{3f}	168.7	-
ξ_{af}	8	%

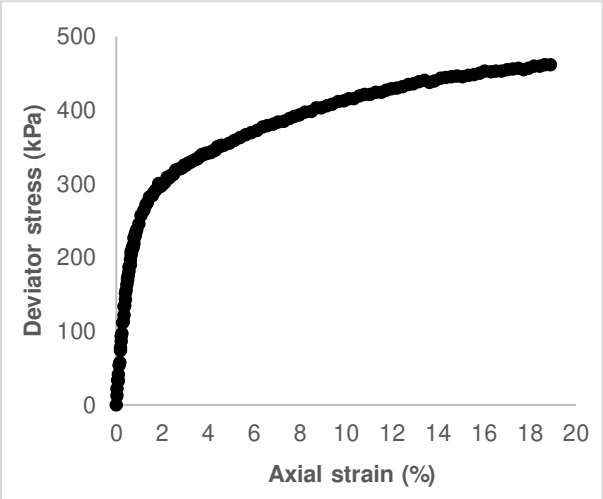

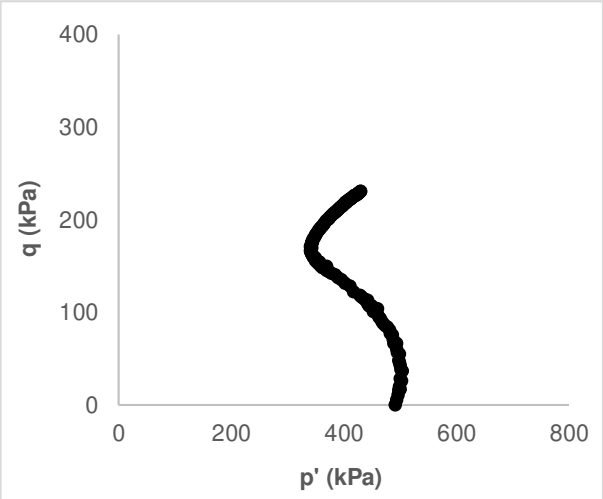

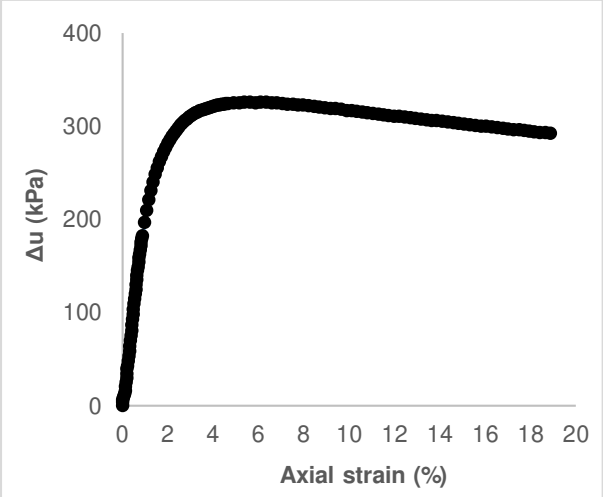

Material: **Dense Tailings**
Test: **100kPa**

Failure criterion: K_f Line

σ'_c	96.71	kPa
ρ_d	1.66	g/cm^3
ρ_t	1.95	g/cm^3
e_0	0.67	-
B	100	%

$\Delta\sigma_{df}$	161.5	kPa
u_{ef}	293.9	kPa
σ'_{1f}	219.6	kPa
σ'_{3f}	58.2	-
ξ_{af}	3	%

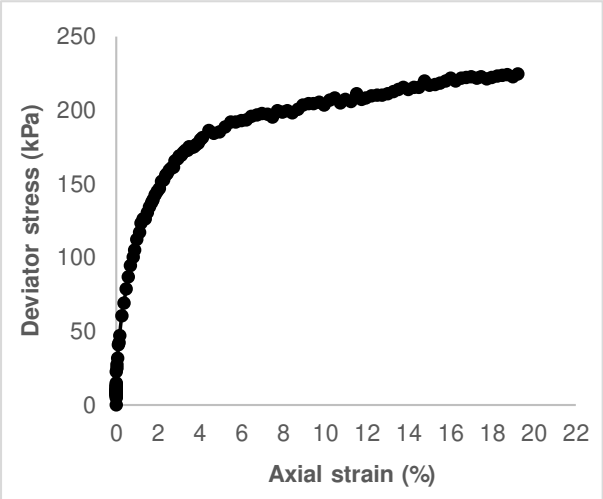

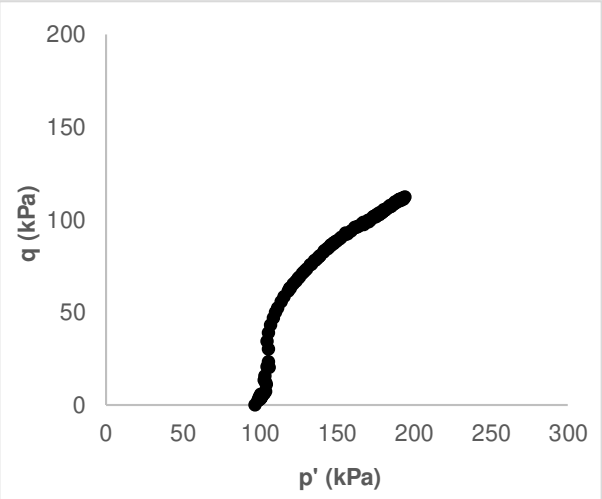

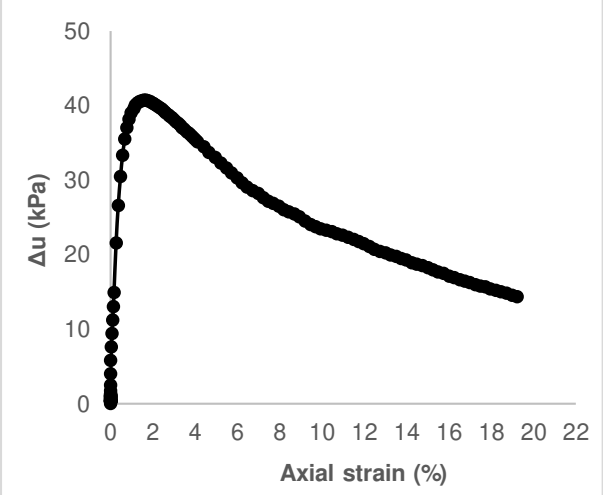

Material: **Dense Tailings**
Test: **250kPa**

Failure criterion: K_f Line

σ'_c	248.23	kPa
ρ_d	1.69	g/cm^3
ρ_t	2.00	g/cm^3
e_0	0.63	-
B	100	%

$\Delta\sigma_{df}$	266.6	kPa
u_{ef}	375.2	kPa
σ'_{1f}	361.8	kPa
σ'_{3f}	95.2	-
ξ_{af}	5	%

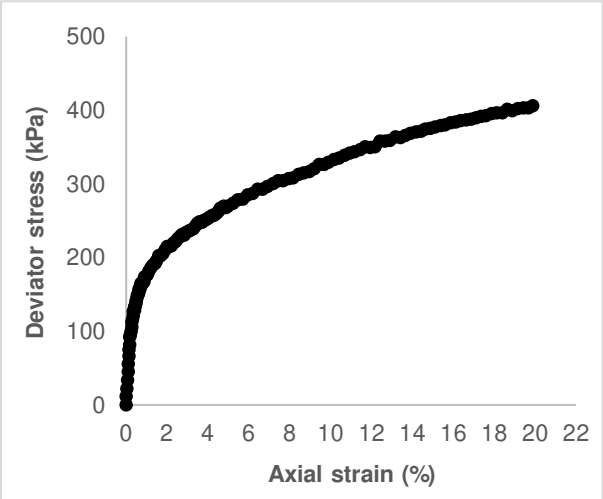

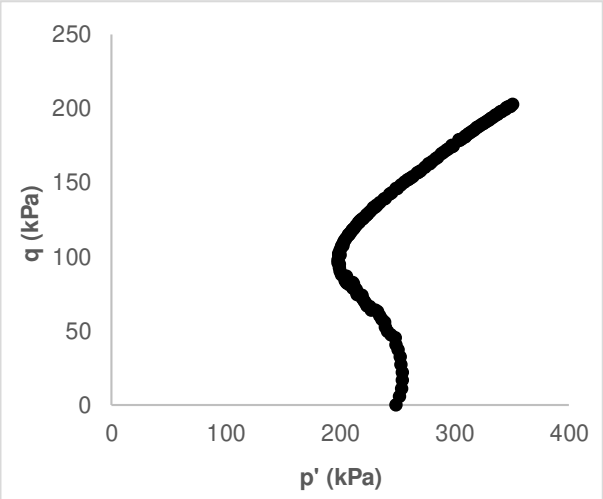

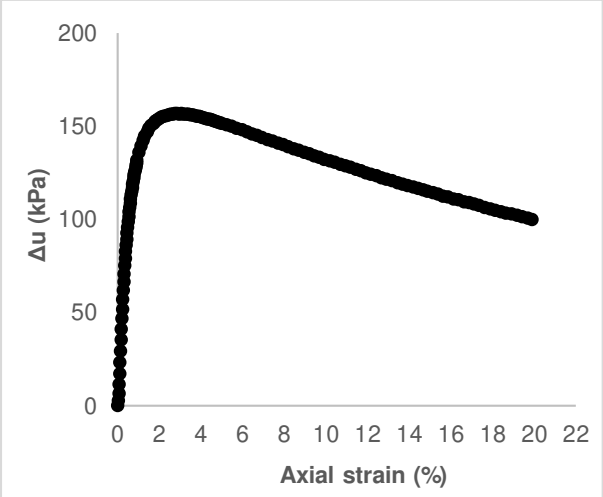

Material: **Dense Tailings**
Test: **500kPa**

Failure criterion: K_f Line

σ'_c	506.00	kPa
ρ_d	1.73	g/cm^3
ρ_t	2.03	g/cm^3
e_0	0.59	-
B	97	%

$\Delta\sigma_{df}$	403.7	kPa
u_{ef}	440.7	kPa
σ'_{1f}	582.5	kPa
σ'_{3f}	178.9	-
ξ_{af}	4	%

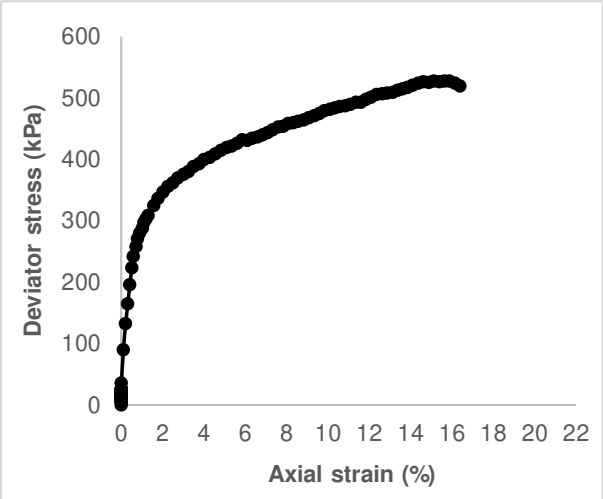

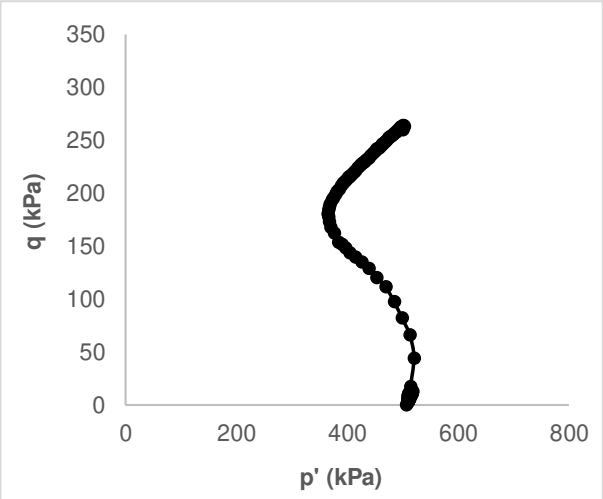

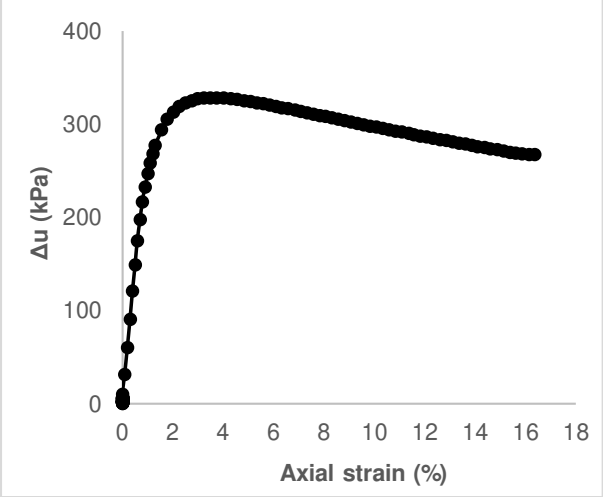

Material: **Paste Tailings**
Test: **100kPa**

Failure criterion: K_f Line

σ'_c	97.18	kPa
ρ_d	1.24	g/cm^3
ρ_t	1.77	g/cm^3
e_0	1.22	-
B	98	%

$\Delta\sigma_{df}$	122.1	kPa
u_{ef}	58.2	kPa
σ'_{1f}	174.4	kPa
σ'_{3f}	52.3	-
ξ_{af}	9	%

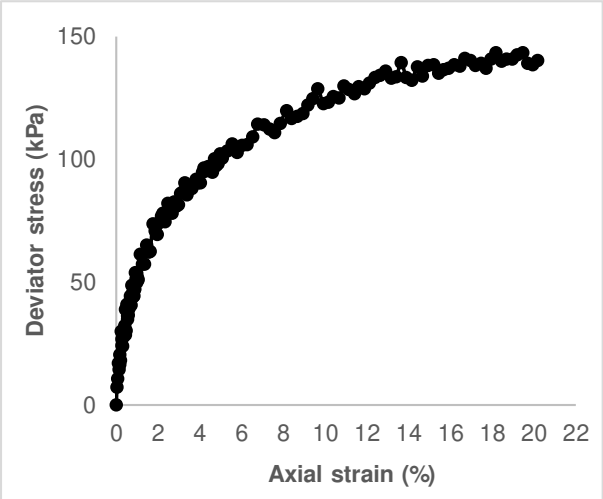

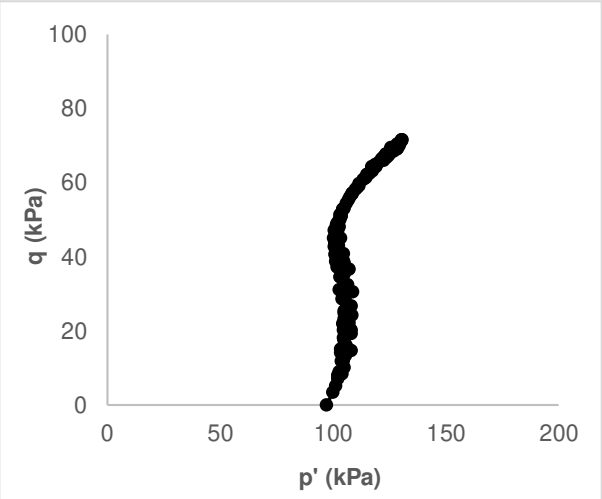

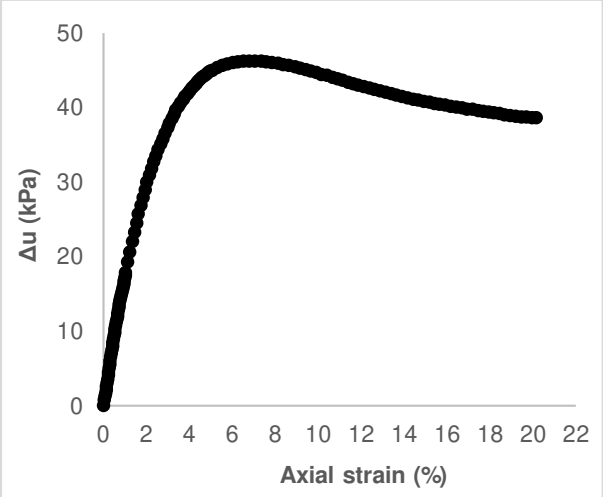

Material: **Paste Tailings**
Test: **250kPa**

Failure criterion: K_f Line

σ'_c	248.88	kPa
ρ_d	1.19	g/cm^3
ρ_t	1.62	g/cm^3
e_0	1.32	-
B	100	%

$\Delta\sigma_{df}$	207.5	kPa
u_{ef}	442.1	kPa
σ'_{1f}	300.5	kPa
σ'_{3f}	92.9	-
ξ_{af}	4	%

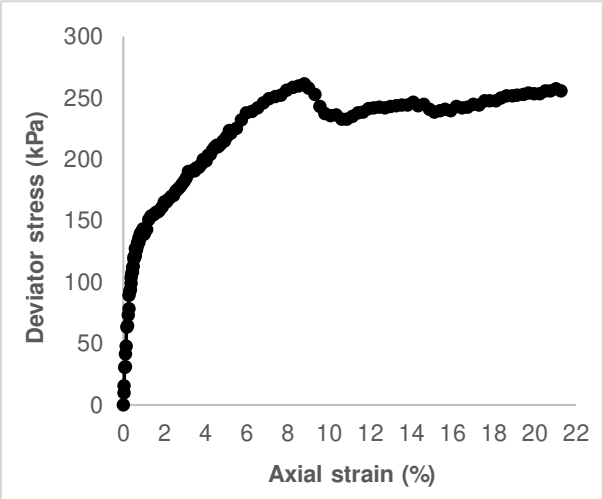

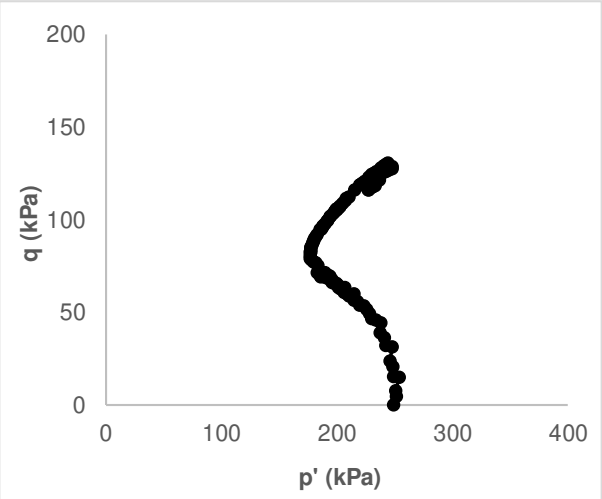

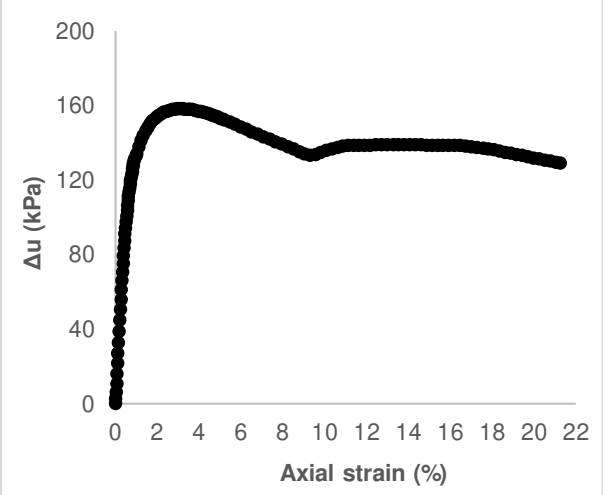

Material: **GeoWaste**
Test: **50kPa**

Failure criterion: K_f Line

σ'_c	49.68	kPa
ρ_d	1.73	g/cm^3
ρ_t	1.90	g/cm^3
e_0	0.58	-
B	95	%

$\Delta\sigma_{df}$	42.4	kPa
u_{ef}	298.3	kPa
σ'_{1f}	63.9	kPa
σ'_{3f}	21.5	-
ξ_{af}	12	%

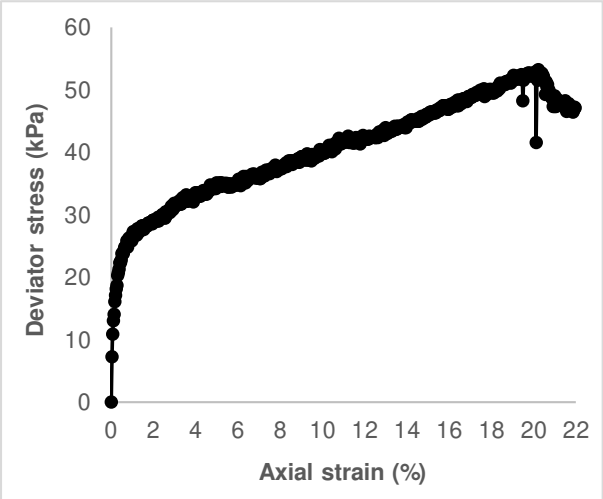

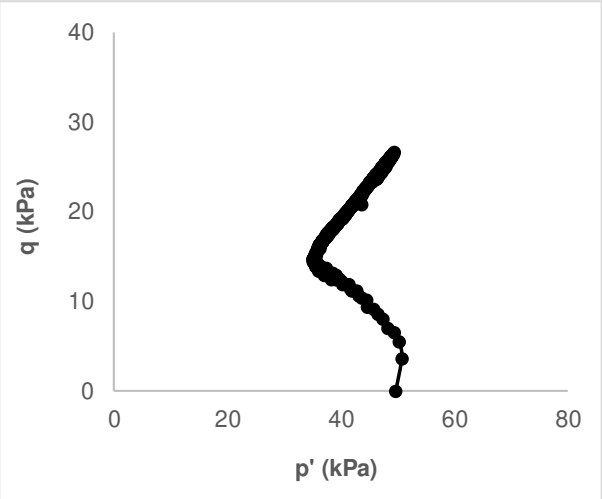

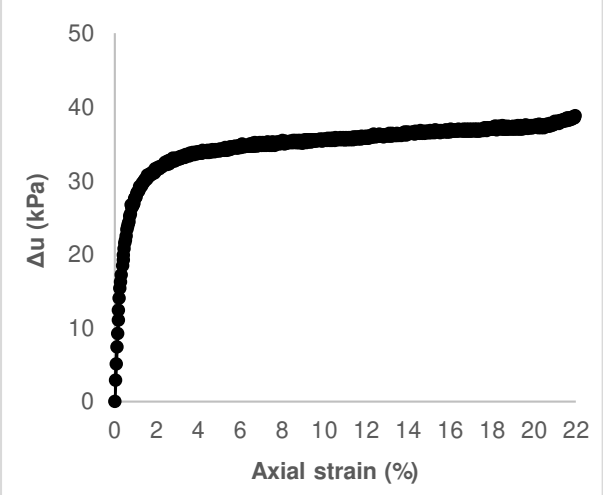

Material: **GeoWaste**
Test: **100kPa**

Failure criterion: K_f Line

σ'_c	96.72	kPa
ρ_d	1.95	g/cm^3
ρ_t	2.14	g/cm^3
e_0	0.40	-
B	97	%

$\Delta\sigma_{df}$	75.6	kPa
u_{ef}	429.6	kPa
σ'_{1f}	105.3	kPa
σ'_{3f}	29.7	-
ξ_{af}	9	%

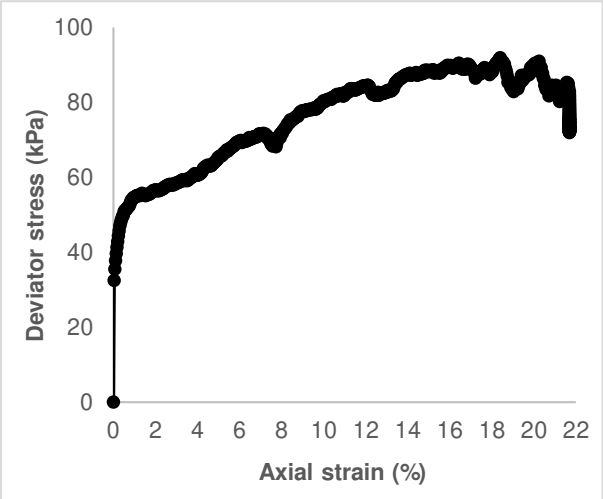

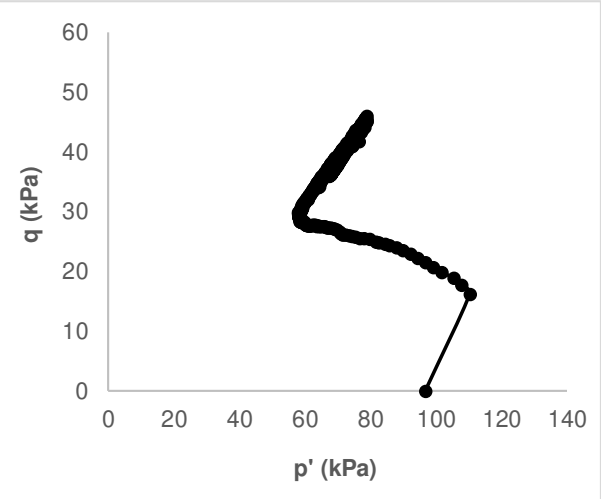

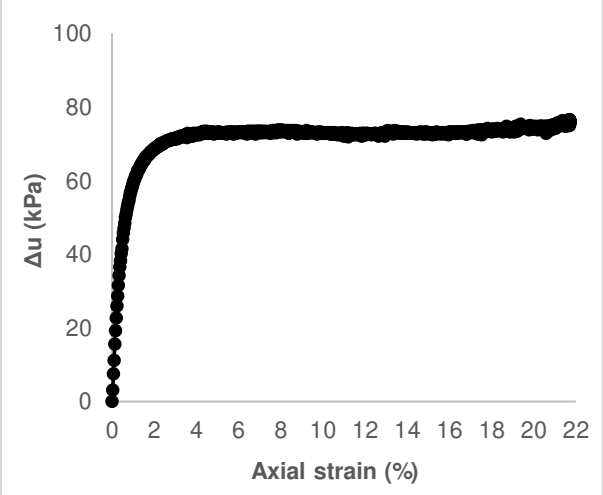

Material: **GeoWaste**
Test: **500kPa**

Failure criterion: K_f Line

σ'_c	476.15	kPa
ρ_d	1.88	g/cm^3
ρ_t	2.03	g/cm^3
e_0	0.46	-
B	96	%

$\Delta\sigma_{df}$	655.3	kPa
u_{ef}	469.3	kPa
σ'_{1f}	843.3	kPa
σ'_{3f}	188.0	-
ξ_{af}	9	%